EPA # 600/R-02/070
September 2002

Guidelines for the Application of SEM/EDX Analytical Techniques to Particulate Matter Samples

by

Robert D. Willis and Fredrick T. Blanchard
ManTech Environmental Technology, Inc.
Research Triangle Park, NC 27709

and

Teri L. Conner
National Exposure Research Laboratory
U.S. Environmental Protection Agency
Research Triangle Park, NC 27711

Contract 68-D-00-206

Project Officer
Curtis Morris
Human Exposure and Atmospheric Sciences Division
National Exposure Research Laboratory

Work Assignment Manager
Teri L. Conner
National Exposure Research Laboratory
U.S. Environmental Protection Agency
Research Triangle Park, NC 27711

National Exposure Research Laboratory
Office of Research and Development
U.S. Environmental Protection Agency
Research Triangle Park, NC 27711

Notice

The information in this document has been funded wholly by the United States Environmental Protection Agency under contract number 68D00206 to ManTech Environmental Technology, Inc. It has been subjected to the Agency's peer and administrative review and has been approved for publication as an EPA document.

Abstract

Scanning Electron Microscopy (SEM) coupled with Energy-Dispersive X-ray analysis (EDX) is a powerful tool in the characterization and source apportionment of environmental particulate matter (PM), providing size, chemistry, and morphology of particles as small as a few tenths of a micrometer. Such information can reveal information about emission sources which cannot be determined through bulk chemical analysis. Automated SEMs capable of routinely analyzing hundreds of particles per hour have dramatically increased the throughput of SEM/EDX, making it feasible to conduct statistically meaningful analyses of PM samples and to generate large data sets for source apportionment studies.

The National Exposure Research Laboratory (NERL) of the U.S. EPA has been developing and evaluating the use of SEM/EDX to characterize ambient and source-derived particles. The present document, which evolved over several years as a product of research carried out in support of the U.S. EPA/NERL SEM/EDX Laboratory, is intended to provide guidelines for researchers using SEM/EDX for aerosol characterization and source apportionment. Topics include laboratory procedures for sample handling, sample preparation, guidelines for successful manual and automated SEM/EDX analyses, data interpretation, issues relating to data quality and method validation and case studies highlighting the use of SEM/EDX in PM research.

Foreword

The National Exposure Research Laboratory, Research Triangle Park, North Carolina, conducts intramural and extramural research in the chemical, physical, and biological sciences. The research is intended to characterize and quantify ambient air pollutant levels and the resulting exposures of humans and ecosystems; to develop and validate models to predict changes in air pollutant levels; to determine source-receptor relationships affecting air quality and pollutant exposures; and to solve scientific problems relating to EPA's mission through long-term investigation in the areas of atmospheric methods, quality assurance, biomarkers, spatial statistics, exposure assessment, and modeling. The Laboratory provides support to program and regional offices and state and local groups. This support includes technical advice, methods research and development, quality assurance, field monitoring, instrument development, and modeling for quantitative risk assessment and regulation. The Laboratory also collects, organizes, manages, and distributes data on air quality, human and ecosystem exposures and trends for the program and regional offices, the Office of Research and Development, the scientific community, and the public.

Gary J. Foley, Ph.D.
Director
National Exposure Research Laboratory
Research Triangle Park, NC 27711

Contents

Notice i
Abstract ii
Foreword iii
Figures vii
Tables viii
Acronyms and Abbreviations ix
Acknowledgments x

Chapter 1: Introduction 1
Chapter 2: Overview of SEM/EDX Techniques and Instrumentation 3
2.1 Overview of SEM/EDX 3
2.1.1 Overview of SEM 3
2.1.1.1 Image Formation 3
2.1.1.2 Electron Beam Production 4
2.1.1.3 Probe Size and Beam Current 5
2.1.1.4 Accelerating Voltage 5
2.1.1.5 Guidelines for Imaging 6
2.1.2 Overview of EDX 7
2.1.2.1 Effective X-ray Volume 8
2.1.2.2 Choice of Primary Beam Energy 9
2.1.2.3 Choice of Spot Size or Probe Current 9
2.1.2.4 Spectral Artifacts and X-ray Line Overlaps 9
2.1.2.5 Guidelines for Qualitative EDX Analysis 10
2.1.3 Overview of CCSEM 10
2.2 Description of NERL Facilities 10
2.2.1 LEO/PGT System 11
2.2.2 Aspex Personal SEM System 11
2.2.3 Vacuum Evaporators and Other Supporting Equipment 12
Chapter 3: Recommended Techniques and Procedures for SEM/EDX and CCSEM 13
3.1 Sample Receipt, Tracking, and Storage 13
3.1.1 Sample Submittal Form 13
3.1.2 Log-in Procedures 13
3.1.3 Sample Tracking 13
3.1.4 Sample Storage 13
3.2 Sample Preparation 14
3.2.1 Choice of Filter Media 14
3.2.2 Particulate Loadings 15
3.2.3 Mounting Filter Samples 15
3.2.3.1 Mounting Polycarbonate Filters 16
3.2.3.2. Mounting Teflon Filters 16

3.2.4 Preparing Bulk Dusts for SEM . . . 16
3.2.4.1 Procedure for Wet Preparation of Bulk Dusts . . . 16
3.2.4.2 Procedure for Dry Preparation of Bulk Dusts . . . 17
3.2.5 Coating Mounted Samples . . . 18
3.3 SEM/EDX Data Acquisition . . . 18
3.3.1 Manual . . . 19
3.3.2 CCSEM . . . 19
3.3.3 Semi-Automated SEM/EDX . . . 21
3.3.4 Size-Only . . . 21
3.3.5 Dedicated Particle Searches . . . 22
3.4 Particle Classification . . . 22
3.4.1 Default Four-Element Typing . . . 22
3.4.2 User-Defined Rules . . . 25
3.4.3 Cluster Analysis . . . 25
3.4.4 Spectrum Matching . . . 27
3.4.5 Neural Networks . . . 29
Chapter 4: Data Quality and Validity . . . 31
4.1 Instrument Calibration and Maintenance . . . 31
4.1.1 Magnification Calibration . . . 31
4.1.2 EDX Spectrometer Gain Calibration . . . 31
4.1.3 Window Contamination Check . . . 32
4.2 Precision and Accuracy of Particle Volume Estimates . . . 32
4.3 Precision and Accuracy of Particle Mass Estimates . . . 33
4.4 Analysis of Ultrafine Particles . . . 34
4.4.1 Limitations of the Present NERL SEM Facilities . . . 34
4.4.2 Other Microscopic Techniques . . . 35
4.4.3 Non-Microscopic Techniques . . . 36
4.4.4 Ultrafine Summary . . . 36
4.5 Carbonceous and Submicron Particles . . . 36
4.6 CCSEM Data Quality and Validity . . . 38
4.6.1 Precision of CCSEM (Repeat Analyses of Same Sample) . . . 39
4.6.2 Representativeness of Data . . . 40
4.6.3 Errors Associated with CCSEM . . . 41
4.6.4 EDX Acquisition Time . . . 42
Chapter 5: Examples of Research Applications . . . 45
5.1 Examples from the Literature . . . 45
5.1.1 Aerosol Characterization . . . 45
5.1.1.1 Fly Ash . . . 45
5.1.1.2 Carbonaceous Particles . . . 45
5.1.1.3 Sulfates . . . 46
5.1.1.4 Marine Aerosol . . . 46
5.1.1.5 Miscellaneous . . . 47
5.1.2 Source Apportionment . . . 47
5.1.3 SEM/EDX Methodology . . . 47
5.2 Phoenix $PM_{2.5}$ Samples . . . 48
5.2.1 Unmix Receptor Model Findings . . . 48
5.2.2 SEM/EDX Findings . . . 48
5.2.3 Summary of Results . . . 50
5.3 Fort Hall Source Apportionment Study . . . 50
5.4 Baltimore Retirement Home Study . . . 53
5.4.1 Methods . . . 53
5.4.2 Summary of Manual SEM/EDX Analysis Results . . . 54
5.4.3 Summary of CCSEM Analysis Results . . . 54
5.4.4 Conclusions . . . 57

5.5 World Trade Center Study 57
5.5.1 Verification of XRF Results 57
5.5.2 Analysis of Bulk Sample 57
5.5.3 Analysis of Ambient Air Sample 58
5.6 Source Particle SEM/EDX Data 58
Chapter 6: References 61
Appendix A 66
Example of LEO/PGT Data Output 67
Example of PSEM Data Output 69
Appendix B 71
Submittal Form for SEM/EDX Samples 72
Assignment of SEM IDs 73
Sample Log-In/Log-Out 74
Appendix C 75
Particle Classification Rules for $PM_{10-2.5}$ (Coarse) Particles 76
Particle Classification Rules for $PM_{2.5}$ (Fine) Particles 77
Appendix D: Particles from Ambient Air Sample Collected in NYC Near WTC Site 78
Appendix E: Source Particle Atlas 83

Figures

Number **Page**

2-1 Photomicrograph of Ambient, Coarse-Fraction Air Sample Collected in Baltimore. 3
2-2 Photomicrograph of Lead-rich House Dust. Left: SE Image. Right: BSE Image 4
2-3a Photomicrograph of Particulates from a Cement Kiln: Tungsten gun, 2.5 nA Probe Current, 1000 cps 5
2-3b Identical Field Imaged with LaB6 Gun, 0.55 nA Probe Current, 1000 cps 5
2-4 Photomicrograph of Pollen Grain Imaged with the LEO S440 at 30, 10, and 5 keV 5
2-5 EDX Spectrum of Iron-Rich Aluminum Silicate Particle 7
2-6 EDX Spectra of 0.16, 0.3, and 1.0 μm Aluminum Silicate Particles. 8
2-7 Photo of the LEO S440 SEM with PGT IMIX EDX System 11
2-8 Photo of the Personal SEM (PSEM) System 11
2-9a Photomicrograph of Salt Crystals (PSEM with Tungsten Gun) 12
2-9b Photomicrograph of Salt Crystals (LEO 440 with LaB6 Emitter). 12

3-1 Photomicrographs of Four Filter Substrates Commonly Used for Aerosol Sampling. 14
3-2 Vacuum Filtration Apparatus Used for Wet Preparation of Bulk Dusts 16
3-3 "Mini-cyclone" Apparatus Used for Dry Preparation of Bulk Dusts 17
3-4 "Puffer" Apparatus Used for Dry Preparation of Bulk Dusts 18
3-5 Photomicrographs and EDX Spectra of Mercury-Rich Particles Collected Downwind of Elemental Phosphorus Plant. Left: SE Image. Right: BSE Image 23, 24
3-6 Plot of Cluster Analysis "Stopping Rules" Calculated for a Simulated Data Set 26
3-7 Plot of Hierarchical Cluster Analysis Populations of Simulated Data Set 26
3-8 Plot of Revised Cluster Populations After Non-Hierarchical Cluster Analysis 27
3-9a Plot of Source Apportionment Results Using Least-Squares Spectrum Matching 29
3-9b Refined Source Apportionment Results Using Least-Squares Spectrum Matching 29

4-1a PGT Versus PSEM Volume Errors for Spherical Particle, as Function of Magnification 32
4-1b PGT Versus PSEM Volume Errors for Flat Particle, as Function of Magnification 32
4-2 PSEM Particle Size Distributions for Two Measurement Thresholds 34
4-3 LEO 440 Photomicrograph of Ultrafine Particle 35
4-4a FE-SEM Photomicrograph of Gold Particles 35
4-4b FE-SEM Photomicrograph of TiO_2 particles 35
4-5 Superimposed EDX Spectra for Polycarbonate Filter and Formvar 37
4-6 Photomicrograph of Submicron Diesel Soot Particle 37
4-7 Superimposed EDX spectra of Diesel Soot Particle and Blank Formvar 37
4-8 Top: EDX Spectrum of a 0.22-µm Aluminum Silicate Particle on Polycarbonate Substrate. Bottom: EDX Spectrum of a 0.24-µm Aluminum Silicate Particle on Formvar. 37
4-9 Precision of Repeated CCSEM Analyses 39, 40
4-10 CCSEM Particle Classification Results for Repeat Analyses at Different X-ray Collection Times. 44

5-1 Photomicrographs and Spectra for $PM_{2.5}$ Particles Collected in Phoenix Air Sample 49
5-2a Photomicrograph and Spectrum for Fine-Fraction Ambient Sample Collected Downwind of Elemental Phosphorus Plant 51
5-2b Photomicrograph and Spectrum for Coarse-Fraction Ambient Sample Collected Downwind of Phosphorus Plant 51
5-3 Photomicrograph and Spectrum of Fine-Fraction Ambient Sample Collected Downwind of Phosphorus Plant During PM10 Exceedance. 51
5-4 Top: Photomicrograph and Spectrum of Fine-Fraction Sample Collected Downwind of Phosphorus Plant. Bottom: Photomicrograph and Spectrum of Ground Flare Plume Sample. 52
5-5 Photomicrograph and Spectrum of Phos-Dock Source Sample... 52
5-6 Photomicrograph and Spectrum of Fly Ash Sphere from the Burden Level of the Furnace Building. 52
5-7 Comparison of Ambient, Coarse-Fraction Particle Classes at Residential Indoor Site, Residential Outdoor Site, and Community Site... 55
5-8 Comparison of Ambient, Fine-Fraction Particle Classes at Residential Indoor Site, Residential Outdoor Site, and Community Site... 56
5-9 Photomicrograph of Gold Particle in World Trade Center Dust Sample. 57
5-10 Photomicrographs of Particulate Matter in Bulk Sample Collected Near the WTC Site 58
5-11 Photomicrographs and Spectra of Individual Fibers in Bulk Sample Collected Near the WTC Site 59
5-12 Photomicrographs and Spectra of Individual Particles (<10 μm) in Bulk Sample Collected Near the WTC Site 60
5-13 Low-Magnification Image of VAPS Coarse-Fraction Filter Showing "Honeycomb" Particle Distribution 61

Appendix D: Photomicrographs and Spectra of Individual Particles in Ambient Air Samples Collected Near the WTC Site 80
Appendix E: Selections from the NERL SEM/EDX Source Particle Atlas 85

Tables

Number **Page**

4-1 LEO-PGT and PSEM Analysis of a 22-μg Lutetium Oxide Sample: Estimated Particle Mass Using Different Volume Formulas and Associated Errors 33
4-2 EDX Collection Time versus CCSEM Particle Composition (in weight percent concentration) . . . 43

Acronyms and Abbreviations

aed	aerodynamic diameter
AEM	analytical electron microscope
AFM	atomic force microscopy
ANN	artificial neural network
BSE	backscattered electron
CCSEM	computer-controlled SEM
CMB	chemical mass balance
CPC	condensation particle counter
DMPS	differential mobility particle sizer
EDX	energy-dispersive X-ray
EF	enrichment factor
ELPI	Electrical Low Pressure Impactor
FE	field emission
FE-SEM	field-emission SEM
FMC	FMC Corporation
HgP	particle-bound mercury
LaB_6	lanthanum hexaboride
MCE	mixed cellulose ester
MSEM	manual SEM
NAAQS	National Ambient Air Quality Standard
NERL	National Exposure Research Laboratory
NIST	National Institute for Science and Technology
PCB	particle class balance
PGT	Princeton Gamma-Tech
PM	particulate matter
PSEM	Personal SEM
ROI	Region of Interest, or X-ray “energy window”
RSD	relative standard deviation
SAED	selected-area electron diffraction
SE	secondary electron
SEM	scanning electron microscopy
SMPS	scanning mobility particle sizer
SOP	standard operating procedure
STEM	TEM operated in the scanning mode
TEM	transmission electron microscopy
WAM	Work Assignment Manager
WD	working distance in mm
WDX	wavelength-dispersive X-ray
XRF	X-ray fluorescence
Z	atomic number

Acknowledgments

The authors wish to thank Mr. Gary Casuccio and Mr. Steven Schlaegle of R.J. Lee Group, Inc., for many useful discussions and suggestions.

Chapter 1
Introduction

In July 1997, the U.S. EPA (U.S. EPA, 1997) promulgated a new National Ambient Air Quality Standard (NAAQS) for particulate matter (PM). The new standard is aimed at regulating ambient concentrations of PM_{10} and $PM_{2.5}$, particles with aerodynamic diameter (aed) <10 μm and $\leq$2.5 μm, respectively. The new NAAQS was developed in response to studies that showed a significant association between human morbidity and mortality and PM concentrations (Dockery et al., 1993; Dockery and Pope, 1994; Schwartz, 1994; Pope et al., 1995). Other studies indicate that transition metals may play a significant role in the health consequences of particle exposure (Ghio et al., 1992, Ghio et al., 1996). These studies coupled with the new NAAQS have generated increased interest in analytical techniques capable of measuring the size, morphology, and chemical composition of individual aerosol particles. These data are essential to the understanding of particle formation, transport and transformation, and deposition mechanisms as well as the impact of particles deposited in the respiratory system. Furthermore, chemical and physical characterization of individual particles can reveal source information that cannot be determined through bulk chemical characterization such as X-ray fluorescence (XRF). Individual particle analysis is thus a complement to bulk elemental analysis techniques as well as a potentially powerful tool in source apportionment research.

The National Exposure Research Laboratory (NERL) of the U.S. EPA has been developing and evaluating the use of scanning electron microscopy (SEM) to characterize coarse and fine ambient and source-derived particles. Modern SEMs exhibit a large depth-of-field and spatial resolution on the order of 30 Å or less. Typically, particles as small as 0.05 μm can be imaged by SEM, providing information on the physical properties of particles including size, shape, and surface morphology. SEMs equipped with energy-dispersive (EDX) or wavelength-dispersive (WDX) X-ray spectrometers are, in addition, able to provide information on the chemistry of individual particles: elemental associations within individual particles can be revealed, and particle chemistry as a function of particle size can be determined. The importance of individual particle analysis as a complement to bulk analysis has been highlighted in many studies.

The advent of computer-controlled SEM (CCSEM) in the past two decades has enabled automated physical and chemical characterization of filter-based aerosol samples at throughputs that can approach 1000 particles per hour, making it possible to examine a statistically significant sample of particles in a reasonable time (Johnson et al., 1981; Casuccio et al., 1983a; Bernard et al., 1986; Anderson et al., 1988; Saucy et al., 1987; Germani, 1991; Van Borm et al., 1989). Whereas bulk analytical techniques such as XRF yield quantitative elemental concentrations averaged over the entire filter, CCSEM typically provides qualitative composition data on individual particles comprising the aerosol sample. Elemental composition data combined with physical properties of the particle provide the basis for classifying individual particles into different classes, using user-defined classification rules or statistical methods, which can often be related to known emission sources. To the extent that particle morphology and chemistry can be used to define distinct particle types, CCSEM can quantitatively characterize the composition of a sample in terms of the number percent (or mass percent, if sufficient information is available) represented by each particle type. Multivariate analysis of a large set of such ambient CCSEM classifications can provide information on source-receptor relationships.

The present document evolved over several years as a product of research carried out in support of the U.S. EPA/NERL SEM/EDX laboratory. It is intended to provide guidelines for researchers using SEM/EDX in both a manual and computer-controlled fashion for aerosol characterization and source apportionment. It is not intended to be a comprehensive manual for SEM analysis; a number of excellent, general-purpose textbooks are available for this purpose (e.g., Goldstein et al., 1992.) Neither is it intended to serve as a standard operating procedure (SOP) for the analysis of samples by SEM/EDX or CCSEM. Samples are submitted for SEM/EDX or CCSEM analysis in a wide variety of forms to support a wide variety of projects and research objectives. It is often necessary to develop customized

sample preparation and analysis procedures to meet the specific research objectives. Moreover, different research laboratories have different analytical and support equipment. For these reasons, it is not practical to develop a generic SOP for SEM/EDX or CCSEM that is applicable in all situations. While the procedures and applications described in this document often are specific to the instrumentation available in the NERL SEM/EDX laboratory, readers can hopefully adapt some of these recommendations to instrumentation available in their own laboratories.

Chapter 2 of this document provides an introduction to the SEM/EDX techniques, including basic concepts and hardware, and a description of the NERL SEM/EDX facilities. Chapter 3 presents recommended procedures for sample preparation and analysis. Chapter 4 presents research related to SEM/EDX data validity and quality assurance and quality control issues. In Chapter 5, examples of research applications are presented.

Chapter 2
Overview of SEM/EDX Techniques and Instrumentation

2.1 Overview of SEM/EDX

2.1.1 Overview of SEM

2.1.1.1 Image Formation

The SEM operates by scanning an energetic, finely focused electron beam over an individual feature or a field of features. This primary electron beam interacts with the specimen producing a variety of secondary signals that can be monitored with appropriate detectors. These signals can be collected in synchronization with the position of the scanned electron beam to generate high-resolution images providing detailed spatial and composition information. Figure 2-1 is a secondary electron photomicrograph of a fairly typical field of coarse-fraction particles (2.5 μm aed < particle diameter < 10 μm aed) from an urban air sample. The sample was collected in Baltimore on a 37-mm polycarbonate filter (0.4 μm pore size) over a 24-h period, using a Versatile Air Pollutant sampler (VAPS). Particle size is indicated by the scale bar in the lower left corner. The particles display a variety of sizes, morphologies, and compositions reflecting different sources. The large, fluffy particle in the upper left center is a soot agglomerate, perhaps from diesel combustion. Two bright, micrometer-sized, iron-rich spheres are observed: probable products of combustion from iron works or steel mills. The elliptical particle in the lower left of the field is carbonaceous and appears to be a pollen or spore. Most of the remaining particles are various crustal-related quartz, aluminum silicates, and calcium-rich particles representing resuspended dust. The small, submicrometer holes observed in the background are the pores of the polycarbonate filter.

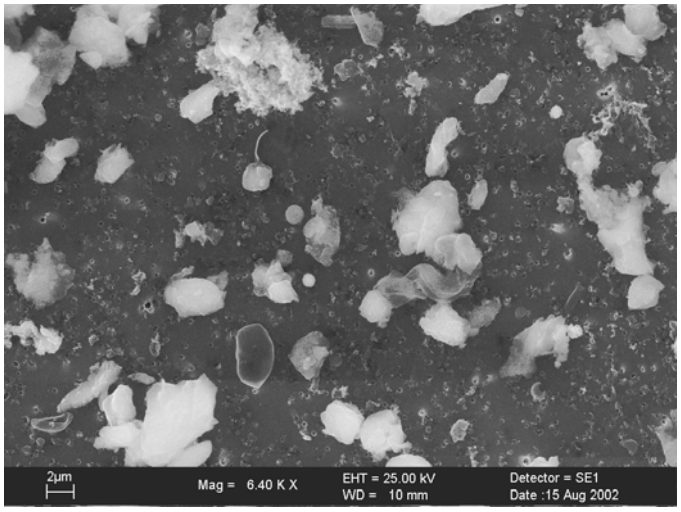

Figure 2-1. Photomicrograph of ambient, coarse-fraction air sample collected in Baltimore, MD.

When the primary beam interacts with the specimen, the electrons undergo two types of collisions: (1) elastic collisions in which the energy of the incident electrons is unchanged, and (2) inelastic collisions in which the primary electrons lose energy in a succession of collisions, leaving the electrons with lower energy. Elastic collisions give rise to the backscattered electron (BSE) signal, which forms the BSE image. Inelastic collisions give rise to the secondary electron (SE) signal, which forms the SE image. The SE and BSE images provide different but complementary information. Secondary electrons are emitted from the atoms occupying the top surface and produce a readily interpretable image of the surface. The contrast in the image is determined by the sample morphology. The SE image possesses three-dimensional perspective, high depth of field, and the appearance of overhead illumination. A high-resolution image can be obtained because of the small diameter of the primary electron beam. Backscattered electrons are primary beam electrons, which are "reflected" from atoms in the solid. The contrast in the BSE image is determined largely, though not exclusively, by the atomic number of the elements in the sample. The image can therefore show the distribution of different chemical phases in the sample. Because backscattered electrons are emitted from a depth in the sample, the resolution in the image is not as good as for secondary electrons.

Figure 2-2 illustrates the difference in information provided by the two types of images. The image on the left is the SE image and the image on the right is the BSE image of the same particle. The particle is from a sample of lead-rich house dust

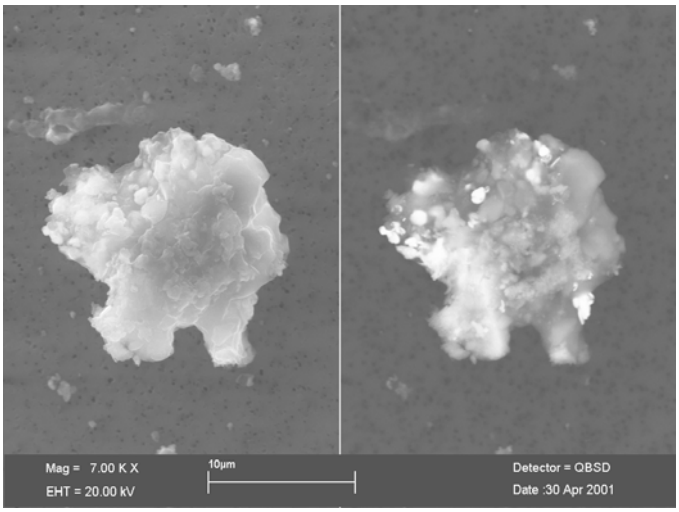

Figure 2-2. Photomicrograph of lead-rich house dust particle. Left image: secondary electron (SE) image. Right image: backscattered electron (BSE) image. Bright inclusions in BSE image are lead-rich. The bulk of the particle is aluminum-silicate. Outlying particles that nearly disappear in the BSE image are carbonaceous.

and has been collected on a polycarbonate filter. The SE image is superior for displaying surface detail and particle morphology but does not generally show chemical heterogeneity. Changes in brightness within the BSE image correspond to changes in effective atomic number: the small, very bright inclusions on the order of one micrometer are lead-rich particles. The host matrix (medium-gray areas) is an aluminum-silicate mineral. Areas that are intermediate in brightness, such as the bottom left quadrant of the particle, have a higher Si/Al ratio. (Although differences in particle thickness can also account for brightness variations in the BSE image, the higher Si/Al ratio was confirmed by EDX analysis). Some smaller, neighboring particles that appear in the SE image have approximately the same brightness level as the polycarbonate substrate and hence are nearly invisible in the BSE image. These particles are mostly carbonaceous.

2.1.1.2 Electron Beam Production

Primary electron beams for electron microscopy can be generated using different emission sources: the tungsten hairpin gun, the lanthanum hexaboride (LaB_6) gun, and the field-emission (FE) electron gun—in order of increasing brightness, cost, and complexity. Perhaps the most important measure of electron gun performance is gun brightness. Brightness is defined as the electron current density per solid angle of the electron beam. The microscopist can optimize the primary beam energy and/or the beam spot size (beam current) depending on the analytical objectives: highest resolution images are obtained with the smallest possible probe diameter (diameter of the electron beam at the particle surface), while maximum image brightness and efficient X-ray microanalysis is obtained with the largest possible probe current. The brighter the electron gun, the better these competing requirements can be satisfied. Other performance factors important in comparing electron guns are lifetime and stability. Compared to tungsten, LaB_6 offers longer life and higher current density. Not only does LaB_6 provide a factor of 10 increase in brightness over tungsten, it also has a smaller effective source size, hence smaller spot size. Disadvantages of LaB_6 are its long warm-up time (about 15 min) and its extreme chemical reactivity when hot. In practical terms, this means that the vacuum in the gun chamber must be approximately two orders of magnitude better than the pressure required to operate tungsten. Typically, the required low pressures are achieved by adding a dedicated ion pump in the gun chamber.

The improved image quality and image resolution obtained with the LaB_6 gun compared to the tungsten hairpin gun is shown in Figures 2-3a and 2-3b. These figures show images of the same particle field acquired with tungsten (Figure 2-3a) and LaB_6 (Figure 2-3b). Probe diameter was adjusted for each gun

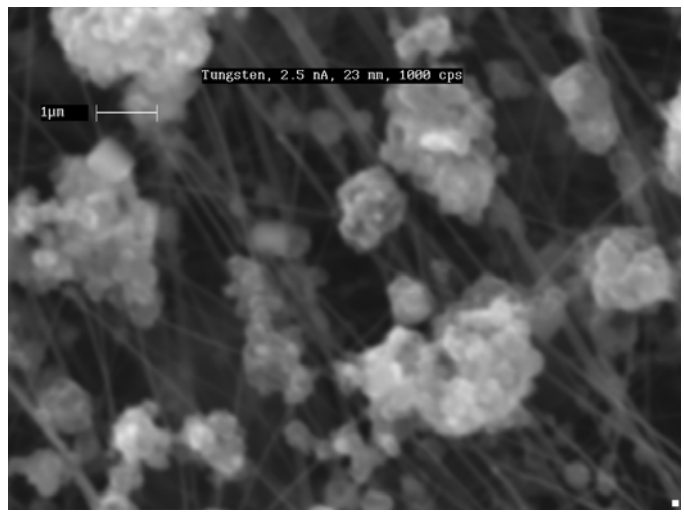

Figure 2-3a. Photomicrograph acquired with tungsten filament. The probe current was 2.5 nA, which yielded an EDX count rate of 1000 cps.

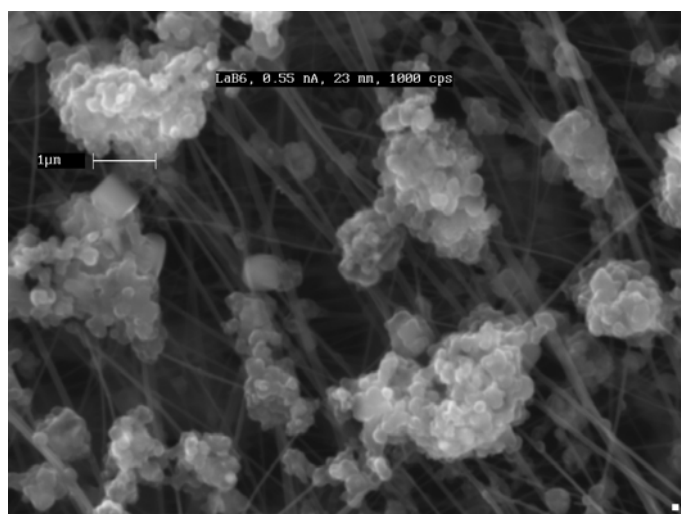

Figure 2-3b. Photomicrograph (identical field) acquired with LaB_6 filament at 0.55 nA probe current and 1000 cps.

to yield the same X-ray count rate of 1000 cps, which approximates a typical EDX analysis count rate. The LaB_6 gun, operating at a probe current of 0.55 nA, shows improved resolution due to the smaller probe diameter compared to the tungsten image acquired at 2.5 nA. Moreover, if X-ray microanalysis were the primary interest, the LaB_6 probe diameter could be increased to match the image resolution of the tungsten gun, with a sizable increase in X-ray count rate and decreased X-ray analysis time. LaB_6 crystals are more expensive to replace than tungsten filaments, but the lifetime of the LaB_6 crystal is approximately 10 times that of tungsten.

Conventional tungsten and LaB_6 filaments are thermionic sources in that the electrons are liberated from the filament by heating the filament. In FE sources, the electrons are drawn from a finely pointed filament tip (usually a tungsten crystal) by means of an electric field. FE is 10–100x brighter than LaB_6 and ~1000x brighter than tungsten. In addition, FE sources exhibit a much greater depth of field than thermionic sources (tungsten and LaB_6). On the negative side, FE sources must be operated at high vacuum (~10^{-9} torr) to stabilize electron emission and to avoid contamination of the FE tip.

2.1.1.3 Probe Size and Beam Current

Source brightness increases approximately proportionally to the beam energy. Thus the probe size and beam current are intimately related and are a function of beam energy in addition to gun type. For high-resolution imaging it is desirable to maintain a probe diameter of 10 nm or less. At 30-keV beam energy, a 10-nm spot size corresponds to a beam current of ~0.01nA for tungsten and ~0.2 nA for LaB_6 (Goldstein et al., 1992). Note that X-ray microanalysis typically requires about 0.1 nA of current. Thus, with tungsten it is difficult to carry out efficient X-ray microanalysis simultaneous with high-resolution imaging.

2.1.1.4 Accelerating Voltage

The energy of the primary electron beam is typically adjustable over a range from approximately 1 keV to 20 or 30 keV. This enables the user to optimize the instrument for image quality objectives or for X-ray microanalysis. The highest feature resolution, in theory, is provided by the most energetic electron beam (higher energy = shorter wavelength = better resolution). However, higher energy also means that the SE electrons that form the particle image are generated over a much larger volume of the specimen due to the deeper penetration of the electron beam. Lowering the beam energy shifts the production of detected secondary electrons toward the surface of the particle, with a consequent enhancement of surface detail in the SE image. The effect of primary beam energy on the image of a pollen grain is shown in Figures 2-4a, b, and c acquired at 30, 10, and 5 keV, respectively. The difference in resolution among the three images is subtle, but the images acquired at 5 and 10 keV are clearly superior to the 30-keV image in terms of surface detail.

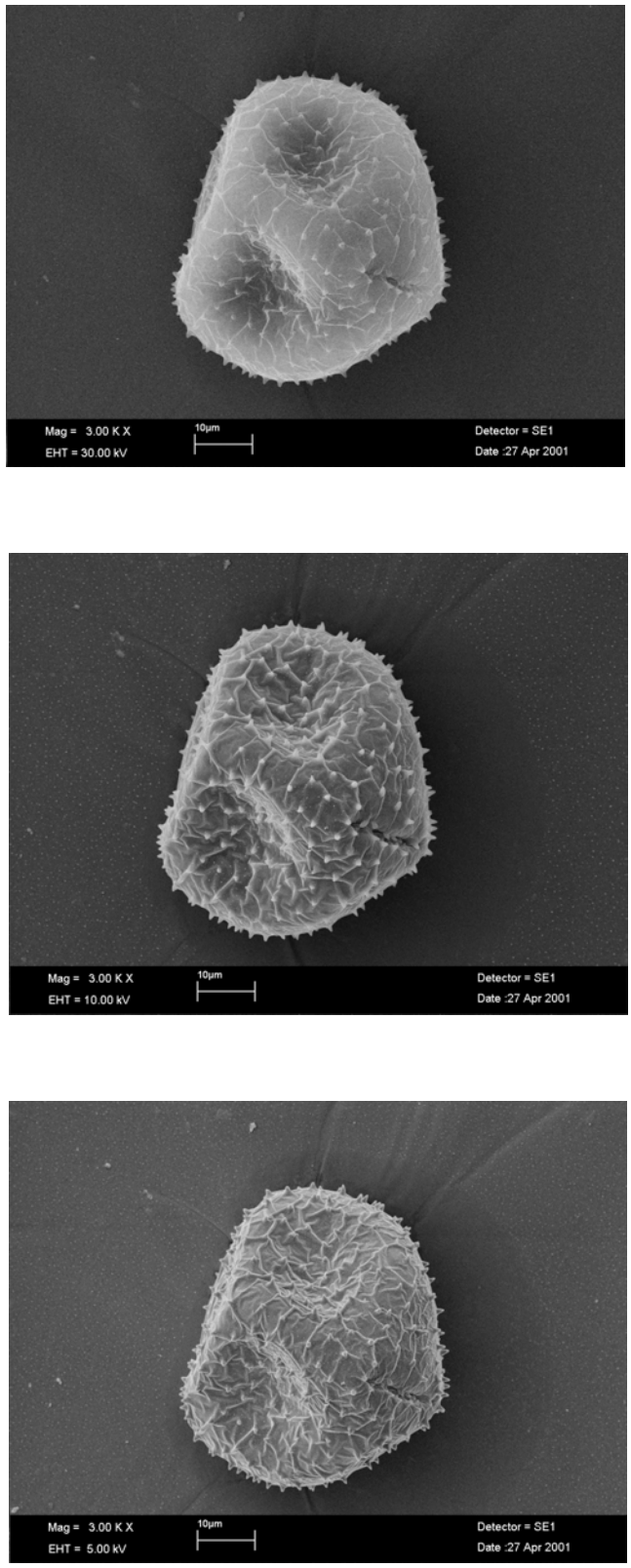

Figure 2-4. Pollen grain imaged with the LEO S440 at different accelerating voltages. Top: 30 kV. Middle: 10 kV. Bottom: 5 kV.

2.1.1.5 Guidelines for Imaging

The following steps are recommended for obtaining the best images and are summarized from Goldstein et al. (1992), which has an excellent chapter on image formation and interpretation.

- **Choose the accelerating voltage appropriate for your objectives:** high keV for best image resolution, low keV to enhance surface detail.
- **Optimize working distance (WD).** WD is the distance between the sample surface and the lower surface of the pole piece. Generally the best image resolution is obtained at the shortest working distances. Typical imaging WDs are on the order of 10 mm. However, for many instruments, the *analytical* WD (the optimum working distance for EDX analysis) is often larger than the optimal imaging WD due to EDX detector/sample geometry. The two SEMs in the NERL SEM laboratory, for example, have analytical WDs of about 17 mm (Personal SEM) and 24 mm (LEO S440). This is a significant inconvenience requiring the user to successively raise the stage for the best particle image, then lower the stage for the EDX analysis. If automated analyses are being conducted in which both images and X-ray spectra are collected, the working distance typically must be set to the analytical WD, with some corresponding loss of image quality.
- **Optimize final aperture size D_{ap}.** The depth of focus for a given magnification is roughly proportional to WD/D_{ap}, where D_{ap} is the diameter of the final aperture. If depth of field is of primary importance in the image, then increase the WD and/or decrease aperture size, if that is an option. (Some SEMs have a single, fixed-diameter final aperture.)
- **Optimize probe size.** Electron scattering within the sample (determined by the accelerating voltage and the effective atomic number of the sample) causes the effective signal-producing area on the specimen to be significantly larger than the physical spot size of the incident probe, especially for BSE signals, which comprise more energetic electrons. Reducing probe current generally yields improved image resolution, until at some point, image quality suffers due to decreasing brightness and contrast. For low-magnification work (<5000x), a larger probe diameter (current) will probably work better than a finely focused, high-resolution probe. Typically one needs a minimum of approximately 0.01 nA of beam current for imaging.
- **Minimize specimen charging.** Specimen charging occurs when one or more areas of the specimen cannot dissipate the incident electronic charge which arrives at the surface via the incident or scattered electron beam. Charging is largely a function of the local surface conductivity of the specimen as well as the primary beam energy and probe current. Charging causes a variety of undesirable effects in electron micrographs, including abrupt brightness changes within the image, image shift/image distortion, and particle displacement (the buildup of electrostatic forces can actually cause charging particles to move or completely leave the sample substrate). The conductivity of insulating or nonconductive PM specimens has traditionally been made acceptable by overcoating the sample with approximately 100–200 Å of conductive carbon or metal. This is accomplished in the NERL laboratory using a vacuum coater. If a coated specimen still exhibits charging problems, the user can minimize charging by a combination of (1) reducing the primary beam energy, (2) reducing the probe current, and (3) acquiring images in the frame-averaging mode rather than the line-averaging mode (if this option is available on the SEM). Reducing beam energy and/or probe current, however, is likely to conflict with the needs for EDX analysis. Alternatively, "environmental" or "variable pressure" SEMs, which allow operation at high pressure (in the range of 0.1–1 kPa), effectively eliminate specimen charging (hence also the need to coat samples) even for insulating samples.

The following tips are suggested for optimizing BSE images:

- **Long WD yields best contrast but least topographic detail.** Medium and short WD gives best BSE signal, topographic detail and good contrast.
- **Beam energy must be high enough for good Z contrast.** Higher Z elements require higher keVs. At lower keVs atomic number discrimination is reduced and at really low keVs one can get reversal of contrast of high Z elements.
- **Signal level is very important.** One cannot get good Z contrast if the BSE signal is too low! Lower signal equals a reduction in contrast.
- **BSE amplifier gain also plays a role in contrast and noise in the final image.**

A final word on the importance of placing a reference scale bar in the image. Image magnification is defined as the linear dimension of the scan on the output device (monitor or printer device) divided by the linear dimension of the scan on the sample. Magnification is thus a hardware-dependent parameter. The same feature image acquired at the same nominal magnification but with different output devices (polaroid film, thermal printer, computer monitor, etc.), may have very different sizes so that magnification does not immediately convey the size of the features in the image. Rather than magnification, it is generally recommended that a scale bar (micrometer marker) be included in each image to calibrate feature size.

2.1.2 Overview of EDX

Interaction of the primary electron beam with atoms in the sample causes inner electron shell transitions, which result in the emission of X-rays. Two types of X-rays are generated: (1) Bremsstrahlung or continuous X-rays, which generate a broad and slowly-varying background over the entire X-ray spectrum, and (2) characteristic X-rays, which are narrow, discrete peaks in the spectrum whose energies are characteristic of specific elements present in the sample. A fraction of the X-rays emitted by the specimen are collected and analyzed by means of an EDX and/or WDX analyzer. EDX provides a far more rapid analysis and is therefore much better suited for CCSEM; WDX is generally more sensitive and accurate, especially for the lighter elements. Our discussion will focus on EDX analysis since this is the approach used in the NERL laboratory and by the great majority of CCSEM users. Detection and measurement of the characteristic X-ray energies yields an analysis of the elements present in the feature. EDX spectroscopy can provide rapid, qualitative analysis, or, with adequate standards, quantitative analysis of elemental composition with a sampling depth of 1–2 µm. X-rays can be collected in synchronization with the image-forming electron beam to form two-dimensional maps or one-dimensional line profiles showing the distribution of elements in a sample surface. For an excellent discussion of X-ray analysis, the reader is referred to the text by Goldstein et al. (1992).

Figure 2-5 shows a representative EDX spectrum. The spectrum is that of an Fe-rich aluminum silicate particle from a Phoenix air sample. The spectrum was collected for 200 s at a primary beam energy = 20 keV, probe current = 100 pA, WD = 23 mm, and X-ray count rate = 1000 cps. Note the discrete characteristic X-ray peaks superimposed on the Bremsstrahlung background which varies slowly with X-ray energy.

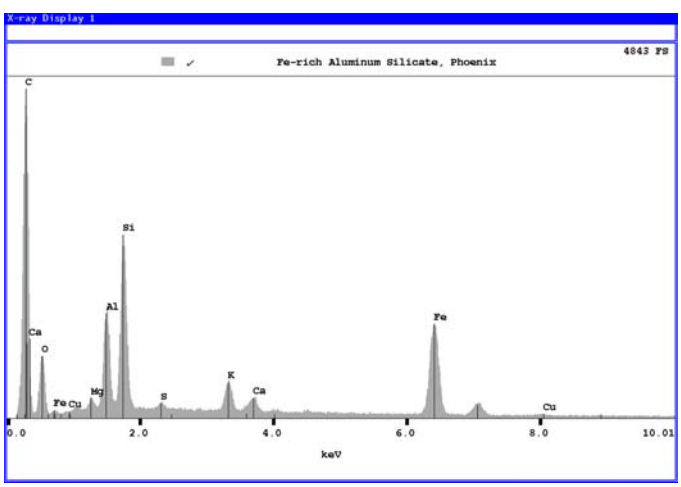

Figure 2-5. EDX spectrum of an iron-rich aluminum silicate particle from a Phoenix air sample. Spectrum was collected for 200 s at a beam energy of 20 keV, probe current of 100 pA, count rate approximately 1000 cps, and working distance of 23 mm.

EDX detectors can be supplied with no window, a thin window, or a thick window depending on the requirements of the user. Thick window detectors have poor or zero transmission of low-energy X-rays and are typically insensitive to elements lighter than Na. Thin window detectors (which are perhaps most commonly used in the general area of environmental analysis) and windowless detectors provide limited detection of elements below Na and poor or no detection of elements below beryllium or boron.

EDX detectors are characterized by their energy resolution. Typical detector resolutions are 130–150 eV at 5.9 keV (Mn K_α line). This resolution is much too broad for inferring chemical states (e.g., elemental sulfur vs. sulfate vs. sulfite), but is generally adequate to separate characteristic X-ray lines from neighboring elements. Nevertheless, interference between peaks of different X-ray line families is a potentially serious problem for EDX. This issue is discussed in more detail in Section 2.1.2.4.

The EDX detection limit for elements Na to U in bulk materials and in individual particles larger than about 2 µm is on the order of 0.1 wt % (Buseck and Bradley, 1982). In a 1-µm particle, the detection limit increases to about 0.5 wt %. These are only rough rules of thumb since the detection limit will also depend on the X-ray collection time, which typically varies from 3 to 100 s. One needs to distinguish these EDX detection limits from the ability of SEM to detect rare or exotic particles. Dedicated computer-controlled SEM/EDX searches, for example, can detect and provide semi-quantitative mass concentration estimates for exotic species, typically heavy metals such as Pb or Hg, which are present in the bulk sample at sub-ppm concentrations but which are present in a few isolated particles at high wt % concentration. An example of this capability is presented in Section 3.3.5. The ability to conduct "needle-in-the-haystack" analyses potentially makes computer-controlled SEM/EDX an extremely sensitive technique and a powerful complement to bulk analytical methods. In general, however, if a species has a bulk mass concentration <0.1 wt %, and is distributed homogeneously among all particles, it will probably not be detected by EDX.

EDX analysis can be performed at two levels of sophistication: quantitative EDX or qualitative EDX. Under optimal conditions (appropriate samples, relevant standards, controlled experimental setup, and sophisticated data-reduction procedures), EDX can yield elemental compositions of flat, polished specimens with accuracies and precisions approaching 1%. Quantitative analysis of individual particles, however, turns out to be much more complicated than analyzing flat, polished specimens. Armstrong and Buseck (1975) and Buseck and Bradley (1982) discuss the difficulties inherent in quantitative EDX analysis of individual particles. These difficulties largely result from the need to correct X-ray yields from particles with irregular surfaces and thicknesses less than the incident electron range. For particles larger than a few micrometers, geometry-dependent absorption effects become severe, while for smaller particles, corrections for atomic number and thickness effects

become critical. Using a correction procedure that accounts for differences in atomic number, depth distribution of generated X-rays, and absorption characteristics between the sample and a standard, Armstrong and Buseck (1975) and Grasserbauer (1977) claim that errors can be reduced to 2–5% (relative) for silicate particles > 0.5 µm in diameter. In addition to requiring a suitable standard, their correction procedure requires an estimate of particle thickness, which would seem to necessitate time-intensive manual analysis. While this approach appears feasible for manual EDX analysis of a few selected particles, to our knowledge, quantitative EDX analysis of individual particles is presently not a reality in automated SEM/EDX analysis.

For the remainder of this document, we will understand EDX analysis to mean qualitative analysis since this is the approach used in most research efforts that employ SEM/EDX for source apportionment. Thus, the same QA/QC considerations that relate to precision and accuracy of quantitative techniques such as XRF cannot be applied to SEM/EDX analysis. To the extent that particle morphology and elemental chemistry can be used to define distinct particle types, then the SEM/EDX technique can quantitatively characterize a sample in terms of number percent by particle type or chemical class. However, with respect to particle sizing or particle mass, SEM analysis provides only semi-quantitative results since the technique uses two-dimensional information to infer a three-dimensional quantity (size or volume).

2.1.2.1 Effective X-ray Volume

Proper interpretation of microanalysis results requires that users be constantly aware of the difference between image resolution and X-ray spatial resolution. Secondary electrons that form the SE image typically come from only a very thin surface layer of less than approximately 0.01 µm in depth. (Secondary electrons generated at deeper depths within a particle do not have sufficient energy to escape the particle and hence do not contribute to the SE image.) Higher energy backscattered electrons can escape from much greater depths than secondary electrons, explaining the relatively poorer surface resolution of BSE images. The effective volume for X-ray production can be still greater because X-rays penetrate matter far more readily than electrons. The user must understand that the SE or BSE image of a particle and its accompanying X-ray spectrum are generated from largely different volumes of the particle. Features seen in the image may, in fact, have little correspondence to the X-ray spectra collected simultaneously with the image. Because electrons scatter as the primary beam penetrates the target, the effective interaction volume is considerably greater than the simple product of the incident probe area and the range of a 20-keV electron. The effective interaction volume depends strongly on both the primary beam energy and the atomic number of the specimen. High beam energies and low-Z targets result in large interaction volumes, while low beam energies and high-Z targets result in small interaction volumes. It is important to note that despite the fact that the incident probe diameter is well under 1 µm in diameter, the interaction volume in a low-density, low-atomic-number target has dimensions of cubic micrometers. Anderson and Hasler (1966) developed the following expression for the X-ray range:

$$R = 0.064(E_0^{1.68} - E_c^{1.68})/\rho$$

where R = X-ray range or X-ray spatial resolution (µm)
E_0 = accelerating voltage (keV)
E_c = critical absorption energy (keV)
ρ = mean sample density (g/cc)

Note that in the above formulation, changing the probe size has *no* effect on X-ray spatial resolution. The effective X-ray range is determined by the beam energy and the sample density.

The effective range of 20-keV electrons (equivalent to the radius of a circle centered on the target surface at the beam's impact point whose circumference defines the envelope of the interaction volume) is approximately 5.3, 4.2, 1.5, and 0.9 µm in C, Al, Cu, and Au, respectively (equivalent semi-spherical volumes ranging from 312 μm^3 to 1.5 μm^3). The lower size limit for qualitative X-ray analysis of a particle is ultimately determined by signal statistics, signal to noise, and particle composition, but is on the order of 0.2 µm for tungsten and LaB_6 guns [Field emission SEMs (FE-SEMs) are capable of reaching considerably lower size limits - see Section 4.4.2]. This limit is illustrated in Figure 2-6 which shows EDX spectra acquired on aluminum silicate particles of different sizes collected on a polycarbonate filter. The instrument parameters included an electron energy of 20 keV, probe current of 200 pA, and

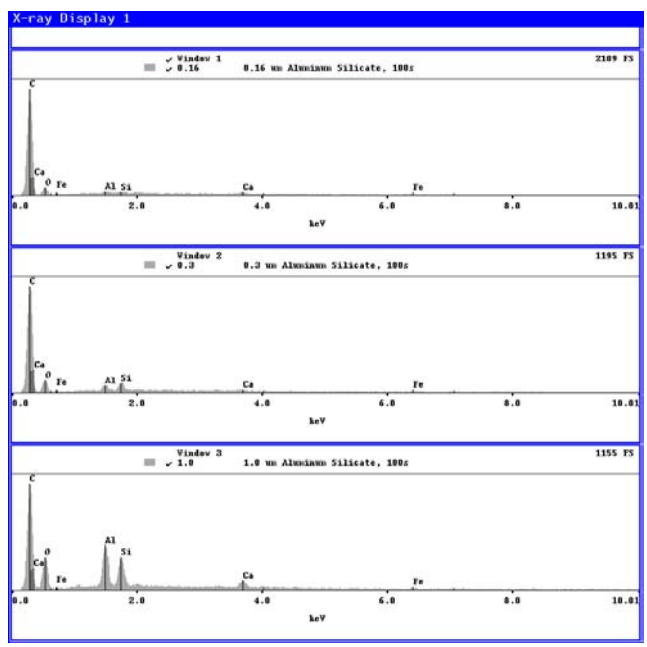

Figure 2-6. EDX spectra acquired on 0.16 μm (top), 0.30 μm (middle), and 1.0 μm (bottom) aluminum silicate particles on a polycarbonate support. The signal (Al + Si peaks) to background (C peak) ratio improves with increasing particle size.

counting time of 100 s. For a 0.16-μm diameter particle (top spectrum), the Al and Si signals are barely above the noise level and are swamped by the carbon signal generated by the polycarbonate filter substrate. Even with the 1.0-μm particle (bottom spectrum), the polycarbonate substrate contributes almost half of the total X-ray counts.

2.1.2.2 Choice of Primary Beam Energy

The choice of primary beam energy for X-ray microanalysis represents a compromise between the need to efficiently excite characteristic X-ray production from the specimen and the desire to minimize specimen self-absorption of the X-rays. The latter occurs because X-rays produced deep within a particle may be absorbed within the particle before they can escape the particle to be detected. The higher the primary energy, the greater the penetration of the primary beam, and the greater the self-absorption losses—especially for low-energy X-rays generated by low-Z elements. A general rule of thumb is that characteristic X-ray production is maximized for primary beam energy roughly 1.7 times the energy of the X-ray line being excited. This is called the *overvoltage factor*. X-ray microanalysis is typically carried out at 15–20 keV, which represents a compromise between the need for adequate overvoltage to efficiently excite most elements of interest and the desire to minimize particle self-absorption losses. With a beam energy of 15 keV or more, all possible X-ray lines of an element in the range of 0.1–10 keV will be efficiently excited (i.e., elements from Be to Ge, plus heavier element L and M X-ray lines.). Still, in larger particles, self-absorption losses of light elements will be significant at primary beam energies of 20 keV. If low-Z elements are especially important, the microscopist may want to work at a reduced beam energy such as 5–10 keV to enhance sensitivity to the low-Z elements while at the same time shifting the analysis towards surface analysis and away from bulk analysis.

2.1.2.3 Choice of Spot Size or Probe Current

Probe current determines the X-ray count rate, which in turn determines analysis time and sample throughput. Typical probe currents vary greatly depending on the brightness of the gun. More useful parameters are the counting times (3–100 s) and typical count rates (1000–3000 s^{-1}). These count rates can be achieved with the PSEM (Section 2.2.2) using a spot size of about 30% (corresponding to roughly 200 nm). Increasing the count rate significantly above a few thousand s^{-1} can result in high detector dead time and degraded detector resolution, and introduce artifacts in the spectrum such as sum peaks. It is generally recommended to keep detector dead time below 30%. The typical probe current for the LEO S440 SEM (Section 2.2.1) using a lanthanum hexaborate (LaB_6) gun is 100 pA yielding a count rate of approximately 1000 s^{-1}, and corresponding to a probe diameter of about 10 nm. There is a tradeoff between image quality, analysis time, and spot size: the best imaging is obtained with a small spot size. However, for best backscatter imaging and X-ray acquisition, a large spot size is needed. To perform automated analysis with reasonable speed, imaging quality must be sacrificed in favor of less noisy BSE images and higher EDX count rate: when no microimages are to be collected, a very large spot size is acceptable. Microimages of submicrometer particles, however may dictate that spot size, and therefore analysis speed be reduced in order to improve image quality. Note also that measurements of particle size, especially for submicrometer particles, is improved when spot size is reduced.

2.1.2.4 Spectral Artifacts and X-ray Line Overlaps

Users must be on guard against misidentified peaks in the EDX spectrum. Even with commercial EDX software, X-ray peaks can be misidentified due to spectrum artifacts (sum peaks and escape peaks which are most prominently associated with high-intensity peaks) and interelement interferences. In general, it is very difficult to unravel two peaks separated by less than 50 eV. Two types of interferences can be distinguished. For the first series of transition metals, the K_β line of an element overlaps with the K_α line of the next element in the series (K through Zn). Second, the heavy metals have *L*- and *M*-family X-ray lines in the 1–5 keV range that can interfere with the *K*-family lines of Na to Ca. Some classic interferences relevant for PM research include the difficult overlap between the Pb M_α (2.34 keV), S K_α (2.31 keV), and Mo L_α (2.293 keV) lines. The lead L_α line (10.549 keV) overlaps the As K_α line (10.532 keV). Zn L_α (1.009 keV) interferes with Na K_α (1.041 keV); Ba L_α (4.467 keV) interferes with Ti K_α (4.508 keV); and Br L_α (1.480 keV) interferes with Al K_α (1.487 keV).

Different EDX systems may employ different methods for handling X-ray line interferences. In most cases, spectral peak overlaps can be dealt with successfully by a combination of user experience, peak deconvolution software provided with the EDX system, and/or longer X-ray counting times. Improved counting statistics in the EDX spectrum can significantly improve the accuracy of peak deconvolution software, especially software that fits the spectrum using stored libraries of X-ray lines for each element. In cases where the *M*- or *L*-lines of a heavy metal overlap with the *K*-lines of a lighter element (e.g., Pb M_α and S K_α), the particle's brightness in the BSE image can often provide definitive confirmation that the heavier element is present. Finally, off-line data review software allows the analyst to review EDX spectra and to correct misidentified peaks. On rare occasions, peak overlaps in the EDX spectrum cannot be resolved and the user must resort to WDX.

Goldstein offers specific "bookkeeping" suggestions to facilitate accurate qualitative EDX analysis: Identify peaks as you work backwards from the high-energy end of the EDX spectrum to the low-energy end; begin with the lines of highest intensity and mark off all lines associated with an identified element before proceeding, including sum and escape peaks; low-energy *L* or *M* lines should be accompanied by *K* or *L* lines, which should aid in identification; proceed with identification of low-intensity lines associated with minor or trace elements.

2.1.2.5 Guidelines for Qualitative EDX Analysis

The following is a brief summary of guidelines for qualitative EDX analysis. For greater detail, the reader is referred to Goldstein et al. (1992). For accurate peak identification, the EDX spectrometer should be calibrated periodically to ensure that the spectral peak positions are within ± 10 eV of the tabulated values. [*Note:* a piece of Cu attached to any sample holder provides a simple energy calibration check for two lines (the K_β line at 8.907 keV and the L_α line at 0.928 keV) which span most of the typical EDX spectral range]. A beam energy of 20 keV is generally considered a good compromise between adequate overvoltage and minimum X-ray absorption. However, at these energies there is still a potential for absorption of X-rays below 2 keV (P and lighter elements). X-ray acquisition time should be adequate to meet the 3σ criteria for statistical significance, i.e., the minimum peak area *P*, after background subtraction, should be three times the standard deviation of the background at the peak position.

2.1.3 Overview of CCSEM

Traditionally, SEM analyses have been conducted manually. However, manual SEM (MSEM) is very time- and labor-intensive and therefore limited in terms of particle throughput. Furthermore, because microscopy is by nature a subjective technique, the results of MSEM are unavoidably operator-dependent to some degree. Advances in digital SEM technology have spurred the development of CCSEM. Developed in the mid-1970s and early 1980s (Lee et al., 1979; Hanna et al., 1980; Kelly et al., 1980; Lee and Kelly, 1980; Johnson et al., 1981; Casuccio et al., 1983a), CCSEM combines an SEM, an EDX analyzer, and a digital scan generator under computer control. CCSEM can determine particle size, shape parameters (e.g., aspect ratio, perimeter), and major elemental content of particles larger than approximately 0.2 μm (depending on particle chemistry and other factors). Once the user has set up the sample for analysis and initialized instrument parameters, the SEM automatically locates features in the size range of interest; determines the size, shape, and major elemental content of individual particles; acquires images of fields and individual particles; and stores all this information electronically for later review and interpretation.

User-defined classification rules or statistical methods such as cluster analysis, artificial neural networks or multivariate analysis can subsequently be employed to sort particles into distinct particle classes based on size, shape, and chemistry. The size and chemistry for individual particles can be used (with varying degrees of success—see Section 4.3) to estimate particle mass, which can be summed, and scaled in order to estimate bulk properties of the sample. However, the great strength of CCSEM is the sheer quantity of information that can be obtained from the analysis of hundreds or thousands of individual particles. With current technology, the throughput of CCSEM can approach 1000 particles per hour on appropriately prepared samples, a dramatic increase in throughput over conventional manual SEM analysis. CCSEM is capable of collecting statistically meaningful data sets from a large number of particles in a timely and cost-effective manner. This breakthrough in particle throughput opens up the possibility of using CCSEM in data-intensive studies such as source apportionment studies.

Numerous applications of CCSEM to environmental studies, aerosol characterization, and source apportionment are reported in the literature. Interested readers are referred to papers by Johnson and Twist (1982), Casuccio et al. (1983b, 1988), Anderson et al. (1988, 1992), Kim and Hopke (1988a,b), Dzubay and Mamane (1989), Mamane (1990), Mamane et al. (1995), Saucy et al. (1991), Vander Wood and Brown (1992), Xhoffer et al. (1992), Katrinak et al. (1995), Johnson and Hunt (1995), and Jambers and Van Grieken (1997).

Despite substantial use of CCSEM, the quality and accuracy of CCSEM data have received limited attention. Some data quality studies have been conducted and are discussed in Section 4.6. Johnson et al. (1981) described a methodology to determine a sample's bulk elemental composition from individual particle data. Potential sources of error associated with CCSEM were discussed, including particle volume and density calculations, assumptions about particle stoichiometry, and particle classification. Watt (1990) discusses some of the difficulties and analytical pitfalls of CCSEM, including misidentification of particles (especially organic particles or particles with low X-ray count rate) arising from the use of "normalized" X-ray data, and analysis of aggregate particles. Germani (1991) evaluated the effects of critical instrumental parameters on the time and accuracy of automated gunshot residue (GSR) analysis (see Section 4.6). GSR analysis is similar in many ways to CCSEM analysis of aerosol samples. Mamane et al. (2001) examined a number of issues affecting the quality and validity of CCSEM data: Stable operation of the SEM instrument during a multi-hour CCSEM analysis of a sample is obviously an essential requirement. Sampling error is a concern for both manual SEM and CCSEM since only a very small fraction (typically less than 0.1%) of the particles on an ambient filter is typically analyzed. A sufficient number of particles must be analyzed to obtain a representative sample (Section 4.6.2). Finally, automated particle recognition algorithms lack the sophistication of the trained human eye; errors can be made by CCSEM that are typically avoided by an experienced operator performing manual analysis (see Section 4.6.3). Such errors may include incorrect sizing of complex particles; incorrect X-ray analysis, especially of aggregate particles or organic and carbonaceous particles, which leads to particle misclassification; missed particles (e.g., due to poor contrast); and analysis of nonexistent features (contrast artifacts).

2.2 Description of NERL Facilities

The NERL SEM/EDX laboratory houses two digital automated SEM/EDX systems: (1) the Personal SEM (PSEM) manufactured by Aspex Instruments (Delmont, PA, formerly R.J. Lee Instruments, Ltd.), and (2) a LEO S440 SEM (LEO Electron Microscopy, Inc., Thornwood, NY, formerly Leica) integrated

with a Princeton Gamma-Tech (PGT) IMIX EDX system (Princeton Gamma-Tech Inc., Rocky Hill, NJ). In addition to these two SEM systems, the laboratory is equipped with supporting equipment. These facilities are described separately below.

2.2.1 LEO/PGT System

The LEO/PGT system comprises a LEO S440 SEM integrated with a PGT IMIX EDX system (Figure 2-7). The LEO S440 is a digital SEM equipped with secondary and backscatter electron detectors. The S440 operates with either a lanthanum hexaborate (LaB_6) electron gun or a tungsten gun. The IMIX system employs a thin-window, large-area (50 mm^2) EDX detector with digital pulse processing. This enables X-ray detection of carbon and heavier elements. The S440 is equipped with a computer-controlled, eucentric sample stage, and the IMIX EDX system includes software for automated feature analysis (CCSEM). An example data output is shown in Appendix A. Both the LEO/PGT and PSEM systems are capable of routinely characterizing particles down to approximately 0.2 μm. The S440, however, provides better imaging resolution (nominally 4.5 nm at 30 kV) and is the instrument of choice for generating highest quality photomicrographs.

Figure 2-7. The LEO S440 SEM with PGT IMIX EDX system.

2.2.2 Aspex Personal SEM System

Like the LEO S440 SEM, the Personal SEM (PSEM) (Figure 2-8) is a digital SEM/EDX system capable of automated SEM/EDX analyses. An example data output is shown in Appendix A. The two SEM systems are distinguished primarily by imaging resolution, on-line and off-line software, and the PSEM's variable pressure option. The PSEM uses a tungsten gun exclusively. The X-ray detector employs a thin window similar to the PGT detector.

Figure 2-8. The Personal SEM (PSEM) system.

The PSEM is generally the instrument of choice for routine work and for automated SEM/EDX analyses when image resolution is not critical. Much of the enhanced speed and ease of use of the PSEM is due to the fact that it is a fully integrated system with both SEM and EDX operations controlled by a single PC using one keyboard and one mouse. In contrast, the LEO/PGT system requires two computers using different platforms (PC and UNIX), two keyboards, and two mice. The serial-line communication between the two computers significantly slows CCSEM analyses compared to CCSEM analyses performed on the PSEM. Additionally, the PSEM software for automated feature analysis offers more flexibility in setting up CCSEM analyses, faster particle throughput, improved ease of use, and better options for off-line data processing and analysis. Overall, the PSEM is significantly easier for the novice to use than the LEO/PGT system and for this reason has become a multi-user facility.

Particle relocation software (program XLATE, R.J. Lee Group, Inc.) allows features of special interest in the PSEM to be physically relocated in the LEO S440. This has made it possible to combine the superior CCSEM capabilities of the PSEM and the superior imaging capabilities of the LEO S440. The PSEM, unlike the LEO S440, can be operated in the variable-pressure or low-vacuum mode in addition to the conventional high-vacuum mode. The variable-pressure capability of the PSEM is provided by a microprocessor-controlled valve and pumping configuration that allows user-selected pressure up to 1 torr to be maintained in the sample chamber while keeping the gun at high vacuum. SEM analysis of samples at elevated pressure has the advantage that charging of insulating samples is largely or completely eliminated, obviating the need for carbon-coating the samples, with no significant loss of image resolution. The advantages of reduced sample preparation time are somewhat offset by the fact that only the backscatter mode

of analysis can be employed in the variable-pressure mode. Nevertheless, the variable-pressure feature has proven to be extremely beneficial for samples prone to charging and when the user simply wants a rapid evaluation of a sample without the need to first coat the sample.

Figures 2-9a (PSEM) and 2-9b (LEO S440) provide a comparison of image quality for the two instruments. Both images are of the same feature at approximately the same magnification. Instrument parameters for both SEMs were optimized to produce the best possible image.

2.2.3 Vacuum Evaporators and Other Supporting Equipment

Samples that are to be examined by SEM in high vacuum (rather than high pressure) typically require a thin conductive coating on the order of 200 Å to conduct charge away from the sample and prevent sample charging. The ideal coating would not contribute X-rays to the X-ray spectrum of the coated particle. Although the coatings are very thin, conductive metal coatings such as chromium, gold, or palladium can generate non-negligible X-ray peaks that interfere with particle-generated peaks in the EDX spectrum. For this reason, carbon is generally the element of choice for conductive coatings if the samples are to be analyzed by EDX, since X-rays produced by the carbon film will interfere significantly only with the carbon X-ray peak generated by the sample. Unless one is analyzing a sample for carbon, the carbon peak contributed by the coating is usually of no concern. (Section 4.5 discusses the problems associated with the analysis of carbonaceous particles). If high-resolution imaging is of primary importance, a thin coating of gold or Au/Pd evaporated from a tungsten basket can be applied to the sample. This enhances image contrast compared to carbon coating, but also introduces unwanted X-ray lines in the EDX spectrum.

Supporting facilities in the SEM/EDX laboratory currently include two vacuum evaporators for coating SEM samples with thin carbon and/or metal conductive films. Both evaporator units employ tilting, rotating specimen holders to ensure uniform coatings and to minimize shadowing, and both are capable of applying carbon or metal coatings. Plans currently include upgrading to more modern coating devices with dedicated carbon and metal coating capabilities.

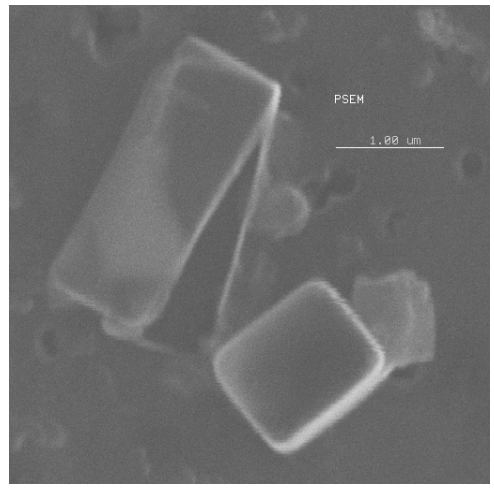

Figure 2-9a. Salt crystals. Image acquired with PSEM at 20 kV, 7-mm working distance, 10% spot size, and tungsten filament.

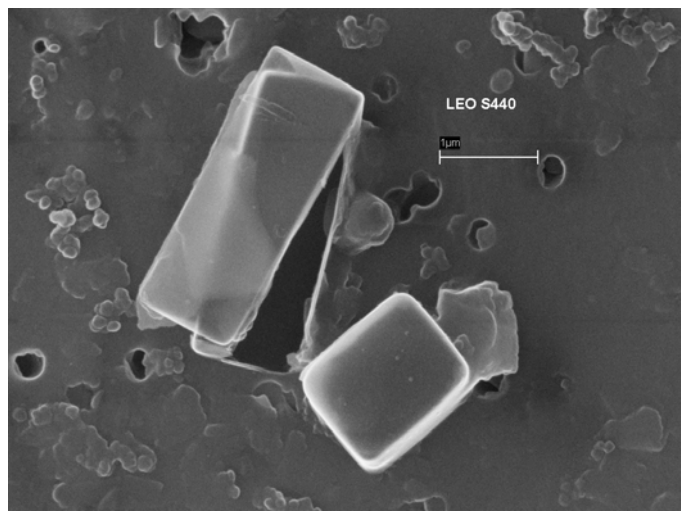

Figure 2-9b. Same salt crystals imaged with LEO 440 SEM at 30 kV, 7-mm working distance, 3-pA probe current and LaB_6 emitter.

Chapter 3
Recommended Techniques and Procedures for SEM/EDX and CCSEM

3.1 Sample Receipt, Tracking, and Storage

The following describes the procedures used by the NERL SEM/EDX Laboratory to manage the flow of samples through the laboratory. These procedures can be easily adapted to the needs of other laboratories.

3.1.1 Sample Submittal Form

It is highly recommended that individuals interested in having analysis done in the NERL SEM/EDX laboratory discuss their needs with laboratory personnel as early into their project as possible. The submitting of actual samples to the laboratory is formalized and tracked through the use of a Sample Submittal Form, a copy of which is included in Appendix B. An electronic version of the form is made available to the requesting researcher/client, who submits the completed form back to the SEM laboratory contact. The client provides a project name and contact person, a description of the samples, the analytical objectives and expected outputs, and a target delivery date for results. Duplicates of the submitted forms are kept in a binder in the SEM laboratory and in the hard-copy file folder created for the associated study. The Sample Submittal form initiates the sample tracking process discussed below, and provides a basis for follow-up discussions.

3.1.2 Log-in Procedures

Samples received for analysis are assigned a project name and a SEMID, a four-digit identification number used by the SEM laboratory to track samples. ID numbers are assigned by the SEM laboratory staff after consulting the "Assignment of SEM IDs" notebook in the SEM laboratory. This notebook is a record of all project names and the ID numbers assigned to all substudies. An example page from this notebook is presented in Appendix B. Analogous to the assignment of IDs in the NERL XRF laboratory, the first three digits of the SEMID represent the project name and the fourth digit is reserved for substudies within the same project (maximum of 10 possible substudies for each project). If the samples represent a new project, a new three-digit code followed by a zero (first substudy of the project) is assigned to the samples.

After assigning a SEMID, the staff enters the requested information into the Sample Log-In/Log-Out notebook (Section 3.1.3) maintained in the laboratory. A file folder is created for each SEMID and kept in a file cabinet in the SEM laboratory. This folder contains all information relevant to that substudy, including a copy of the Sample Submittal form, communications between the client and the SEM laboratory, and hard copies of data and outputs from the SEM analysis such as photomicrographs and reports. If the submitted samples were previously analyzed in the NERL XRF facility, that should be noted on the sample submittal form, and hard copies of the XRF data are included in the file folder. The XRF data can be very useful in guiding the SEM/EDX analysis of the same sample.

3.1.3 Sample Tracking

Samples are tracked by means of Sample Log-In/Log-Out notebook maintained in the SEM laboratory. The Sample Log-In/Log-Out notebook is a record of samples logged into the laboratory for analysis and logged out of the laboratory for any purpose. All samples that are removed from the SEM laboratory must be logged out, including those whose return is requested on the SEM Sample Submittal form. "Sample" in the above discussion refers both to the samples as submitted (filters, raw dusts or powders, etc.) and to SEM sample stubs prepared from the as-submitted samples. However, SEM stubs are removed from the laboratory only under exceptional circumstances since they are useful only to people with access to a SEM. Information recorded in the Sample Log-In/Log-Out notebook includes the following: date the samples were received, project name and SEMID, number of samples, name of a contact person or client, and number of samples returned and to whom returned. An example Sample Log-In/Log-Out page can be found in Appendix B.

3.1.4 Sample Storage

Samples include as-submitted samples as well as the SEM stubs prepared from the submitted samples. As-submitted samples may include air filters, loose samples such as soil or dust samples, or liquid suspensions. At the present time these samples are stored in cabinets in the SEM laboratory unless the client requests their

return on the Sample Submittal form. This policy may be revised as storage space becomes limited. Half-inch SEM stubs are typically stored in plastic stub boxes with the project SEMID and individual stub IDs (Section 3.2.3) marked on the box lid. Recent SEM stubs or samples for active projects are typically stored at room temperature in low-humidity Lucite sample storage boxes in the SEM laboratory. Alternatively, sample stubs are stored in vertical filing cabinets labeled by project name. Periodically, old stubs that have been determined to be non-essential are destroyed and the aluminum stubs are cleaned and reused.

3.2 Sample Preparation

Proper sample preparation is a prerequisite for successful SEM analysis. The nature of the sample preparation will be governed by the nature of the sample and the analytical objectives. Suitable samples include most solids that are stable under vacuum and exposure to an energetic electron beam (metals, ceramics, polymers, minerals). Microscopists should be constantly aware of the potential for loss of volatile particles in vacuum during carbon coating and/or SEM analysis. For example, Parungo et al. (1986) reported the loss of sulfate particles due to sublimation during EDX analysis.

The range of motion of the SEM stages limits the physical size of samples to about 50 mm. Typically, only a few square mm of an air filter sample are sufficient. Sample preparation for PM samples is relatively simple since we typically deal with dry, non-biological specimens. Usually PM samples are analyzed as is, with no additional preparation other than mounting on a stub and overcoating with a thin carbon film to provide conductivity. Quantitative X-ray microanalysis, which generally requires flat, polished specimens is rarely required in the analysis of aerosol samples.

3.2.1 Choice of Filter Media

Several types of filters are commonly used in sampling aerosols, but not all are compatible with SEM/EDX analysis. The ideal filter medium for SEM/EDX would have the following properties: (1) a *screen* membrane (in contrast to a depth membrane), providing uniform contrast, in which the aerosol particles are deposited on top of an optically smooth, flat surface; (2) transparent to 20-keV electrons so that it contributes minimally to the EDX spectrum of the sample; (3) thermally stable (insensitive to localized heating from the electron beam) and compatible with high vacuum; (4) electrically conductive to minimize sample charging; (5) high purity/low blank to facilitate EDX analysis; and (6) mechanically rugged.

Figure 3-1 shows micrographs of four of the most commonly used filter types. Teflon, quartz, and MCE (a mixture of inert cellulose nitrate and cellulose acetate) are "depth" filters, which trap particles throughout the depth of the filter rather than on the surface. The three-dimensional fibrous structure of these filters and their chemical composition greatly complicate the task of identifying particles embedded in the filter. Depth filters have greater sampling capacity than screen membrane filters but are clearly less than ideal for microscopy purposes. In addition, the EDX spectra generated by Teflon and quartz filters may interfere significantly with the X-rays from the particles. (Teflon produces high F and C peaks, while quartz produces high Si and O peaks.) Whenever possible, aerosol samples should be collected on polycarbonate screen membranes (Poretics Corporation, Livermore, CA). Polycarbonate membranes, also called Nuclepore, are mechanically rugged and are an excellent substrate for automated particle analysis. Polycarbonate filters are available in diameters ranging from 13 mm to 47 mm and greater and with pore sizes ranging from 0.01 μm up to 20 μm. The smooth two-dimensional surface upon which the particles are collected has a very low EDX blank, being composed of light elements (C, H, and O). This composition provides excellent BSE image contrast with particles of higher Z. A major drawback of polycarbonate membranes is that they provide poor imaging contrast for carbonaceous particles, making CCSEM analyses of small carbonaceous particles especially difficult. Furthermore, these filters are nominally 10 μm thick and therefore not transparent to 20-keV electrons. Thus, the filter generates carbon and oxygen X-rays as well as bremsstrahlung radiation, which increases background levels and degrades signal to noise for EDX analyses, especially of biological or carbonaceous particles.

In many cases, the microscopist is presented with samples that have already been collected on non-polycarbonate filters, most often Teflon or quartz membranes. For certain types of analyses, it may be possible with considerable care and effort to analyze aerosol samples on quartz or Teflon filters by automated SEM/EDX (although the huge Si signal generated by the quartz substrate will make it difficult, if not impossible, to determine the chemistry of particles collected on quartz filters). For example, automated searches for heavy metals can be carried out

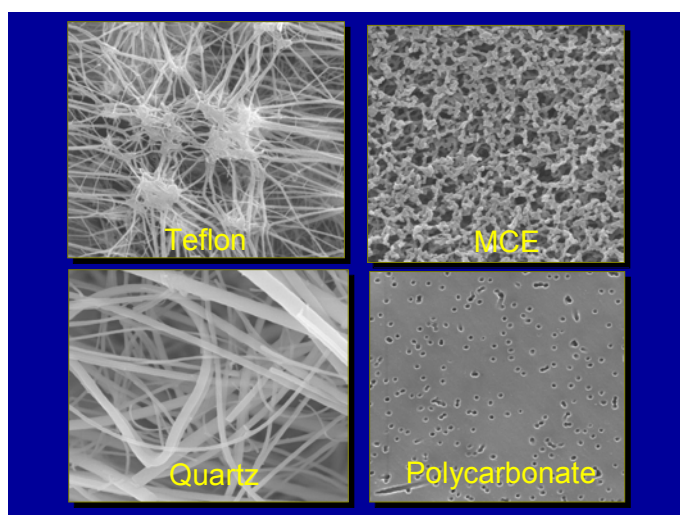

Figure 3-1. Four filter substrates often used for aerosol sampling. Teflon (upper left), quartz (lower left), and MCE (upper right) are depth filters, while the polycarbonate (lower right) is a screen membrane. The polycarbonate filter is ideal for SEM/EDX because of its low blank for Z>12, and its optically flat, low-contrast surface.

successfully, since the "noisy" low-Z filter substrate can be largely eliminated by use of a high-Z video threshold. For more general applications involving particle sizing or classification of low-Z as well as high-Z particles, one is usually faced with the choice of either manual analysis or transferring the aerosol sample onto a polycarbonate filter. Some laboratories have reported success in redepositing particles from Teflon or quartz onto polycarbonate filters (Casuccio, 2002). The redeposition process involves sonication of the original filter in filtered acetone (depending on the sample, hexane or distilled water may also be used) to liberate the aerosol particles followed by redeposition of the particles onto a polycarbonate substrate using vacuum filtration apparatus. The major concerns with particle transfer are the possibility that the redeposited particles have been chemically or morphologically altered during the sonication and filtration steps, or that the redeposited sample is not representative of the original sample. To ensure quality, it is a good idea to mount a section of the original filter side by side with a section of the redeposited filter and to manually compare the two samples looking for differences. Obviously, particles that are soluble in the carrier liquid (e.g., salt crystals in distilled water) will be lost during the sonication process.

In addition to sample preparation procedures, some online SEM analysis software has been developed which can provide some help in the analysis of fibrous filters. On-line software for the PSEM, for example, includes a semi-automated mode of analysis (I-P66 program, R.J. Lee Group, Inc., Monroeville, PA) developed especially for Teflon or quartz filters in which the features to be analyzed in each field are selected by the user, but the analysis otherwise proceeds automatically (Section 3.3.3).

3.2.2 Particulate Loadings

For aerosols in the submicrometer to 20-μm range, ideal mass loadings for SEM/EDX analysis are in the range of 5 to 20 $\mu g/cm^2$, though up to 30 $\mu g/cm^2$ may be acceptable in some cases. As loadings increase above 30 $\mu g/cm^2$, more particles come in contact with each other and it becomes increasingly difficult to analyze individual particles by CCSEM. The average distance between neighboring particles should be at least four times the average diameter of the particles being analyzed. If the loading is too light, the time required to analyze a representative number of particles may become impractical because of the time required to move the sample stage over many fields. Particle loading is particularly critical for CCSEM analyses for which automated feature analysis software lacks the ability of the human eye to resolve overlapping particles. Uniform distribution of the particles is desirable for both manual and automated SEM and is a prerequisite for estimating bulk properties of a sample (e.g., the number or mass of particles per unit area or the overall mass loading) based on a partial sampling of fields.

3.2.3 Mounting Filter Samples

Filter specimens are typically mounted on aluminum or carbon sample stubs. Stubs are available in 1/2-in and 1-in diameters with 1/8-in-diameter posts compatible with the PSEM and LEO stub holders. In mounting samples, it is critical that there be good electrical conductivity between the sample and the specimen stub in order to avoid charge build-up. Filter sections should lie flat on the stub with maximum surface area in contact with the stub (or underlying carbon tab if a tab is employed). Powder-free gloves are recommended whenever handling anything that goes into the SEM in order to maintain the cleanliness of the SEM column. (Oils from the skin can ultimately contaminate the SEM column due to volatilization.) The following procedure is recommended for preparing sample stubs:

1. Label the stub on its underside with a six-digit ID number (the "Stub ID") using a permanent marking pen. The first four digits of the stub ID are the SEMID assigned to the project. The last two digits (0–99) identify the individual sample mounted on the stub.
2. Label a plastic stub box (holding up to twelve 1/2-in stubs) with the project name and the date. Label each stub position in the box with the six-digit stub ID numbers.
3. Prepare the stub by applying conductive adhesive (silver paint, dag, or carbon tabs) for an approximately 10-mm^2 filter section. Carbon tabs are disks of carbon with adhesive on both sides. They are available in the laboratory in 1/2-in and 1-in diameters. They provide good electrical conductivity between the filter and the stub. They are also excellent substrates for viewing particles by SEM because they provide a flat, artifact-free background; they withstand electron beam heating moderately well; are stable in vacuum; and have a clean (carbon only) EDX spectrum. Carbon dag is a dispersion of graphite or carbon particles in a volatile carrier such as isopropyl alcohol. It provides excellent electrical conductivity and adequate adhesion between the stub and the mounted filter section. Apply a thin layer of dag to the stub by brush. Wait until the dag has dried slightly but is still moist. For typically loaded aerosol samples, a 10-mm^2 or larger section of filter should give adequate statistics for most purposes, but selecting a random subset of fields from a larger area may provide a more representative analysis if the sample loading is somewhat inhomogeneous.
4. Lay the filter section onto the carbon tabs or the wet dag. In our experience, the dag method seems to be most effective in minimizing charging problems.
5. Refer to Sections 3.2.3.1 and 3.2.3.2 for mounting polycarbonate and Teflon filters and Section 3.2.5 for coating the mounted samples.
6. Place the mounted samples in plastic stub boxes to prevent contamination. From this point on, use special forceps designed for gripping the SEM stubs to handle the stubs.

3.2.3.1 Mounting Polycarbonate Filters

Examine the filter to verify which side of the filter is the loaded side. (The shiny side should be the loaded side, but occasionally the dull side has been mistakenly loaded.)

1. Place the filter on a clean, flat, glass surface.
2. Using a clean stainless steel scalpel or razor blade, cut a square section (approximately 5 mm by 5 mm) from the interior of the filter.
3. As an alternative to step 2, cut the section using clean scissors.
4. Affix the section of filter to the stub with dag or carbon tabs.

3.2.3.2 Mounting Teflon Filters

1. Verify that the loaded side of the filter is face up.
2. Place the area of the filter to be removed on top of a stub covered with a sticky carbon tab.
3. With a clean scalpel or razor blade, cut a 5-mm by 5-mm section of filter.
4. Gently lift the filter from the stub leaving the desired section attached to the stub.

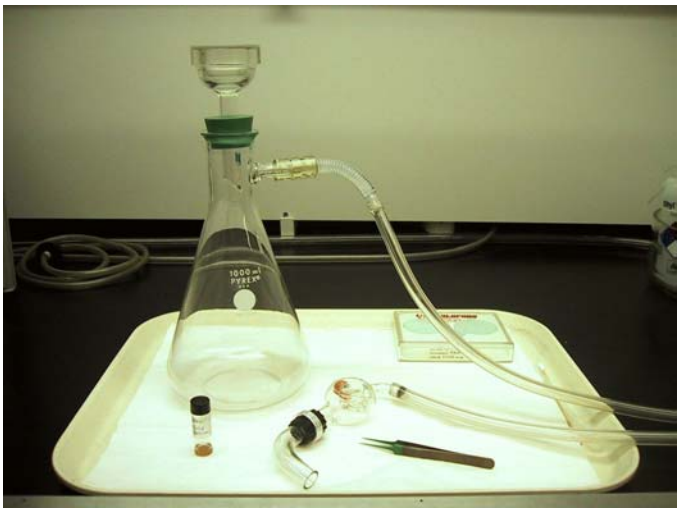

Figure 3-2. Vacuum filtration apparatus used for wet preparation of bulk dusts. A fritted glass base supporting a 37- or 47-mm filter extends into the vacuum flask through the stopper. The flask is evacuated through its side arm. The sample (in a liquid suspension) can be introduced to the filter either through a funnel clamped on top of the filter, or by using a glass nebulizer (foreground) to spray the exposed filter.

3.2.4 Preparing Bulk Dusts for SEM

In addition to characterizing filter samples, it is frequently necessary to analyze bulk samples, such as dusts, soils, or powders. Both wet and dry methods have been developed in the laboratory for the preparation of bulk particle samples.

3.2.4.1 Procedure for Wet Preparation of Bulk Dusts

We have used several options for wet preparation in the NERL SEM laboratory. Particles in a liquid suspension can be deposited onto a filter using glass microanalysis vacuum filtration apparatus (Fisher Scientific, Pittsburgh, PA. Vacuum filtration apparatus is available for 25-, 47-, and 90-mm filters). This method is easy to carry out and generally yields a uniform particle distribution on the filter. In this approach, an aliquot of bulk dust is suspended in reagent-grade acetone. A blank, tared polycarbonate filter is clamped between a fritted glass support base and a glass funnel. The base is coupled through a rubber stopper to a vacuum flask whose side arm is connected to a source of vacuum. (Figure 3-2 shows the vacuum flask closed with a rubber stopper attached to the fritted glass base. The glass funnel is not shown.) The liquid suspension is sonicated for approximately 1 min and an aliquot is placed in the glass funnel. Gentle vacuum is applied to the flask causing the liquid suspension to be sucked through the polycarbonate filter. As the liquid level in the funnel drops, rinse the sides of the funnel with clean acetone using a spray bottle. When the filter appears completely dry, remove the clamp and the funnel while continuing to evacuate the flask. Then, shut off the vacuum and remove the filter with clean tweezers.

Alternatively, suspended particles can be sprayed onto a clean stub or filter using a glass nebulizer or a miniature air brush. (We have used the Model 250 Air Brush, Badger Air-Brush Co., Franklin Park, IL.) The following details the air brush and wet nebulizer methods:

1. Suspend approximately 10–20 mg of sample (ground if preparing for XRF, or if altering particle size is not important.) in a 4-mL glass vial containing 2 mL of reagent-grade 2-propanol or acetone.
2. Sonicate for approximately 1 min to break up agglomerates.
3. Aerosolization is accomplished in a vented hood using a miniature air brush. Connect the air brush to 20 psi of dry nitrogen. Alternatively, put the suspension in a glass nebulizer attached to the hood nitrogen fitting.
4. Mount a blank polycarbonate filter in an open-faced 47-mm aluminum filter holder (Model 1220, Gelman Sciences Inc., Ann Arbor, MI) attached to a 500-mL Pyrex (Corning Labware and Equipment, Big Flats, NY) vacuum filtration flask.
5. Insert air brush siphon fully into the sample vial.
6. Apply vacuum to the backside of the filter assembly to accelerate the evaporation of the propanol or acetone carrier.
7. Raster the air brush evenly over an area approximately 10 times larger than the filter to improve deposit uniformity. (A metal splashboard surrounding the filter catches the excess spray.)
8. Turn off vacuum, unmount loaded polycarbonate filter, and mount section on SEM stub as described in Section 3.2.3.

Note: The use of a wet technique for sample preparation raises concerns that the 2-propanol or acetone carrier may alter particle

chemistry, size, or morphology. Many salts and organic compounds are soluble or slightly soluble in propanol, which leads to a potential for biasing the results for such species, although we have not investigated these effects to date. Likewise, we are not aware of studies comparing size distributions for raw versus wet-prepped aliquots of the same sample.

3.2.4.2 Procedure for Dry Preparation of Bulk Dusts

A dry sample preparation procedure was developed for creating a uniform deposit of powders or dusts on Teflon or polycarbonate filters. In contrast to other preparation techniques for dry powders, this technique employs a miniature cyclone device (John and Reischl, 1980), which, by adjusting the airflow rate, allows one to select the size range of particles collected on the filter. Figure 3-3 is a photo of the mini-cyclone device. The motivation for developing the technique was to be able to prepare powder samples suitable for quantitative XRF analysis, which requires particles smaller than 10 μm, aed. But the method is also useful for preparing samples for SEM/EDX The procedure is simple and easy to perform. Test samples examined by SEM show very uniform particle distributions. The procedure is outlined below.

Materials needed:

- 37- or 47-mm Teflo (2-μm pore size) or polycarbonate filters
- Quartz filter for backing
- Cyclone and cyclone flowchart
- Vacuum pump with flow gauge (lpm)
- Teflon tweezers, spatula, plastic 47-mm petri dish, filter holder

Procedure:

1. Label petri dish with sample ID number and date.
2. Equilibrate untared, clean filters in petri dishes for 24 h in climate-controlled weighing room.
3. Record filter tare weights and return filters to petri dishes.
4. Place filter in holder with backing filter.
5. Attach vacuum line from pump to filter holder.
6. Set flow rate on vacuum pump for desired particle size according to cyclone flowchart.
7. Use a spatula to feed sample into inlet tube.
8. Run vacuum for 1–2 minutes; turn off vacuum pump.
9. Remove backing filter and place loaded filter in labeled petri dish.
10. Weigh loaded filter after 24-h equilibration in weighing room.
11. Repeat procedure if necessary until desired loading is attained. (Note: For XRF analysis, desired loadings are approximately 0.5–1 mg for 37-mm filters and 1–2 mg for 47-mm filters, which are up to 20 times the desired loadings for SEM.)
12. Clean cyclone after each loading to prevent contamination.

The NERL SEM Laboratory also prepares dry dusts and powders using a custom-designed glass resuspension apparatus (the "puffer") shown in Figure 3-4. The puffer is a glass chamber with a volume of 900 mL. The lid to the chamber has a built-in mesh grid for supporting a 47-mm filter. Air can be pulled from the chamber through the filter by means of a

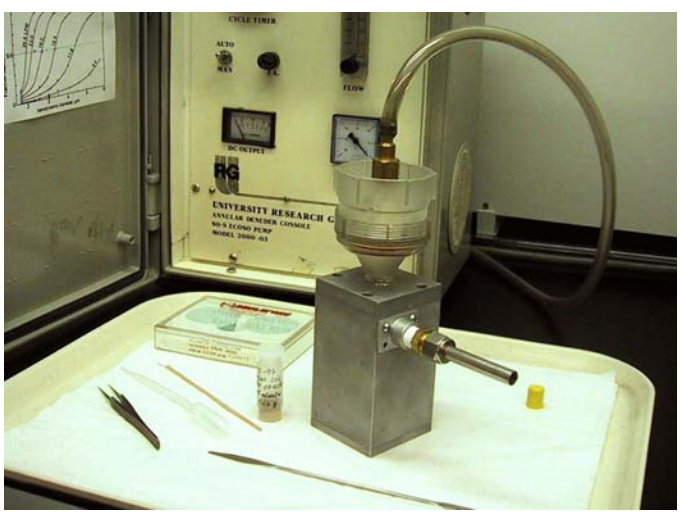

Figure 3-3. "Mini-cyclone" apparatus used to prepare filter samples of bulk dusts and powders. Raw sample is sucked into the cyclone through the horizontal section of tubing. The filter to be loaded is placed in the filter holder on the top of the cyclone. A vacuum pump is shown in the back.

Figure 3-4. "Puffer" apparatus used to prepare filter samples of bulk dusts and powders. The side arm below the shut-off valve is connected to a vacuum pump.

vacuum connection on the lid. The lid also has four air (or gas) jets connected to a central inlet with a shut-off valve. The jets extend via tubes into the resuspension chamber and are arranged symmetrically about the base of the chamber. Clean, filtered air or inert gas can be introduced into the chamber via the four jets. To operate the puffer, approximately 0.1 mg of sample is placed in the bottom of the clean chamber. A blank, tared 37- or 47-mm filter is placed on the filter support grid and secured in place by a Delrin cap. Vacuum is applied to the backside of the filter and the lid is then closed over the chamber so that the chamber is evacuated. The air inlet valve is then opened allowing a burst of clean air or inert gas into the chamber via the four jets. The burst of air resuspends the sample material, a fraction of which is then pulled onto the vacuum-backed collection filter. SEM examination of filters prepared with the puffer show very uniform loadings. During the preparation of a sample with the puffer, most of the resuspended sample dust redeposits on the internal surfaces of the chamber; to avoid cross-contamination of samples, the puffer must be thoroughly cleaned between uses. It is possible that filter samples prepared in the puffer show some size fractionation relative to the original sample material, but size fractionation effects in the puffer have not been investigated.

3.2.5 Coating Mounted Samples

The mounted samples are coated with a thin conductive film prior to SEM/EDX analysis to minimize sample charging problems. General guidance for coating samples is given below.

1. Use a vacuum evaporator device to overcoat specimens with carbon, or a vacuum evaporator or sputter coater to overcoat specimens with metal (typically gold). It is helpful to have a one-page instruction sheet for using each coating device kept with each unit.
2. Coat specimens to be analyzed by EDX only with carbon, since metal coatings will complicate the X-ray spectrum of the particle. Metal coatings are often used to enhance image resolution on specimens that are not to be analyzed by EDX.
3. Produce carbon films by evaporating 1/8-in carbon rods. Thicknesses on the order of 200 Å usually provide adequate charge conductivity. If charging is still a problem, an additional C-coat may be required.
4. Metal films (typically Au, Pt, or Au/Pd) are produced by evaporating a length of pure metal wire in a resistance-heated tungsten wire basket (vacuum evaporator) or sputtering metal targets (sputter coater). A typical gold coating with the vacuum evaporator uses two inches of 0.008-in-diameter wire placed in the tungsten basket.
5. Ensure that samples are not subject to the full power of the coating process for an extended period. The process of coating the sample subjects the sample to considerable heat, which can alter the sample chemically and physically. Maximizing the distance between the evaporation source and the sample can reduce the potential for thermal damage.
6. A rotary/planetary/tilting stage helps to ensure a uniform coating and eliminate shadowing effects.
7. Protect your eyes. Metal and carbon evaporations produce extremely bright and potentially damaging light visible through the glass bell jar or sample chamber. The user *must* wear eye protection (welding glasses) or view the process through the optically dense glass plates attached to the outside of the bell jar or chamber.

Some coating devices are equipped with a thickness controller/monitor. If the coater is not equipped with a thickness monitor, a convenient technique to estimate the thickness of the carbon coating is to place a polished brass stub in the coater along with the samples to be coated. Thin-film interference causes the polished brass to take on different colors, depending on the thickness of the carbon coating, according to the following color scale:

Color	Carbon Thickness (Angstroms)
Orange	150
Indigo red	200
Blue	250
Bluish green	300
Greenish blue	350
Pale green	400
Silver gold	450

The carbon coating is easily removed from the brass stubs by using metal polish applied to a cotton swab.

Gold by itself has relatively poor wetting properties. In order to improve the quality of the gold thin film, a thin film of carbon may first be evaporated onto the sample. Or gold and carbon may be evaporated simultaneously by wrapping gold wire around a sharpened carbon rod and doing a normal carbon coat. A popular alternative to Au is Au/Pd which has improved wetting properties.

3.3 SEM/EDX Data Acquisition

SEM/EDX analyses can be conducted in fully manual mode, fully automated mode, or interactive (semi-automated) mode. For each mode of analysis, the analytical objective may be particle size distribution only, size and chemistry, images only, or a targeted particle searches. These modes are discussed below. These discussions are specific to the Aspex Instruments (Denton, PA) Personal SEM (PSEM) and/or the LEO (Thornwood, NY) SEM and PGT (Princeton, NJ) IMIX EDX system. Users of other SEM/EDX instruments may need to adapt these guidelines to their own instruments.

3.3.1 Manual

Despite the impressive throughput of automated SEM, there will always be a need for manual SEM (MSEM). Many samples are unsuitable for CCSEM because of particle loading or inappropriate substrate, and therefore require MSEM. Moreover, MSEM examination is strongly recommended for all samples before proceeding with either a more detailed manual analysis or a CCSEM analysis. Preliminary manual examination of a sample familiarizes the microscopist with the sample and provides vital quality control. A preliminary examination can reveal if the sample is charging and needs another carbon coating or if the sample has been seriously compromised (e.g., tears or holes in filter-based samples, foreign objects or other evidence of contamination, gross non-uniformity in particle loading, filter sample mounted wrong-side up). The sample should be scanned at low magnification to identify any obvious non-uniform or irregular particle deposits, sample artifacts, or areas of the sample that should be avoided.

Because of the low particle throughput of manual analysis, sampling error is always a major concern. If the objective of the manual analysis is to provide an accurate representation of the sample, then the microscopist must examine enough fields and enough particles to ensure representative sampling. Studies suggest that this requires a minimum of several hundred particles (Mamane et al. 2001). Because the eye is naturally attracted to larger features or those with distinctive morphology, fields should be selected at random (with eyes closed), and *all* particles within each field should be analyzed to minimize the potential for bias or operator subjectivity. Although manual analysis is very tedious, there is an opportunity in MSEM to bring one's intelligence and experience to bear on the sample that is not so direct in CCSEM. The microscopist can interact in real time with the sample, making observations and drawing inferences about the sample that cannot be done in the automated mode.

Observations from a MSEM analysis session are typically recorded in a lab notebook, accompanied by hardcopies of photomicrographs of fields of particles as well as micrographs of selected particles of interest. A common approach is to work from a hardcopy photomicrograph of a field of particles which have been numbered by the analyst. The analyst successively analyzes each particle within the field, recording relevant data (e.g., date, sample ID, field number, particle number, particle size, morphology, chemistry, and particle class) in the notebook. Photomicrographs of fields and individual particles are saved to disk.

Although MSEM is indispensable for many samples, especially novel samples, it is so labor intensive that it generally cannot provide the statistical depth needed for data-intensive studies such as source apportionment where differences among samples must be quantified.

3.3.2 CCSEM

Samples that are suitably prepared (proper loading, compatible filter substrate, uniform particle distribution) may be candidates for fully automated, computer-controlled SEM (CCSEM). The PSEM uses vendor-supplied software (ZepRun, Aspex Instruments, Delmont, PA) to perform a computer-controlled analysis of the sample once the initial instrument conditions are set up. These parameters include the physical boundaries for the analysis, video threshold, magnification(s) at which the analysis will be conducted, number of particles and/or fields to be characterized, method of field selection (random, manual, in order), particle size range, aspect ratio range, X-ray acquisition time, list of elements to be quantified, and numerous other parameters that affect data acquisition. The user may also create customized rules to specify how often and for what types of particles images should be acquired or to exclude particles that are of no interest. Once the run-time parameters are initialized, the CCSEM analysis can proceed without operator intervention. Data acquired include particle size and shape parameters, particle location, particle and field images (if requested), video level, total X-ray counts, and element concentrations. The data are stored in electronic format for later evaluation. Two software packages (ZepView and ZepSum, Aspex Instruments, Delmont, PA) enable the user to review and summarize data off-line.

During CCSEM analyses, the PSEM relies on a user-selected grayscale video threshold (the detection threshold) to discriminate between a particle and filter background. A carefully chosen threshold is essential for accurately identifying and sizing particles. However, a complex aerosol sample may present a wide range of particle compositions, sizes, and morphologies, which will complicate the strategy for threshold setting.

CCSEM analyses are generally conducted using the BSE mode rather than the SE mode. The BSE signal is better for detecting particles on a filter substrate because of its higher atomic number contrast, its relative lack of topographic detail, and its lower susceptibility to electron beam charging artifacts, which can occur even with carbon-coated samples. (The edges of the holes in Nuclepore filters routinely exhibit charging effects in the SE mode.) The BSE mode thus yields a much more uniform and stable video signal from the filter background, enabling the user to precisely set the detection threshold. Particle brightness in the BSE mode is governed by the effective atomic number (Z) of the particle. Particles with high Z (e.g., Fe-rich) have a high backscattered electron yield and appear brighter on the SEM image, while particles with low Z (carbon, sulfates, organics, biological) will appear dim. Proper setting of the video threshold is extremely important in CCSEM analyses. Ideally, the video threshold is set such that all particles having an effective Z greater than or equal to a threshold value Z_t are detected while all particles with $Z<Z_t$ are rejected. In practice, such precise thresholding is never possible because a particle's video signal is not determined solely by atomic number but is also determined to some extent by particle size, morphology, and shadowing by neighboring particles. Consequently, it is possible that small (submicrometer), low-Z particles are preferentially missed. Errors associated with automated SEM are discussed in the next section.

ZepRun uses a two-step process to locate and measure particles. To identify a feature as a particle, the computer com-

pares the backscattered electron signal collected at each point in a grid to the preset detection threshold. Once a signal above the threshold is detected, the measurement mode is enabled. In this mode, the distance between grid points is much smaller than in the detection mode, and the preset measurement threshold has a lower grayscale value than the detection threshold. The computer draws 16 chords through the particle's center of mass within the confines of the measurement threshold in order to determine the particle's maximum, minimum, and average diameters, aspect ratio, and area. (An alternative approach to sizing, which may yield somewhat better estimates of particle volume for large particles, is to measure the particle perimeter. This "perimeter walk" option is available in ZepRun's I-P66 mode of analysis, Section 3.3.3).

Very abbreviated guidelines for CCSEM are presented below. Users requiring more detailed guidelines are referred to the PSEM ZepRun Users Manual (Aspex Instruments).

How to Obtain Good Results from CCSEM

A. Prepare a good sample

1. Label stub with 6-digit ID
2. Add fiducial marks for particle relocation
3. Ensure representative sample
4. Ensure uniform loading
5. Minimize particle overlap
6. Avoid contamination
7. Eliminate sample charging

B. Setup SEM

1. Saturate filament
2. Align beam
3. Set working distance: 15-20 mm for best EDX, 7-8 mm for best images
4. Set spot size: 30%-40% for EDX; for best imaging, use smallest spot size which still gives adequate brightness and contrast

C. Setup stage

1. Degauss lens until focus is stable
2. Set up analysis area and focus for each sample
3. Set up origin and alignment reference points (for future particle relocation)

D. Preview the sample manually

1. Check particle loading and deposit uniformity
2. Scan sample at low mag to identify areas to avoid
3. Particle size range determines choice of mags
4. Particle types determine choice of elements and on-line analysis rules
5. Optimize EDX countrate and detector dead time on high Z particles and low Z particles by adjusting spot size.

E. Setup CCSEM run parameters

1. Set up Run Parameter File (RPF):
   a. Suggested mags:
      10- 100 μm: 200x 0.2–5 μm: 1200x
      5–50 μm: 400x 0.2–2.5 μm: 2000x
      2.5–10 μm: 800x
   b. Specify SEM run parameters:
      Maximum particles per mag; max fields per mag; max time per mag; particle diameter and aspect ratio limits (minimum and maximum) for search; search grid spacing; search size, search, measure, and image dwell times; guard band; microimage fill%; field image option; field selection method (random, in order, manual).
   c. Specify EDX parameters:
      Minimum and target counts; normal and maximum EDX time; element threshold; X-ray mode (point, chord, raster, perimeter).
2. Set up Element Vector file (VEC)
   a. Put C and O in the element list only if you want to analyze carbonaceous particles.
   b. Be aware of possible peak overlaps:
      Pb *Mα* - S Kα As *Lα* - Mg *Kα* Br *Lα* - Al *Kα*
      Zn *Lβ* - Na *Kα* As *Kα* - Pb *Lα* Ti *Kα* - Ba *Lα*
   c. Require 3-5 sigma counts in secondary or tertiary ROIs (regions of interest or X-ray "energy windows") for potential overlaps: Pb, As, Br, Ba.
3. Set up Analysis Rule file (RUL)
   a. Create rules based on particle size, shape, and/or chemistry for screening on-line data
   b. Specify MAX EDX to increase the EDX time for elements of special importance: e.g., Pb, Br, Zn, As
   c. For each particle type defined by the rule file, specify whether to save microimages and/or spectra, and how frequently (e.g., save for all particles or save for every 10th, etc.)

F. Final Checks

1. Ensure adequate disk space for data
2. Set up auto-threshold feature as desired
3. Move stage to first sample and check that focus is OK
4. Carefully set detection and measurement thresholds
5. Make a thermal print to record threshold settings

G. Run the Analysis

Note: It is imperative that the microscopist monitor the start of a CCSEM analysis for several minutes to verify that the analysis is proceeding normally—i.e., particles are being correctly sized and classified, images of selected particles or fields are being collected as desired, and the estimated run time is adequate for analyzing the desired number of particles or fields. It is not unusual that the operator may iterate between Steps C and D

several times, refining the RPF file and restarting the analysis until the CCSEM run parameters are optimized. It is also recommended that the microscopist check on the analysis periodically (if possible) to ensure that the analysis is proceeding as intended.

3.3.3 Semi-Automated SEM/EDX

The PSEM provides an interactive, semi-automatic mode of analysis (referred to as the I-P66 mode), which operates as follows. The run parameters are essentially the same as for a CCSEM analysis. The semi-automated mode differs from the CCSEM mode in that each time a new field is located during the analysis, the program pauses for user input. On each field, the user manually optimizes the focus and the threshold setting. As with CCSEM, the threshold setting automatically determines which features are detected in the field, but with I-P66 the user can manually select which subset of these features to include in the analysis. Features are selected in one of three ways: (1) The user selects a feature with the cursor, and the software automatically sizes it and determines its shape parameters using the current threshold setting (identical to CCSEM except that the feature selection is done by the user). (2) The user selects a feature and overlays it with a circle of adjustable diameter. The feature shape is then assumed to be spherical with the diameter of the overlaid circle. (3) Rather than define the particle as a sphere, the user can define the particle as a fiber of adjustable length. Once the user has selected the features to be analyzed in the field, the program is restarted. The features are analyzed by EDX and the results are automatically stored so that the output data format is identical to CCSEM. The interactive analysis mode is especially useful for the analysis of particles loaded onto fibrous filters such as Teflon or quartz. The program makes use of the superior ability of the human eye to discriminate aerosol particles from the filter substrate. Although the I-P66 mode of analysis has lower throughput than CCSEM and can also introduce user subjectivity into the analysis, it can be extremely useful for samples when fully automated analysis is inappropriate (e.g., heavy loadings or "noisy" substrates).

3.3.4 Size-Only

Aerosol particle size not only reflects on the sources of the particles, but also relates to their health effects. Some studies conducted in the NERL SEM laboratory require measuring only the size distribution of an aerosol sample without the need for chemical analysis. By size, we mean the two-dimensional projected image of the feature. The Z-dimension or thickness of a feature cannot easily be determined by SEM. Both the PSEM and the LEO/PGT systems can perform automated analyses for geometry in 2 dimensions only. In sizing particles, both systems locate the projected particle's centroid and then draw a series of chords at equiangular intervals through the centroid. Minimum, maximum, and average diameters are then calculated. Obviously it is critical that the particle loading be such that the probability of two particles touching each other is insignificant. Care in setting the threshold is critical for accurate sizing. Automated size-only analyses are selected on the PSEM by specifying an X-ray analysis time of zero seconds (Norm EDX = 0) when setting up the ZepRun analysis.

Even though the Z dimensions of particles are not determined, there is often interest in estimating the mass associated with a particular class or classes of particles identified by SEM. To do so requires both a volume and a density estimate. Given the projected area or diameters of a particle, the PSEM and LEO/PGT (IMIX) software make some assumptions in order to estimate the volume of the particle. The default assumption used by both the PSEM and the IMIX software is that the particle is a prolate spheroid whose volume is calculated as:

$$V = \pi/6 * D_{max} * D_{min}^{2},$$

where D_{max} and D_{min} are the maximum and minimum of 12 (IMIX) or 16 (PSEM) diameters through the particle's projected area. Obviously, not all particles are prolate spheroids, and one volume formula is not appropriate for all classes of particles. For both the IMIX and the PSEM, the user may replace the default volume formula above with another formula of his or her choosing. (The prolate spheroid assumption, however, is probably the most reasonable choice for typical aerosol samples , given our present state of knowledge). As discussed in Section 4.2, the uncertainty in the Z-dimension can result in very large errors in particle volume and particle mass. Users should be forewarned that the accuracy of SEM for sizing and "weighing" particles may diminish rapidly as particles deviate from spherical shape.

It is important to distinguish between geometric size and aerodynamic size. The geometric (physical) diameter (D_g) of a particle is the physical diameter of the particle. The aerodynamic diameter of a particle (D_a) is defined as the diameter of a sphere of unit density (1 g cm^{-3}), which has the same terminal falling speed in air as the particle of interest. D_g and D_a are related to each other through the particle density:

$$Da = Dg \cdot k \cdot \sqrt{(\rho_p/\rho_0)}$$

where ρ_p is the particle density, ρ_0 is unit density (1 g cm^{-3}), and k is a shape factor that is 1 for spherical particles.

Aerosol samplers are typically designed to collect particles within a certain aerodynamic size range (e.g., $PM_{2.5}$ and PM_{10} refer to aerodynamic diameters). If the densities of the collected particles are known, as may be the case for test aerosols used in wind tunnel studies, then the aerodynamic size distribution can be determined directly from a size-only CCSEM analysis. If the particle densities are not known *a priori*, they can be estimated for each particle using the particle's X-ray spectrum. In this way, the PSEM will generate aerodynamic size distributions for samples analyzed for both size and chemistry. The IMIX system presently does not have an algorithm for estimating particle density from the particle's X-ray spectrum and therefore cannot calculate aerodynamic diameters.

3.3.5 Dedicated Particle Searches

The PSEM and the IMIX systems allow the user to set up computer-controlled dedicated searches for particles that meet user-defined criteria for size, shape, and/or chemistry. Since the instrument spends very little time on features that do not meet the search criteria, large areas of a sample can be rapidly analyzed. This mode of analysis is ideal for "needle-in-the-haystack" applications when one is interested in specific rare or exotic particles, which may be present at number concentrations approaching 1 ppm (or lower).

An example of a dedicated particle search is a search for particle-phase mercury in ambient air samples collected downwind of the Astaris elemental phosphorus plant near Pocatello, ID (see Section 5.3).This was the first time that mercury had been observed in samples examined in the NERL SEM/EDX laboratory. The ambient sample was a fine-fraction 24-h dichot sample collected on March 8, 1997, at the Primary monitoring site immediately downwind of the Astaris facility. The sample was collected on a Teflo (Gelman Sciences, Inc., AnnArbor, MI) filter. X-ray fluorescence analysis of the sample showed a mercury concentration of 51.3 ng/m^3. Significant concentrations of Se (49.4 ng/m^3) and Cd (19.1 ng/m^3) were also measured in the sample. The total fine mass concentration was 21 μg/m^3. Mercury thus accounted for 0.24% of the total fine mass.

An automated particle search was carried out on the PSEM to identify individual Hg-bearing particles. Teflo filters typically present a challenge for automated searches because of the "noisy" image background generated by the filter. Mercury, however, because of its high atomic number, is very bright in the BSE mode compared to the Teflo substrate. By setting a high video threshold for the automated search, only particles with a high effective Z are located and analyzed, dramatically improving the efficiency of the analysis. During a 48-h automated search covering 10.3 mm^2 of filter area (1.6% of the total area), 17 Hg-bearing particles were found for which Hg was greater than 5% of the particle's EDX spectrum. Identifications of the particles were verified by returning to each particle at the conclusion of the automated search using the PSEM relocation feature, manually analyzing the particle, and confirming the presence of Hg in the EDX spectrum. A low-mag field image was also collected for each particle to facilitate relocating the particle in the LEO SEM. The sample was then transferred to the LEO SEM for collecting high-resolution images of the Hg-bearing particles. Particles were relocated using XLATE, a relocation program developed by RJ Lee Group (Monroeville, PA).

Figures 3-5a, b, c, and d show images and EDX spectra for four Hg-rich particles. Secondary (left image) and backscatter (right image) electron images were collected for each particle. Very bright areas in the backscatter image show the locations of Hg. In all cases shown, submicrometer Hg-rich particles appear to be embedded in or coated with phosphate, which typically dominates the fine-fraction aerosol at this monitoring site. The EDX spectra for all four particles indicate that Hg and Se are present in most Hg-rich particles in a fairly constant ratio, perhaps as mercury selenide (tiemmanite). In addition, several Hg-rich particles also contained silver, although silver was below XRF detection limits in the bulk filter analysis. The Hg-rich particles display an interesting morphology, often appearing as strands or filaments. Most of the Hg in the ambient samples collected at the Primary site is in the fine-fraction, suggesting combustion sources that include the ground and elevated CO flares (no longer in operation), calciners, and furnace emissions.

3.4 Particle Classification

CCSEM can generate a huge amount of data for a single sample: it is not unusual to analyze 1000 particles per sample, where each particle may be characterized by 50 or more size, shape, location, and chemistry parameters. In addition, photomicrographs may be collected for some or all of the particles and/or fields. In order to facilitate interpretation of CCSEM results, researchers have explored various approaches to reducing the data to more manageable dimensions. Ideally, one would like to be able to reduce a particle's description from 50+ parameters to only two or three parameters: particle size, particle class or particle type, and possibly particle morphology. Methods investigated for particle classification include simple elemental sorting (based on the highest three or four elements in the particle), ruled-based sorting, spectral matching, cluster analysis, and neural networks.

Source apportionment studies have traditionally relied on chemistry data obtained by bulk analysis of ambient and source aerosol samples. However, source apportionment can also be based on CCSEM data acquired on individual particles. In this case, particles are sorted into distinct classes (Kim and Hopke, 1988a), and the masses of those classes are used to provide quantitative source apportionment (Kim and Hopke, 1988b). Particle classes are most often based on particle composition (as provided by EDX data), although, ideally, shape could also be included to refine the classification. A potentially significant advantage of particle-based methods is that the additional information obtained by analyzing hundreds of individual particles, compared to a single bulk analysis of the same sample, may minimize collinearity problems that frequently plague traditional source apportionment approaches. SEM/EDX data have been used in a number of source apportionment studies (see Section 5.1.2).

3.4.1 Default Four-Element Typing

By default, the PSEM offers a choice of one-element, two-element, three-element, or four-element particle classification based simply on the dominant one, two, three, or four elements in the individual particle spectra. The resulting particle types are artificial in that they are not based on measurements of known standards. Furthermore, being sample-dependent they are not directly transferrable from one sample to another. However, the four-element typing approach can be useful as a first cut in classifying particle data and in highlighting differences between samples.

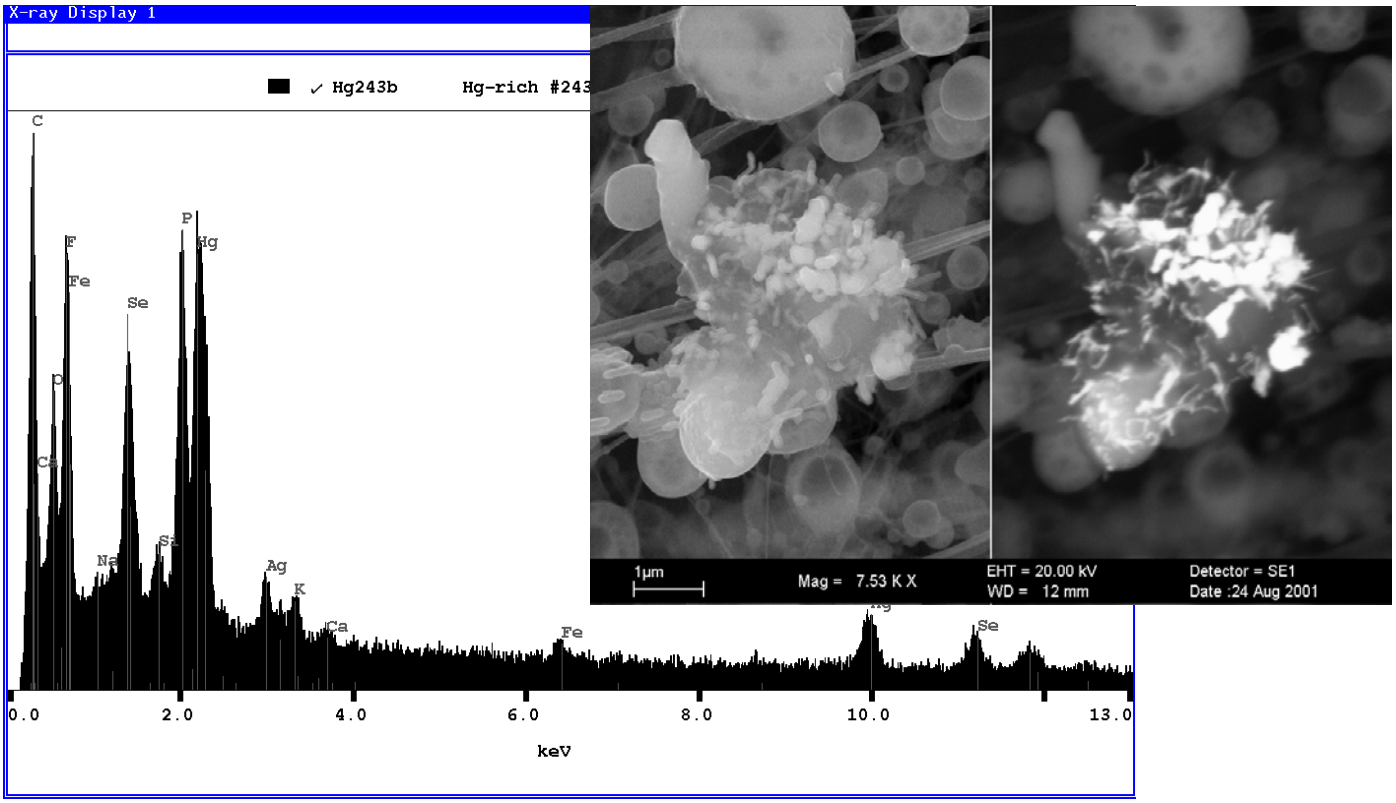

Figures 3-5a, b, c, d. Mercury inclusions in ambient air sample collected downwind of elemental phosphorus plant. Left photos: SE images. Right photos: BSE images showing very bright Hg inclusions.

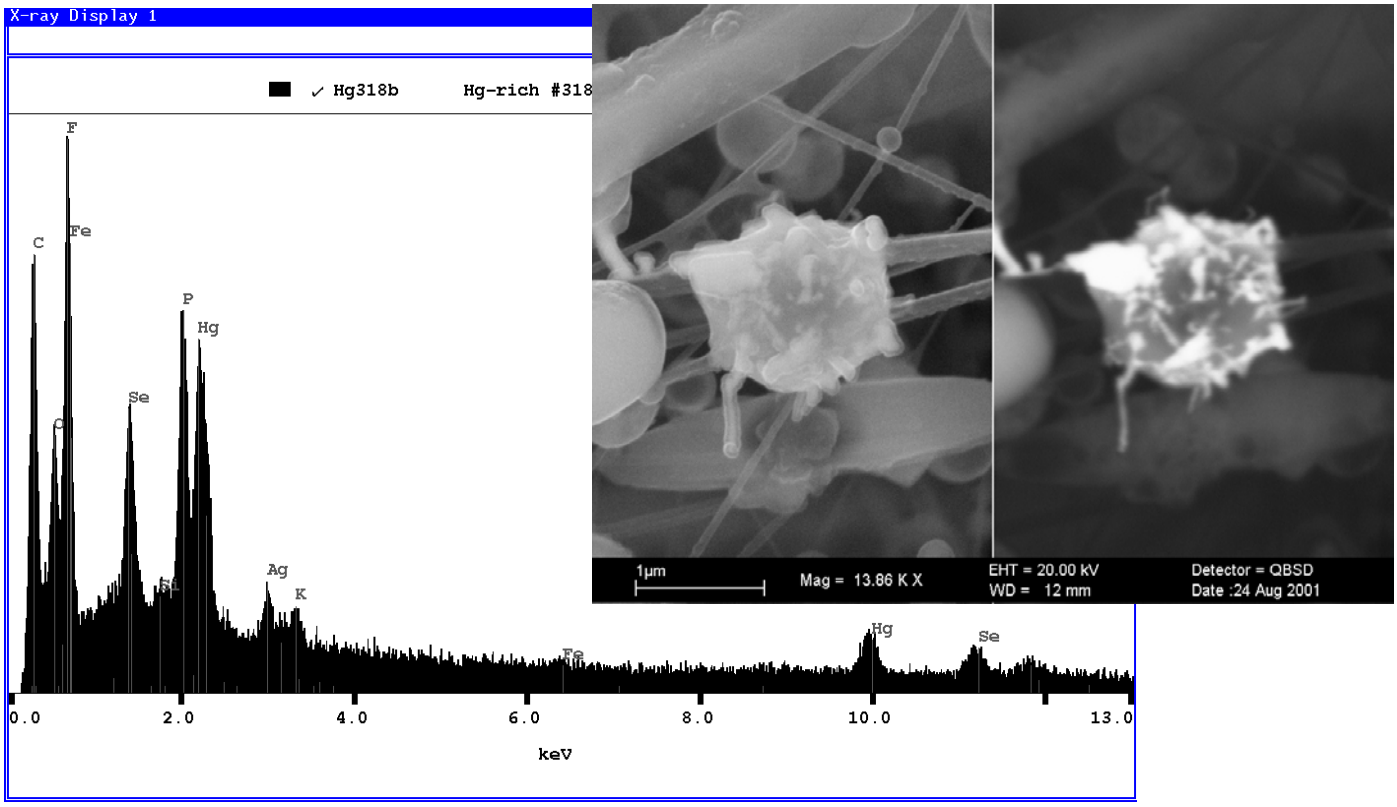

Figure 3-5b.

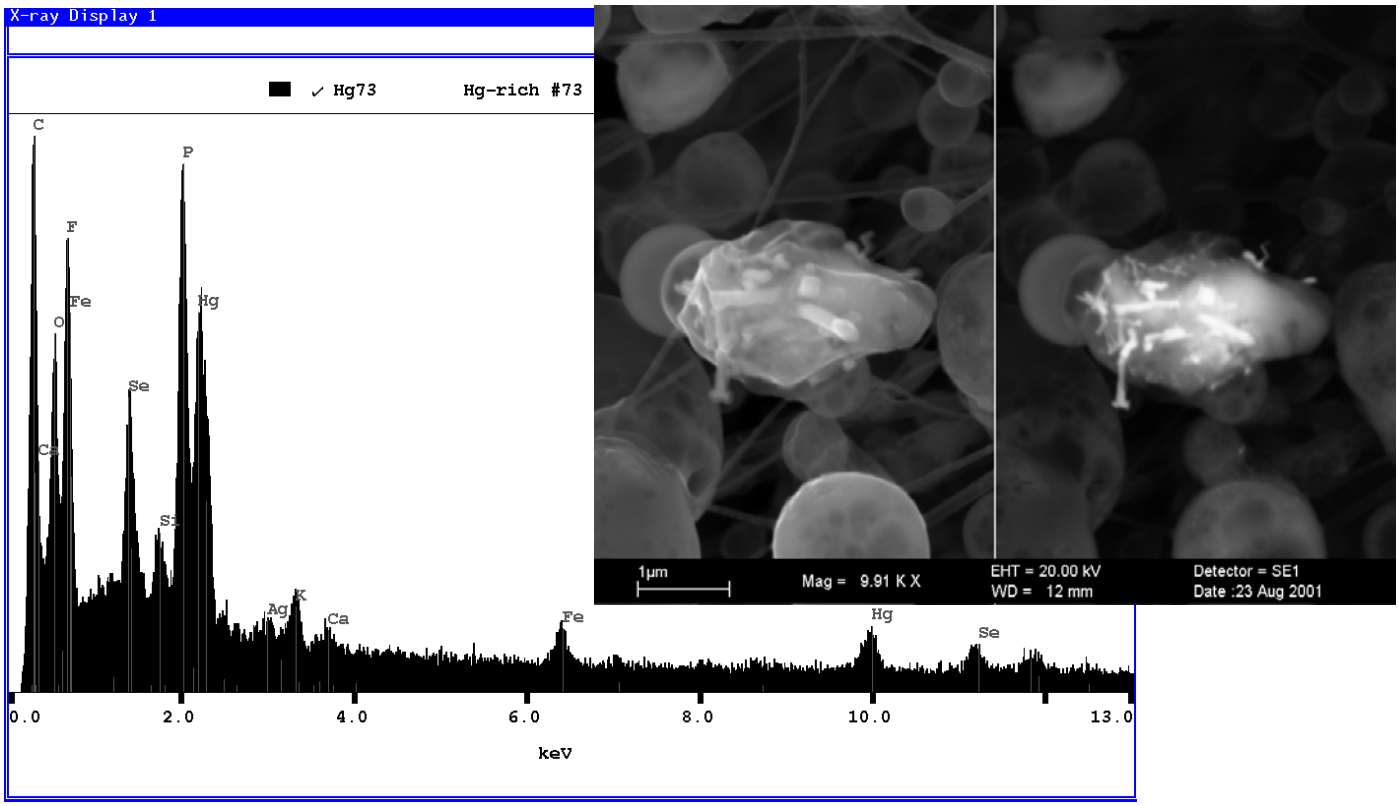

Figure 3-5c.

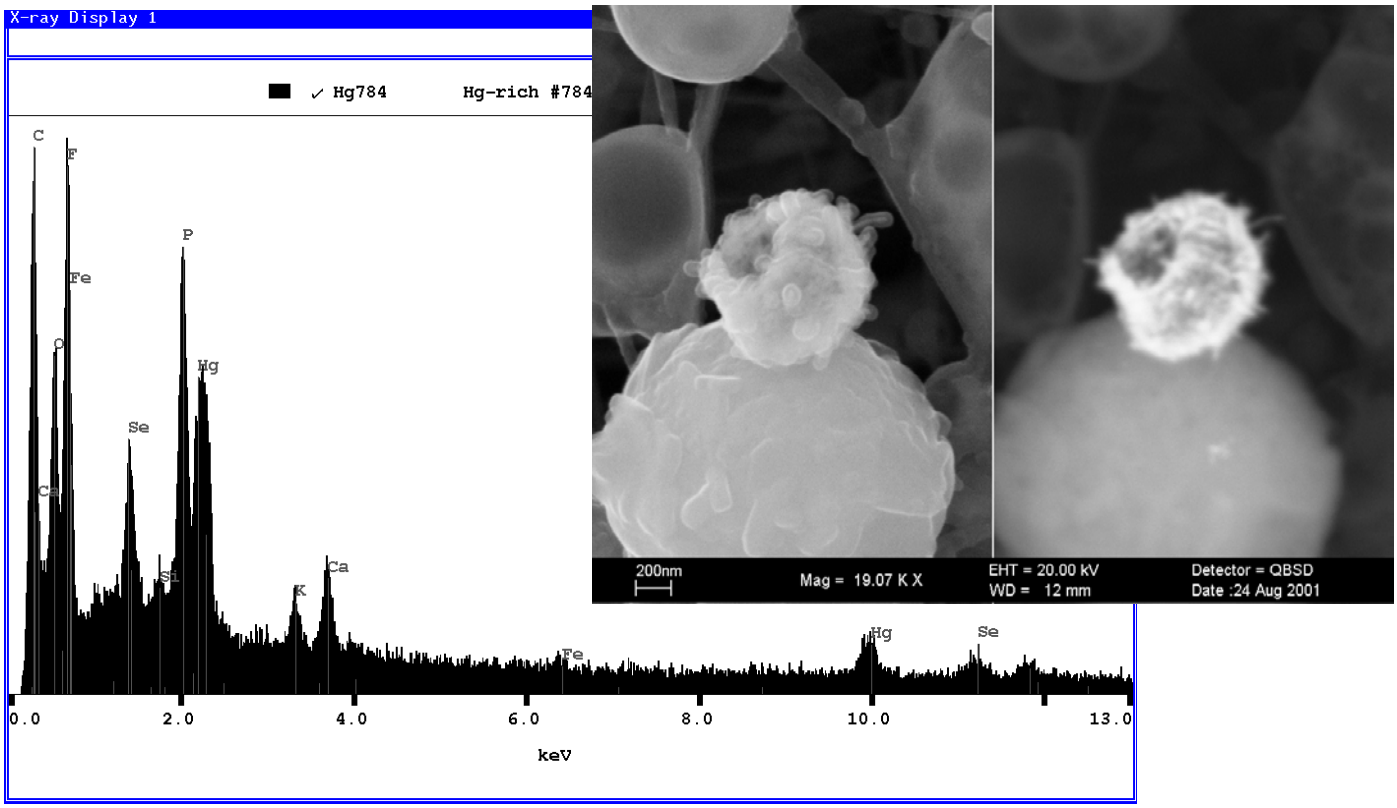

Figure 3-5d.

3.4.2 User-Defined Rules

The PSEM's off-line analysis software includes a program for the analyst to develop custom rules (ZepRule, Aspex Instruments, Delmont, PA). These user-defined particle classification rules can be based on size, shape (aspect ratio), elemental composition, X-ray counts, video level (grayscale brightness, reported as a numeric value) of the particle image, and/or any other parameter measured and recorded during the CCSEM analysis. Examples of user-defined rules are presented in Appendix C. The rules use greater than, less than equal to, addition, and subtraction to put boundaries on the values of each parameter used to define a rule. More than one parameter can be used to define a single rule. Rules are applied in sequential order to each particle until a particle class assignment is made; thus, each particle is assigned to only one class, and the order in which rules are listed is critical. In the examples in Appendix C, the first rule listed for both the fine and coarse particle samples serves to remove particles which were not in the aerodynamic size range of interest from further classification (i.e., coarse particles are excluded from fine particle classification, and vice versa).

Typically, rules are applied to each sample analyzed, and results evaluated by examining both measured parameters and particle images. Rules can then be changed or added based on these evaluations, and the process continues in an iterative manner until the particle classifications are judged by the analyst to be satisfactory, based on the uniformity of chemical and physical characteristics within a particle class. The rules can be applied to other samples to make minor adjustments and to test the robustness of the classification scheme, based on the uniformity of particle characteristics within each particle class both within a single sample and across all samples. It is recommended that the X-ray spectrum be reviewed to verify the identification of elements, such as trace metals, that are typically low in abundance and/or subject to significant interferences.

Particle classification in the PGT IMIX system is facilitated by the "Chemical Classification" program, and can be carried out on-line or off-line. In a similar fashion to the PSEM, particles are classified according to a set of user-defined rules. In contrast to the PSEM, however, the IMIX classification rules are based only on particle chemistry, typically expressed in terms of EDX peak-to-background values and relative peak ratios for the elements of interest. Thus, the IMIX class editor program does not allow one to combine a physical criterion such as "circularity", with EDX criteria (to define, for example, a class called "Spherical Fly Ash"). An example of an IMIX class file is that of quartz which must meet the following four conditions: (1) Net Si / Bkgnd Si > 10; (2) Net O / Bkgnd O > 3; (3) Net O / Net Si > 0.05 and < 0.5, and (4) (Net O + Net Si) / (Net O + Net Al + Net Si + Net S + Net K + Net Ca + Net Fe) > 0.7. The IMIX particle classification program also differs from the PSEM rule-based classification in that each IMIX feature is tested against *every* class file, without regard to order. Thus, one particle can be assigned to more than one class, if the defining rules are not mutually exclusive.

In addition to off-line classification, both the PSEM and the PGT systems allow the user to define rules to screen or constrain the particle data that is collected on-line. The on-line rules or "selection formulas" can employ a comprehensive set of arithmetic operators and functions, as well as basic logic operators which can be applied to virtually any measurable feature quantity. A common application of the on-line rules is to exclude particles from analysis that are either too small or too large. The PSEM allows on-line screening based on both physical and chemistry parameters, while the IMIX system "selection formulas" only screen particles based on physical parameters.

3.4.3 Cluster Analysis

Cluster analysis (CA) is a multivariate statistical technique used to reveal structure in large, multidimensional data sets. In the area of aerosol analysis, CA provides a statistical method for sorting particles into distinct groups separated from each other by chemistry, size, and/or morphological differences. It has been applied by researchers in source apportionment studies to help in the identification of emission sources (Section 5.1.3). The results of CA can also be used to generate user-defined rules for particle classification.

One research group at the forefront of developing cluster analysis techniques for use with electron probe or SEM/EDX data is that of R. Van Grieken and colleagues at the University of Antwerp. This group has developed a Windows-based software package for cluster and factor analysis, called IDAS, and has applied the tools of IDAS in characterizing aerosols by electron probe analysis and identifying their sources (Bondarenko et al., 1996). IDAS provides an easy-to-use interface to carry out two main multivariate analysis techniques, cluster analysis (CA) and factor analysis (FA). CA is implemented as a three-step procedure: Hierarchical cluster analysis (HCA) is the first step. Its results serve as an initial partition for nonhierarchical cluster analysis (NHCA). Finally, the internal structure of the obtained clusters and relationships between them can be revealed with fuzzy clustering analysis (FCA). FCA is implemented in IDAS as a two-step process. First, principal factor analysis (PFA) is used to estimate the "correct" number of factors and to calculate factor loadings and scores. The next stage, meaningful interpretation, can be done either with the help of abstract factor rotation (AFR) or with target transformation factor analysis (TTFA).

The feasibility of using IDAS software to identify sources of particles was explored in studies conducted by the NERL SEM/EDX Laboratory. The hypothesis was that if particle data from known, chemically distinct emission sources were fed into IDAS, the program should be able to sort the particles into distinct clusters in elemental space, with each cluster representing one of the sources. If this proved successful, the next step would be to apply cluster analysis to an ambient sample impacted by these sources and attempt to apportion each ambient particle to a specific source. For the preliminary tests discussed below, the source particle database comprised seven sources of

30 particles each. The 7 sources included six sources sampled in the Czech Republic city of Ostrava (Willis et al., 1997): mobile source emissions, stack emissions from two steel works, a coke oven battery, a sintering plant, a coal-fired power plant, and a coking plant. In addition, residual oil fly ash was characterized and included in the source particle database. In this preliminary attempt to use the cluster analysis software only particle chemistry was used. Future refinements of the technique may be able to incorporate particle size or shape parameters (e.g., aspect ratio or circularity) in addition to chemistry in order to further resolve clusters that may overlap in elemental space.

The first step in cluster analysis with IDAS is HCA. The results of HCA are presented in the form of a dendrogram starting with *N* leaves (*N* = number of particles) and terminating with a single group encompassing all particles. The user, relying on his knowledge of the air shed or on "stopping rules" generated within IDAS, must decide how many clusters are represented in the data, that is, where to terminate the dendrogram. IDAS includes built-in graphical support to display the stopping rules. Figure 3-6 shows a graph of stopping rules calculated for the seven-source data set. Four different tests can be applied to the data to predict the "true" number of clusters up to a maximum of 10. (For each test, a local minimum in the plotted line, or a strong deflection indicates the "best" number of clusters to use in subsequent analysis.) Generally, the "CAIC" test is most successful in determining the number of clusters. In Figure 3-6, the CAIC test (as well as the inflection in the DB plot) indicates seven clusters. Both the WB and SD tests would indicate eight clusters. Choosing seven clusters as the best number, IDAS calculates the population of each hierarchical cluster and identifies the location (cluster) of each individual particle. (HCA and NHCA are both "hard" clustering techniques in that each particle can be assigned to one and only one cluster).

Figure 3-7 is a graph of the resulting cluster populations. With our simulated data set, one would ideally expect a population of 30 particles in each of 7 clusters. As Figure 3-7 indicates, the emission sources are not totally distinct, causing some particles from different emission sources to be grouped together in the same cluster. By examining the location of each particle, we determined the following:

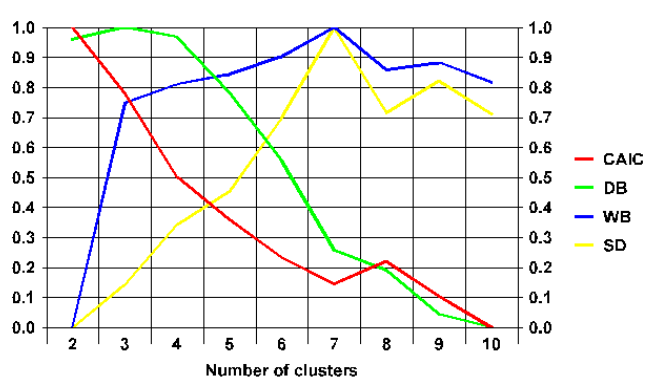

Figure 3-6. A plot of the "stopping rules"calculated for a simulated data set comprising seven emission sources. The plot displays the dependence of four different clustering criteria on the number of clusters. Local minima or inflections in the curves indicate the "best" number of clusters.

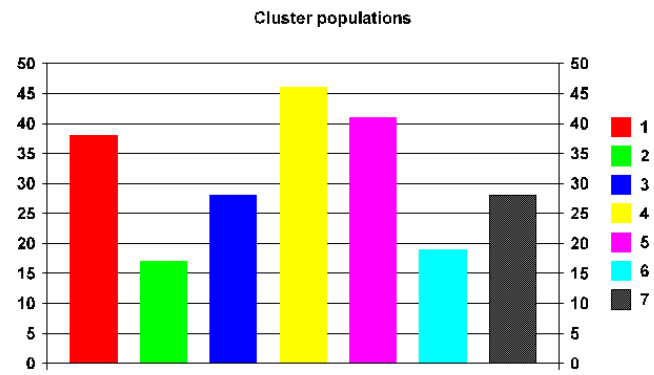

Figure 3-7. Cluster populations resulting from hierarchical cluster analysis. The data set comprised 30 particles from each of seven different emission sources. One would expect each cluster to contain 30 particles if all particles representing a given source were truly distinct from those of all other sources.

Cluster 1 represents the coal-fired power plant and in addition includes some mobile source particles.

Cluster 2 is a weak cluster containing particles from both the coke oven stack emissions as well as from mobile sources.

Cluster 3 represents the steel works source.

Cluster 4 is a combination of the coke oven stack particles and residual oil fly ash.

Cluster 5 represents the sintering plant.

Cluster 6 is dominated by mobile source particles, but includes some oil fly ash particles.

Cluster 7 represents the coke battery emissions.

The results indicate that residual oil fly ash and the coke oven stack emissions are somewhat overlapping clusters, and that the mobile source particles are scattered among four different clusters. The latter observation suggests that the mobile source sample may include particles emitted from other sources. (It is very probable, in fact, that the mobile source signature, which was collected in a busy traffic underpass, is actually a mixture of mobile emissions diluted by ambient aerosol.)

The clusters identified in HCA serve as the initial "seed points" for NHCA. NHCA produces somewhat revised cluster populations as shown in Figure 3-8.

IDAS also calculates statistics for each cluster, including the mean and standard deviations for each elemental species. Ideally, the mean elemental concentrations calculated for each cluster can be interpreted as source profiles. One could use these values to create user-defined rules for the PSEM to facilitate off-line sorting of particles into source-related clusters.

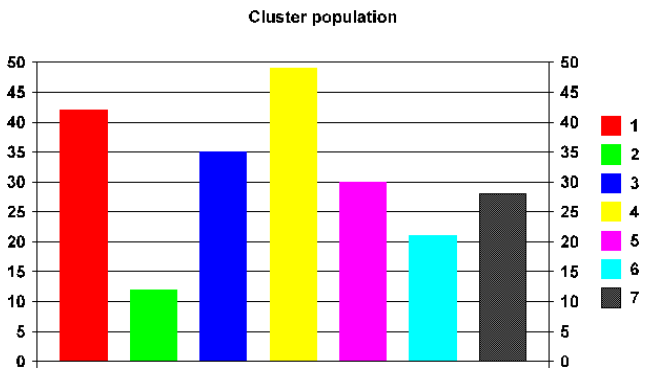

Figure 3-8. Revised cluster populations after non-hierarchical cluster analysis.

The authors of IDAS recommend that any conclusions about the structure of the data set should be based on comparison of the results of all three clustering techniques: hierarchical, non-hierarchical, and fuzzy. (The "fuzzy" technique was not explored in this preliminary study).

In a second application of CA to particle classification, CA was used to classify particles collected downwind from an industrial complex in Pocatello, Idaho. Chemistry and size data were collected by SEM/EDX on 314 particles between 2 and 15 μm in size. Hierarchical cluster analysis (HCA) was first carried out on the data using Ward's method and assuming a Euclidean distance metric (Statistica. Graphical tools estimated the "most likely" number of clusters to be seven. Non-hierarchical cluster analysis (NHCA) was then applied to the data using the seven HCA cluster vectors as initial seed points for NHCA. The identification of the seven clusters (based on the mean elemental composition of each cluster) and their abundance (number %) were as follows: (1) K-P-rich, 16.2%; (2) Ca-P-rich, 15.0%; (3) aluminum silicates, 20.4%; (4) Ca-Si-P, 19.4%; (5) P-O-rich, 6.1%; (6) Carbonaceous, 8.0%; and (7) quartz, 15.0%. Analysis of the particle size distribution within each cluster of particles could probably indicate which of these particle types is predominantly in the coarse-fraction, and therefore likely to be attributable to resuspended dust sources, and which types are predominantly in the fine-fraction, and therefore likely to be attributable to combustion sources.

3.4.4 Spectrum Matching

Another approach to particle classification has been developed on the PGT IMIX system. The IMIX system differs from the PSEM in that the IMIX system stores the complete EDX spectrum for a feature, while the PSEM typically stores only X-ray counts in user-selected elemental regions of interest. In effect the PSEM philosophy is to compress the raw spectral information into a small set of numbers that are easily manipulated and take up less disk space.

In the PSEM, particles are sorted into distinct chemical classes based on simple 4-element typing or more sophisticated user-defined rules involving the particle size, shape, and X-ray data. The process of generating these rules is typically an iterative process that can be very time-consuming and labor intensive and ideally is best done by an experienced microscopist. The ability of the IMIX system to save the raw spectra of particles allows for a purely mechanical particle classification scheme based on the similarity between the sample spectrum and stored standard spectra. The IMIX software includes a program called Spectrum Match, which performs a least-squares fit of an unknown spectrum against a library of (up to 200) standard spectra. The program outputs chi-square for all matches in order of ascending chi-square.

A new program built around the Spectrum Match program shows promise as a method for creating a user-defined number of particle classes from a collection of EDX spectra. The program performs essentially three tasks: (1) Given a collection of particle spectra, the script generates chemically distinct classes based on a least-squares match of the current particle spectrum against an evolving library of standard spectra representing different particle classes. (2) Given a library of standard spectra representing different particle classes, the script determines the best match for each unknown spectrum based on the chi-square of the least-squares match. (3) Given a library of standards (or particle types) the script performs a least-squares fit of all standards (or particle types) against each other in order to identify potential collinearities among the particle types.

Given a collection of source samples, it is envisioned that the new script will be able to generate source profiles each of which consists of one or more particle types and their relative abundance. The program will then match particles from ambient samples against the library of source types to apportion the ambient sample to contributing sources. The source apportionment can be carried out using conventional Chemical Mass Balance (CMB), in which the usual elemental concentrations are replaced with abundances of the different particle types.

In order to generate particle classes "from scratch" (e.g., a new source sample), the user inputs the chi-squared cut point, which determines how many different classes will be created from a collection of particle spectra. A small chi-square will typically result in the creation of more classes, while a large chi-square will produce fewer classes with broader chemical definition. The script operates as follows: Particle spectra are read into the script successively and compared to standard spectra, which are continuously evolving. The very first particle spectrum is matched against itself to create the first standard (Type 1) since no standard spectra exist initially. The second particle is compared to the Type 1 spectrum. If chi-square of the least-squares fit is greater than the user-selected cut point, then the second particle is classified as a new type, and its spectrum becomes the initial spectrum representing Type 2. If, on the other hand, chi-square for the match is less than the cut point, then particles 1 and 2 are both considered to be Type 1, and the Type 1 spectrum

is subsequently replaced by the average of spectrum 1 and spectrum 2. This continues until all particles have been matched.

The least-squares approach described above has some inherent flaws that might invalidate the approach. As the Type 1, Type 2, . . . Type N spectra evolve, particles initially assigned to a particular type may no longer fit that type by the time all particles have been classified. This potential problem is dealt with as follows: At the end of the initial sorting process, the resulting particle types are frozen and the collection of particles is matched against these final, fixed types. Another potential problem with the classification scheme is that the shift in the "centroid" of a given type with the addition of the nth particle is weighted by $1/n$ where n is the number of particles in that class. Although the final spectrum representing the class is the simple arithmetic average of all member spectra, the membership in each type is largely determined by the first few particles in the particle list coupled with the user's choice of chi-square. If the particle list is shuffled and the script is re-run, different particle classes will be generated.

In order to test the new script, approximately 50 particles from each of 20 sources were analyzed by EDX. Spectra for each source were individually run through the script to generate particle types representing that source. A chi-square cutpoint of 1.5 was rather arbitrarily chosen. Some sources were represented by only a single particle type (monodisperse), while other sources, especially soils, were characterized by 10 or more types (multidisperse). A total of 73 source types were generated, but there were a number of collinearities (arbitrarily determined by chi-square $\leq$ 0.5) among the types. The same collection of 1150 spectra used to generate the source profiles were then treated as a proxy for ambient particle spectra and matched against the resulting library of source types. The results of the particle classification are shown in Figures 3-9a and 3-9b.

The 20 different sources are shown along the x-axis of each figure. The number in parentheses is the number of particles used to generate the source types. The sources are listed in more detail below.

Figure 3-9a shows the raw apportionment results after matching the "ambient" particle spectra against the library of 73 particle types. The results are totally unconstrained by source profiles, i.e., all particle types are assumed to be independent from each other. It was hoped that by making use of the source profiles to constrain the model fit that a more accurate source apportionment could be obtained. The results, shown in Figure 3-9b, were obtained using the CMB model and the source profiles obtained from the least-squares approach. The uncertainties in the "ambient" CMB file for each particle type were largely determined by the number of other types judged to be collinear with the selected type. Pairs of types whose spectra matched each other with a chi-square $\leq$0.5 were assumed to be collinear. In the worst case, one soil type was collinear with 19 other particle types. The uncertainty associated with this type in the CMB input file was therefore made to be very large. The raw apportionment results in Figure 3-9a and the refined CMB results in Figure 3-9b are very similar, and it is not obvious that the apportionment results improved with the CMB calculations.

The test results above look promising. Ideally the calculated/true concentration for all sources should be unity. The largest deviation from unity occurs for the "sticky carbon tab" source, for which there was only a single particle represented in the data set. Errors for the highly collinear sources were generally in the range of 20% to 35%. In one sense, the result represents a best case scenario in that the particle types were generated from the same spectra that were subsequently matched against the particle types. On the other hand, the test case presented an unusually difficult challenge for the methodology because of the similarities between the Brownsville Soil, Czech Soil, Arizona Road Dust, Mt. St. Helens Ash, and FMC Shale samples. It must be emphasized as well that individual sources were typically represented by only about 50 particles, whereas studies described in Section 4.6.2 demonstrate that about 500 particles are needed to adequately represent ambient and some multidisperse source samples. Better statistics should improve accuracy and confidence in the source profiles generated by the method, which in turn may improve the CMB results. Finally, for this initial test, the chi-square cut point for creating new particle types was arbitrarily chosen as 1.5. A lower value for the cut point may yield some improvement in the results.

Potential advantages of the least-squares classification scheme are as follows:

- Particle types are generated via a purely mechanical and objective process without the need for experienced human input (other than to select the chi-square cut point that determines the number of particle types).
- The PGT software allows up to 200 different particle types to be used in the classification process. This may permit more highly resolved and more accurate source profiles than can be obtained by user-defined rules.
- The classification script is relatively quick: Particle types can be generated from a collection of 500 particles in roughly 1.5 hours. Matching 500 particles against a library of 73 types takes approximately the same amount of computer time with the present PGT Sparc5 computer. With an upgraded computer, the time required for these tasks could probably be cut in half at least.
- The output of the classification script (source profiles expressed as percent abundance of different particle types and the sorted ambient data) can be input directly into the CMB model for source apportionment calculations. A statistically valid treatment of uncertainties in the source and ambient CMB data files, however, needs to be developed.

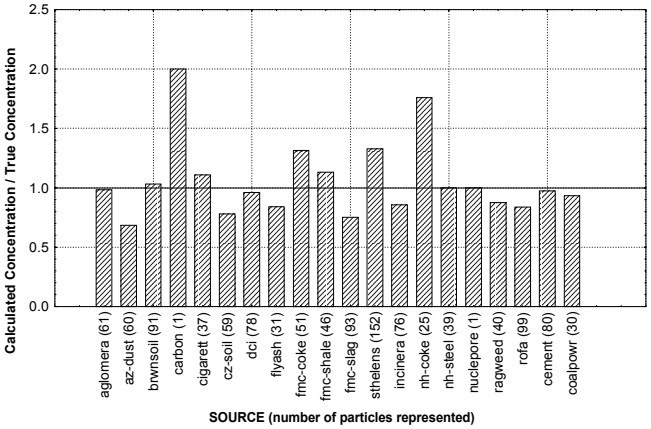

Figure 3-9a. Unconstrained source apportionment results based on least-squares match of "ambient" particle spectrum against a library of chemically distinct source types.

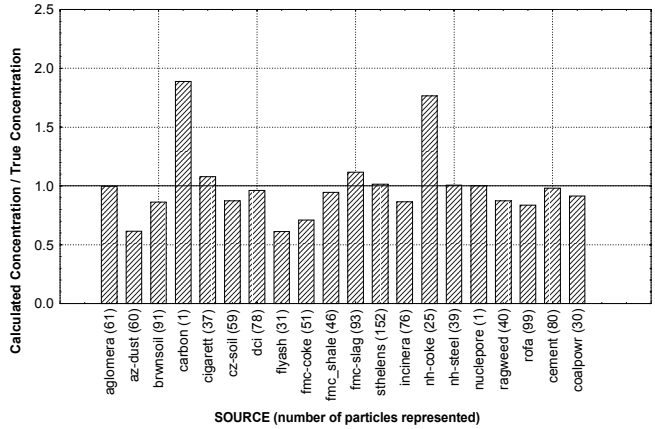

Figure 3-9b. Refined source apportionment results after running raw source apportionment data through the chemical mass balance model. The CMB apportionment results are constrained by the source profiles generated by the least-squares method.

aglomera = Aglomerace sintering plant in Ostrava, Czech Republic

az-dust = Arizona Road Dust

brwnssoil = Brownsville (TX) soil

carbon = blank sticky carbon tab (common substrate for SEM samples)

cigarett = cigarette ash

cz-soil = soil collected in Teplice, Czech Republic

dci = Dade County (FL) resource recovery waste incinerator

flyash = fly ash from coal-fired power plant

fmc-coke = coke used in elemental phosphorus production plant

fmc-shale = phosphorus shale used in elemental phosphorus production plant

fmc-slag = slag product produced at elemental phosphorus production plant

sthelens = volcanic ash from Mt. St. Helens

incinera = medical waste incinerator in S. Florida

nh-coke = Nova Hut coke battery emissions (Ostrava, Czech Republic)

nh-steel = Nova Hut Steel Works emissions (Ostrava, Czech Republic)

nuclepore = blank Nuclepore substrate for SEM samples

ragweed = ragweed pollen

rofa = residual oil fly ash

cement = Tarmac cement plant in S. Florida

coalpwr = emissions from Trebovice coal-fired power plant in Ostrava, Czech Republic

Disadvantages of the PGT classification script are as follows:

- The classification scheme is restricted to using chemistry data only in the least-squares matching algorithm. Particle size and morphology data would be difficult to incorporate into this scheme. This information is, however, collected during the initial EDX analysis of the particles and could be reviewed manually by the microscopist to further refine the particle classification results obtained by using chemistry only.
- The current least-squares approach may have a fundamental difficulty distinguishing spectra that are similar in terms of abundances of major elements but differ in abundances of minor elements. For example, lead-bearing soot particles and biological particles are both dominated by carbon. The least-squares fit to these spectra may be driven largely by the carbon peak, while the crucial differences among the minor Pb, P, K, and Cl peaks may be largely ignored in the least-squares approach. As a result, the least-squares approach may have trouble classifying carbon-rich particles distinguished by minor species. This potentially serious problem needs to be examined in more detail. A weighted least-squares approach may be required where minor peaks are weighted equally with major peaks in the least-squares fit.
- Storage of EDX spectra uses considerable disk space and has already caused some difficulty with the Sparc5 computer. Along with CPU speed, problems of limited disk space might be largely eliminated with an upgraded Sparc workstation.

3.4.5 Neural Networks

During the past decade there has been considerable activity in the application of artificial neural networks (ANNs) to particle classification. Artificial neural networks are algorithms that attempt to mimic the human brain's approach to processing and classifying data. ANNs are a relatively new tool for advanced

information and data processing and have found impressive success in areas such as pattern matching and classification and data clustering. The theory behind ANNs is beyond the scope of this document. However, descriptions of ANNs are numerous on the web and in the literature.

Wienke et al. (1994) and Xie et al. (1995) used a specific type of ANN called adaptive resonance theory or ART-2a (Carpenter et al. 1991) to rapidly identify particle shape from the binary SEM particle image. The resulting shape parameter was then combined with chemical composition data and input into a second ART-2a net to yield a "more intelligent" classification of CCSEM data. The authors investigated the potential of a ART-2a for unsupervised classification (clustering) as well as supervised particle classification using training sets. An important advantage of ART networks, compared to other supervised ANNs is the ability of ART to dynamically create new classes in response to novel particle types which were not represented in the training set. Applications of neural nets in the area of environmental studies have been pioneered by Phil Hopke and colleagues at Clarkson University. (Hopke and Song, 1997; Xie et al., 1994; Song et al., 1999; Song and Hopke, 1996). Conventional receptor modeling has difficulty in determining the contributions of very similar composition source material. Song et al. (1999) used a combination of the ART-2a neural network and the back-propagation (BP) neural network to apportion the mass contributions of three different crustal sources to ambient particle samples. It is conceivable that in the future, a neural network could be trained to monitor a CCSEM analysis, providing data quality control in real-time, identifying statistical outliers in the data, and determining when to terminate an analysis (e.g., when additional data are changing the results negligibly).

Chapter 4
Data Quality and Validity

4.1 Instrument Calibration and Maintenance

Instrumental factors impacting the validity of the SEM/EDX data include (1) accuracy of the SEM magnification (which affects the accuracy of the particle size measurements) and (2) the gain calibration of the EDX amplifier. The latter affects the accuracy of the X-ray peak identification subroutine that assigns element labels to the spectral lines according to the channel (energy) locations of the peak centroids.

4.1.1 Magnification Calibration

The magnification of the SEM is primarily calibrated by using the MRS-3 magnification calibration standard (Geller Microanalytical Laboratory, Topsfield, MA). The MRS-3 comprises a series of precisely etched geometric patterns that allow the SEM mag calibration to be accurately checked at mags ranging from 10x to 50,000x. The MRS-3 is available with or without traceability to NIST. The standard used in the SEM laboratory is not traceable; however, the manufacturer has never seen a pattern that deviated by more than ±0.5 μm for the 50-μm and 500-μm pitch, or ±0.1 μm for the 2-μm pitch. The MRS-3 is used to determine SEM error in measuring spacings on precisely etched grid patterns ranging from 2-μm pitch to 500-μm pitch. The maximum observed errors in either the LEO S440 or the PSEM was have been on the order of +4%. As discussed below, sources of error other than the magnification calibration appear to be as important or more important in determining the SEM's accuracy in sizing particles. Thus, magnification calibration errors of up to a few percent are probably acceptable and do not need to be corrected by the vendor.

The use of polystyrene latex beads for calibrating or checking SEM magnification has been carefully explored in our laboratory with discouraging results. For reasons that are not yet understood, we have been unable to get agreement between the MRS-3 standard and the NIST-certified PSL bead diameters on either the PSEM or the LEO S440. The discrepancy between PSL beads and the MRS-3 standard is greatest for submicrometer beads, where pixel resolution and particle size increase due to gold or carbon coating can cause significant error, but these errors do not appear to explain all of the observed disagreement.

The magnification calibration for both SEMs appears to be quite stable over time, however, a calibration check of the SEM is recommended at least twice a year. Calibrations for both SEMs are routinely checked during the annual preventive maintenance visits for each instrument. Using the MRS-3 standard we will measure the magnification calibration errors of the two SEMs for at least four magnifications spanning the range of 200x to 20,000x. The measured dimensions in both X and Y as well as the ratio of the two must be within spec before the instrument is used. A record of the results should be maintained so that any drift in the magnification of either instrument over time will be noted. If deviations from the MRS-3 standard exceed 5%, the instrument's magnification calibration is adjusted by the field engineer, or we will make the adjustments ourselves if possible.

4.1.2 EDX Spectrometer Gain Calibration

Both EDX systems use software to recalibrate the EDX spectrometer gain. The spectrometer gain determines the keV per channel for the EDX spectrum, which in turn provides the basis for X-ray peak identification. EDX gain can be calibrated using a gold/copper standard since X-ray lines from these two elements span almost the entire spectral range of the detector. In order to recalibrate the spectrometer gain, it is necessary only to acquire a spectrum of the Au/Cu standard and to run the autocalibration routine. Recalibration ensures that the centroids of the Au and Cu X-ray lines (and by extension, the lines of all other elements) coincide with the corresponding line markers generated by the EDX software so that peaks in the EDX spectrum are assigned to the correct elements. EDX peak positions should be within 10 eV of the tabulated values. Periodic checks on the PSEM and IMIX energy calibrations indicate that the calibrations are very stable. The energy calibrations are checked at least once per year as part of each instrument's annual preventive maintenance.

4.1.3 Window Contamination Check

Over time, deposits including ice or oil can build up on the ultra-thin window of the EDX detector, resulting in a loss of detector sensitivity. Changes in detector sensitivity can be monitored fairly accurately by tracking K_α/L_α ratios for Cu or Ni over time. Because X-ray absorption losses due to window deposits will be greater for the L_α line than for the more energetic K_α line, the K_α/L_α ratio will increase over time as deposits build up on the detector window. We typically use a copper grid as a sample. When performing a detector sensitivity check, one should always use the same probe current, working distance, and X-ray count rate whenever checking the K_α/L_α ratio. If loss of sensitivity becomes significant, the detector window can be cleaned, using extreme caution, either by the vendor or by the user.

4.2 Precision and Accuracy of Particle Volume Estimates

Particle sizing error was investigated in the PGT and PSEM systems. In each system, we imaged and sized a roughly spherical gold particle (diameter ~ 1.3 μm) and an irregular, flattish particle of lutetium oxide (average diameter ~ 1.6 μm) at five magnifications (1000, 2000, 4000, 10,000, and 20,000). For the PGT system, field images were acquired at 1024 by 1024 pixel resolution prior to particle sizing. This resolution yields calibration scales of approximately 0.31, 0.156, 0.077, 0.031, and 0.0156 μm/pixel for the five magnifications above. The PSEM software is designed such that once a feature has been located by searching the field along grid points, the spacing of the grid points is reduced to provide higher pixel resolution for sizing the feature. For the PSEM, the measurement grid spacing was set to the highest possible resolution, corresponding to 0.128, 0.064, 0.031, 0.013, and 0.006 μm/pixel at the five mags. Thus, under the conditions of this test, the PSEM has approximately 2.5 times better pixel resolution than the PGT system. The gold and Lu_2O_3 particles selected for sizing comprised approximately 10–12 pixels in the PSEM at 1000x, the minimum recommended number of pixels needed to define a feature. The magnification in the PGT system must be greater than 2000x in order for the minimum pixel size threshold to be exceeded. Even at 4000x, a one-pixel error in the diameter of a 1.3-μm sphere represents a volume error of approximately ±19% in the PGT system and ±7% in the PSEM.

For the PGT system, particle volume was calculated at each mag using the following four volume formulas:

$V_{rjl} = \pi/6 * D_{max} * D_{min}^2$, where D_{max} and D_{min} are the maximum and minimum of 12 diameters (PGT) or 16 diameters (PSEM) through the particle center of mass;

$V_{avg_dia} = \pi/6 * D_{avg}^3$;

$V_{sphere} = 4/3 * \pi^{-1/2} * Area^{3/2}$, where Area = projected area of the particle; and

$V_{prolate} = (8/3\pi) * Area^2 / D_{max}$

The four formulas reduce to the identical formula for perfect spheres, but can yield significantly different volumes for a non-spherical particle. V_{rjl} is the default formula for calculating particle volume in the PSEM. Like $V_{prolate}$, V_{rjl} assumes a prolate spheroid rotated about the semi-major axis. The difference between the two formulas is that $V_{prolate}$ is based on the projected pixel area of the particle, while V_{rjl} uses the product of measured diameters D_{max} and D_{min}. Errors in particle volume were computed relative to the "true" volume which was assumed to be the volume of the particle measured at 20,000x (least affected by pixel resolution error) using the prolate sphere formula, $V_{prolate}$. (This formula yielded the best agreement between the SEM-determined mass and the known gravimetric mass of a lutetium oxide sample - see Section 4.3).

Volume calculation results for the PGT system and the PSEM are shown in Figures 4-1a (gold particle) and 4-1b (lutetium oxide particle). The PSEM and PGT measurements were made on different, but similarly sized, particles. Four different formulas were used to calculate particle volume for the PGT system while a single formula, V_{rjl}, was used for the PSEM. Magnification calibration errors have been corrected at each magnification using a magnification calibration standard.

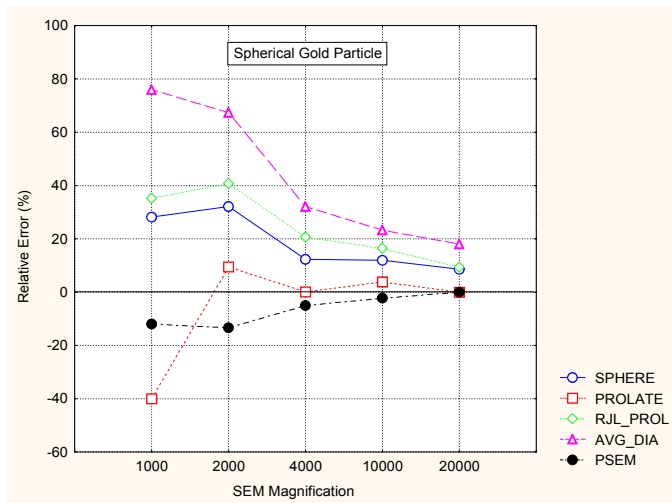

Figure 4-1a. Relative volume error for a 1.3-μm quasi-spherical gold particle as a function of SEM magnification for PGT system (four curves) and PSEM (one curve).

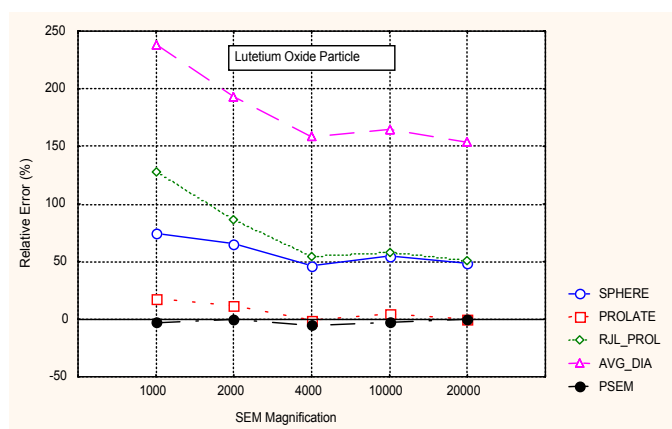

Figure 4-1b. Relative volume error for a 1.6-µm lutetium oxide particle as a function of SEM magnification for PGT system (four curves) and PSEM.

As expected, the PGT errors calculated from the four volume formulas for the quasi-spherical gold particle tend to converge at high magnification. True convergence is not expected, however, since the particle is not truly spherical. Compared to V_{rjl}, V_{avg_dia}, and V_{sphere}, the area-based prolate formula, $V_{prolate}$, and the PSEM volume calculation are less sensitive to changes in the SEM magnification above 2000x.

The four PGT volume estimates for the non-spherical lutetium oxide particle (Fig. 4-1b) show little convergence to the "true" volume as magnification increases, but instead show that, for non-spherical geometry, the four formulas calculate significantly different volumes. Volumes calculated using V_{avg_dia} consistently show the largest errors. Again, $V_{prolate}$, and the PSEM volume calculation are least sensitive to changes in the SEM magnification.

If accurate particle volume is a concern in an automated analysis, these results suggest that, for particles on the order of 2 μm or less, one should use a minimum magnification of 4000x for the PGT system and 1400x for the PSEM. (The magnifications used in Figures 4-1a,b assume the display monitor as the output device. The PSEM magnification is referenced to the thermal printer output and is approximately 2.9 times smaller than the magnification referenced to the display monitor. A mag of 1400x on the PSEM corresponds to about 4000x on Figures 4-1a,b).

4.3 Precision and Accuracy of Particle Mass Estimates

In order to assess the precision and accuracy of mass estimates from SEM data, a sample of lutetium oxide particles was sized in the PSEM. The PSEM-calculated mass of this sample was a factor of 4.33 higher than the gravimetric mass. This discrepancy was attributed to errors associated with the assumption that all particles are prolate spheroids. The same filter was analyzed using the LEO/PGT system in order to verify the PSEM results.

Mass reconstructed from individual particle analysis is critically dependant on volume estimates. Four different formulas (presented in Section 4.2), including the PSEM formula for prolate spheroid volume, V_{rjl}, were used to calculate particle volume and particle mass in data collected with both SEMs. One objective of this exercise was to determine which of the above volume formulas yields the best agreement with the gravimetric mass for nonspherical particles. Results of the PSEM and LEO/PGT analyses are shown in Table 4-1. All SEM mass estimates greatly overestimated the gravimetric mass of the sample (22 μg). Best agreement with the gravimetric mass was obtained using $V_{prolate}$ for the LEO/PGT system (236% error) and V_{rjl} for the PSEM (323% error). The maximum and minimum mass estimates for the LEO/PGT and PSEM systems differed by factors of 2.1 and 1.4, respectively, indicating considerable sensitivity to the choice of volume formula.

The large errors in Table 4-1 are attributed to the flat, plate-like morphology of the Lu_2O_3 particles, which were poorly sized

Table 4-1. LEO-PGT and PSEM Analysis of a 22-μg Lutetium Oxide Sample: Estimated Particle Mass Using Different Volume Formulas and Associated Errors

	$V_{prolate}$	V_{sphere}	V_{rjl}	V_{avg_dia}
LEO/PGT (μg)	74	99	116	157
LEO/PGT error (%)	236	350	427	613
PSEM (μg)	103	132	93	125
PSEM error (%)	368	500	323	468

using the volume formulas above. The shape of the Lu_2O_3 particles is atypical of environmental aerosols which are typically more round than flat; thus the errors in Table 4-1 represent an extreme case. Nevertheless, these results demonstrate that particle shape is a major factor in the error associated with inferring a three-dimensional particle volume from a two-dimensional particle diameter or projected area. For an unusual aerosol sample with aytpical particle shape, one may need to examine the sample first and choose a more appropriate volume formula, before attempting to calculate the bulk mass of the sample.

Similar analyses were performed on Arizona Road Dust since the results would have a more direct bearing on SEM-derived mass estimates for typical PM samples. Arizona Road Dust is a test material with a bulk density of 2.65 g/cc and a well-characterized particle size distribution. Examination by SEM showed that particles were generally more round than flat. Two samples were prepared from the "coarse" size fraction of the Arizona Road Dust. Dust was suspended in propanol, aerosolized using a glass bulb nebulizer, and manually sprayed onto tared 25-mm Nuclepore filters placed on a glass frit and pumped from the backside. After loading, the filters were equilibrated and weighed to determine the mass loadings. The two filters had nearly identical loadings (31 and 32 μg, respectively). Repeat measurements were made on both samples in order to provide a measure of precision in SEM-determined mass loadings via PSEM analysis. Efforts were made to maintain the same measurement and detection thresholds from run to run, if necessary via slight adjustments to the brightness.

The precision of three repeat analyses of the *same* fields (227 fields, 6000 particles) yielded a precision (relative standard deviation) of 3.5%. Eight successive analyses of *random* fields (6000 particles, ~ 110 fields) yielded a precision of 11%. Because of the small mass loadings on these samples, a few anomalously large particles can give a significant positive bias to the SEM mass estimate. In one analysis, for example, the largest particle (after normalizing for the fraction of sample analyzed) accounted for 25% of the total estimated mass loading. In order to eliminate particles that unduly bias the results, all analyses for a given sample were combined into a single analysis and the resulting particle size distribution was plotted. The largest six particles for each of the two samples were identified as outliers and eliminated from the data sets before estimating the mass loadings. The estimated mass loadings for our two Arizona Road Dust samples were 24.4 ± 2.4 μg and 35.9 ± 4.1 μg, respectively, for the 31-μg and 32-μg samples. These

represent errors of -21% and +12%, respectively. Note that without eliminating the six largest particles, this last mass loading was estimated to be 41.1 μg. Given the ability of a few large particles to severely bias the mass results, the accuracy of these mass estimates probably cannot be improved except by analyzing a much larger fraction of the sample. (Each of the individual analyses represented between 0.06% to 0.1% of the total filter.)

The setting of the PSEM measurement threshold is extremely critical in determining a sample's size and mass distribution. This sensitivity is illustrated in Figure 4-2, which shows size distributions for back-to-back analyses (6000 particles in randomly selected fields) of the 31-μg sample.

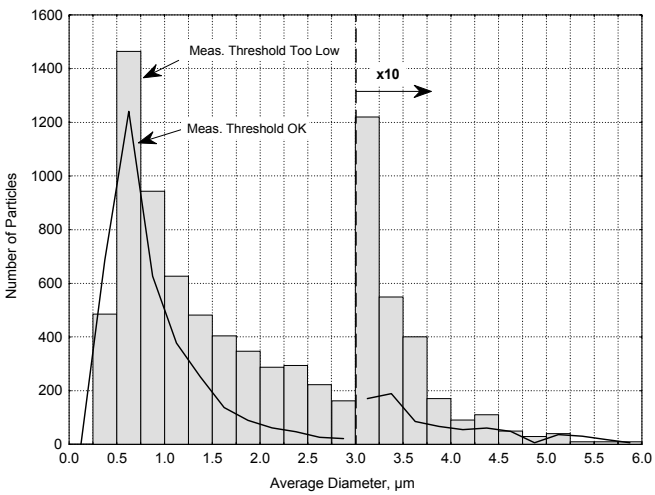

Figure 4-2. Back-to-back particle size distributions using the PSEM with different measurement threshold settings.

The number of particles for both the line plot and the bar plot were normalized to the same analyzed area of the sample and should, in principle, be very similar. The bar plot, however, shows many more particles detected in nearly all size bins than the line plot. Furthermore, the estimated mass loadings were 59.4 μg versus 25.9 μg for the analyses depicted in the bar and line plots, respectively. The large discrepancy in the two size distributions is a consequence of setting the measurement threshold too low (too close to the noise level) in the former plot. Although the threshold appeared to be set properly on the few fields examined prior to the start of the analysis, a number of fields analyzed during the run had slightly higher brightness levels, which elevated the noise level to approximately the measurement threshold. Particles that should have been excluded for being below the minimum size threshold (0.4 μm) were then oversized and counted. Particles already above the minimum size threshold were pushed into larger size bins. These results emphasize the importance of setting the analysis thresholds properly, collecting all field images, monitoring the SEM periodically during a CCSEM analysis, and carefully examining the data on a field by field basis after the analysis.

It is important to keep in mind in this discussion that the mission of SEM/EDX is not to replace bulk analysis, but to complement bulk analysis by providing information not available via bulk techniques. SEM should not be considered as a tool for determining bulk, macroscopic properties of a sample such as the sample mass or the bulk sample composition. However, the "ball park" bulk mass estimates extrapolated from microscopy data should be useful as a QC check on the sample or on the quality of the SEM analysis. SEM-based mass estimates that differ greatly from the gravimetric mass may thus indicate problems with the sample such as highly-non-uniform particle loading, contamination of the sample by foreign particles, or gross overestimate or underestimate of carbonaceous mass.

4.4 Analysis of Ultrafine Particles

In light of recent studies that show an association between human morbidity and exposure to air particulates, especially particles in the fine fraction (< 2.5 μm, aerodynamic), there is interest at the U.S. EPA in identifying tools that can characterize fine and ultrafine particles in the air (size, concentrations, chemical composition). Ultrafine particles are particles smaller than 0.1 μm. The following paragraphs assess the capability of current technologies to characterize ultrafine particles.

4.4.1 Limitations of the Present NERL SEM Facilities

The LEO S440 high-resolution SEM has a practical minimum size limitation of approximately 0.1 μm, the upper size limit for ultrafine particles. This limit is illustrated in the photomicrograph in Figure 4-3, which was obtained with SEM operating conditions optimized for image resolution: The working distance was set to 8 mm, the beam energy was set to 30 kV, and the probe current was minimized at 1 picoamp (pA). The electron source was a lanthanum hexaboride crystal (LaB_6) operated near full saturation. (The S440 can also be operated with a tungsten gun, but LaB_6 is a brighter source and provides superior image resolution.) Figure 4-3 shows the image of a particle approximately 0.1 μm in size sitting on a polished carbon planchet. The feature is poorly resolved and devoid of morphological information. Although the feature could be sized manually, the accuracy would be limited to perhaps 20% due to the "fuzzy" edges. Contrast differences between particles and the background are critical to identifying and sizing particles by automated techniques, which would be essential if such analyses are to be carried out routinely. But feature contrast degrades as the feature size approaches the practical limit. The poor contrast observed in Figure 4-3 would not allow for accurate counting and sizing of ultrafines in the automated mode with the present instrument.

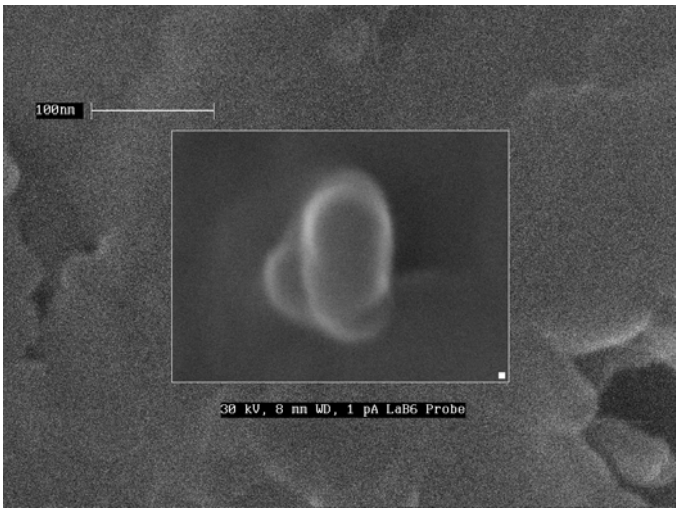

Figure 4-3. Photomicrograph taken with LEO S440 SEM. The particle approximates the minimum feature size that can be analyzed with the present SEM.

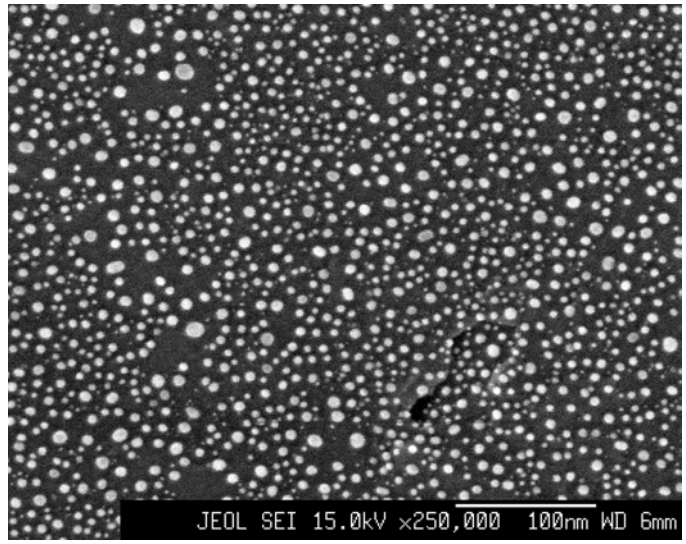

Figure 4-4a. FE-SEM image of gold particles on a carbon substrate. The image was acquired with a JEOL JMS-6340F FE-SEM. (Courtesy of JEOL, Inc., Peabody, MA).

4.4.2 Other Microscopic Techniques

There are two microscopy alternatives available for sizing and counting ultrafine particles: (1) field-emission SEM (FE-SEM), and (2) transmission electron microscopy (TEM). The two systems are similarly priced at about $330K. FE-SEMs have excellent imaging resolution due to the field-emission source and are capable of identifying and sizing particles down to approximately 0.02 μm; smaller particles should be imaged with a TEM. Figures 4-4a and 4-4b are photomicrographs taken with different FE-SEM instruments. Figure 4-4a was acquired with a JEOL Model JMS-6340F FE-SEM and shows gold particles on a carbon substrate. The advertised resolution of this instrument is 1.2 nm at 15 kV. Figure 4-4b was acquired with a LEO 982 FE-SEM and shows TiO_2 particles (the smallest of which is approximately 0.07μm). Note that excellent resolution is obtained at only 3 kV.

TEM is probably a more robust imaging method for the ultrafine size regime (Steel, 2001). The choice between TEM and FE-SEM may depend on whether or not particle chemistry is required. Typically, X-ray analysis requires electron probe energies of at least 15 kV. At these energies, the effective excitation volume from which X-rays are detected is on the order of 1 μm^3, a volume thousands of times larger than the volume of an ultrafine particle. For FE-SEM, in which particles or air filters are analyzed on stubs just as in conventional SEM, EDX analysis of ultrafines would be meaningless since virtually all X-rays would be generated by background. If particle chemistry is required, then a TEM operated in the scanning mode (STEM) with an X-ray detector (typically called an analytical electron microscope or AEM) is the best and perhaps only choice of instrument. In the transmission mode, X-ray analysis can be meaningful since very few X-rays are produced by background. The major disadvantage of TEM is that sample preparation is considerably more difficult and time-consuming. In order to analyze a section of an air filter, for example, the filter substrate would have to be dissolved and the particles redeposited on a thin film supported by a TEM grid. This raises concerns about the potential for altering the particle chemistry or morphology. TEMs and FE-SEMs can have automated feature analysis capabilities, but feature contrast may be a problem, particularly for FE-SEMs, depending on the particle and substrate type.

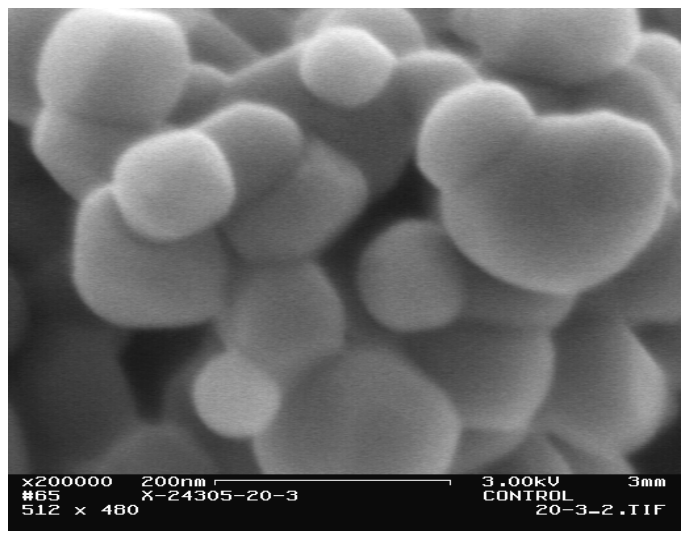

Figure 4-4b. TiO_2 particles imaged by a LEO 982 FE-SEM operated at 3 kV. (Courtesy of Rick McGill, Eastman Chemical Co., Kingsport, TN).

Related to the analysis of ultrafines is the question of how ultrafine samples should be collected for either FE-SEM or TEM. Polycarbonate screen membranes with 0.1-μm pores have essentially unity collection efficiency for particles at least down

to 0.035 μm. One suggestion is to use a micro-orifice impactor with Al-foil impactor substrates for FE-SEM; for TEM, collect ultrafines directly onto a TEM grid mounted in the micro-orifice impactor (Wight, 2001).

The use of atomic force microscopy (AFM) to image ultrafine particles has been investigated in several laboratories. Researchers have found that AFM is limited as a tool for imaging ultrafines by artifacts due to convolution of the tip shape with surface topography (Van Cleef et al., 1996). Using both high-resolution SEM and AFM, Wurster and Ocker (1993) analyzed 0.040-μm indium particles evaporated onto a vitreous carbon substrate. The authors concluded that AFM images have to be carefully interpreted because the unprocessed image represents an interaction of the scanning tip shape with the real sample topography. At this time, it appears that AFM is not a viable alternative to FE-SEM or TEM.

4.4.3 Non-Microscopic Techniques

Non-microscopic approaches for determining size distributions and concentrations of ultrafine particles directly in real-time include the differential mobility particle sizer (DMPS) and the scanning mobility particle sizer (SMPS). Both are capable of measuring airborne particle size distributions in the submicrometer range. The DMPS has a particle size range of approximately 0.01 to 1 μm, while the SMPS has a size range of 0.005 to 1 μm. Both the DMPS and the SMPS systems include a condensation particle counter (CPC) that determines particle concentrations in each size bin. Unfortunately, the particle size measured by such devices are given in terms of the "mobility equivalent diameter" rather than aerodynamic diameter, which is more relevant. The Electrical Low Pressure Impactor (ELPI, Marjamcki et al., 1997) is a new instrument that combines a conventional low-pressure cascade impactor for *aerodynamic* particle size classification and an electrical detection system for aerosol concentration determination. The size resolution of the ELPI is, however, limited by the design of the cascade impactor. The impactor used by Marjamcki et al. has 12 stages evenly spaced between 0.03 μm and 10 μm.

4.4.4 Ultrafine Summary

The NERL SEM/EDX laboratory is presently equipped to routinely count and size particles down to a few tenths of a micrometer in size. More powerful tools are needed to characterize ultrafine particles. If particle chemistry is not required and particles smaller than approximately 0.02 μm are not of primary interest, then the FE-SEM is probably the instrument of choice. Alternatively, if particle chemistry is required in addition to counting and sizing and if particles smaller than 0.02 μm are of interest, then an AEM is recommended with the added caution that there are concerns about sample preparation. If ultrafine size distributions and particle concentrations are of primary interest, these can be measured in real time using differential or scanning mobility particle sizers.

4.5 Carbonaceous and Submicrometer Particles

Conventional wisdom holds that EDX analysis of submicrometer particles is difficult and unreliable. The problem is that scattering of the primary electron beam within the sample substrate generates EDX signal from an effective volume that can be substantially larger than the feature being analyzed. The resulting signal-to-background ratio is poor, with the signal generated by the particle often overwhelmed by background generated from the underlying and surrounding substrate. Furthermore, substrates of choice for aerosol field samples are typically carbon based such as polycarbonate films. Thus, SEM/EDX analysis of small carbonaceous particles is especially problematic due to the inability to resolve the EDX spectra of the particle and substrate, and also because of poor image contrast. A recent journal article (Laskin and Cowin, 2001) describes progress in automated single-particle SEM/EDX analysis of particles as small as 0.1 μm. The fundamental innovation used by the authors is to use extremely thin carbon films (commercially available on TEM grids) as particle substrates. The films are on the order of 25 nm thick and are almost transparent to a 20-keV electron beam. The vast majority of the electrons penetrate the substrate with very little electron scatter, hence, very little EDX background. In this way, Laskin and Cowin have been able to obtain semi-quantitative EDX analysis of submicrometer, low-Z particles in automated SEM/EDX analysis. This work has potentially important implications for computer-controlled SEM/EDX analysis of aerosols, especially $PM_{2.5}$.

Experiments were conducted to verify the basic elements of Laskin and Cowin's work. Submicrometer particles were loaded onto TEM support films similar to those used by Laskin and Cowin and carried out manual SEM/EDX analysis on the particles. Figure 4-5 shows a comparison of the EDX signals generated during 100-s analyses by our normal polycarbonate filters (in black) and by a 25-nm carbon-coated formvar film (in white). The latter is supported on a standard 3.08-mm copper TEM grid. Note that the vertical scale is logarithmic so that the true reduction in background afforded by the formvar film is much greater than the apparent reduction. For carbon, the dominant species in both substrates, the reduction is 100-fold. This low background signal enables semi-quantitative EDX analysis of small and low-Z particles. The formvar film shows small Cu and Al peaks in addition to C. (The Cu is due to scattering of secondary electrons from the Cu support grid.) A key factor in the low count rate generated by the formvar is geometry: After penetrating the formvar film, the probe beam travels through open space for several inches before hitting the bottom of the SEM sample chamber. There is a resulting small solid angle for X-rays produced here to reach the secondary detector, and the sample wheel that holds the TEM grid intercepts any line-of-sight X-rays produced at this location.

Figure 4-6 is a photomicrograph of a submicrometer diesel soot particle taken with the LEO S440 in the secondary electron

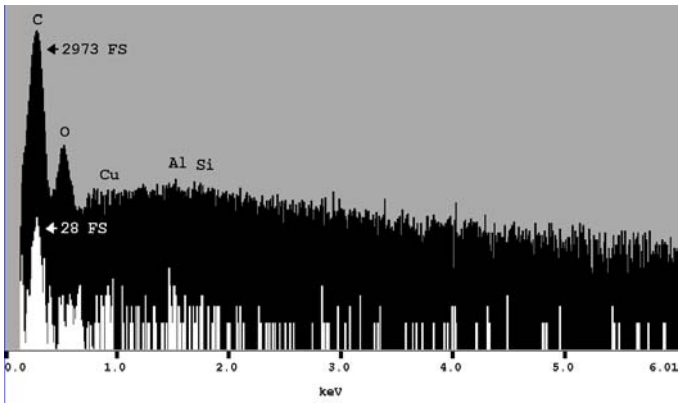

Figure 4-5. EDX spectra for blank standard polycarbonate filter (black) versus 25-nm carbon-coated formvar film (white). Both spectra were acquired for 100 s.

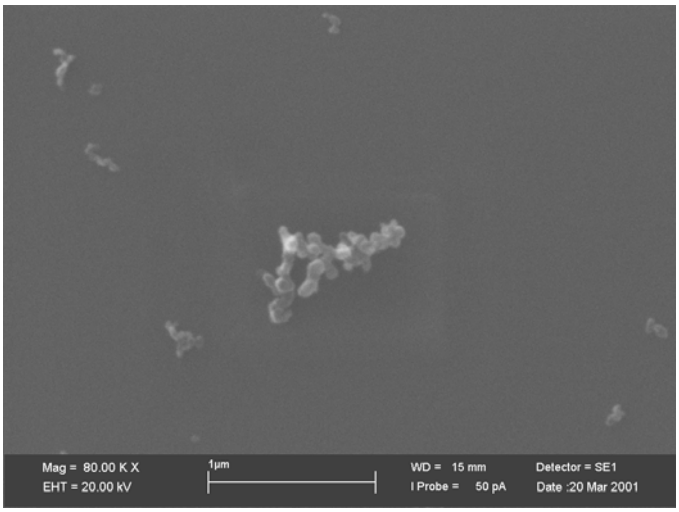

Figure 4-6. Photomicrograph of sub-micrometer diesel soot particle.

mode. The support substrate is a 25-nm carbon-coated formvar film supported on a copper TEM grid. The carbon coating improves the stability of the formvar to localized heating from the electron beam. The formvar film provides uniform contrast and a featureless, optically flat background ideal for imaging. (It should be noted that the image was acquired under conditions optimized for imaging, e.g., low probe current, short working distance, and high pixel resolution. The image would be noticeably degraded using SEM conditions more appropriate for computer-controlled SEM/EDX.)

Figure 4-7 shows the EDX spectrum (in black) of the soot particle shown in Figure 4-6. The spectrum is dominated by C, as expected, but also shows Al, Si, Cu, and O. Superimposed on the spectrum (in white) is the approximate contribution from the substrate, measured by moving the electron beam to a nearby point off the particle. Both spectra were collected for 100 s at a probe current of 200 pA. The carbon peak dominating the soot particle spectrum represents a count rate of 17.3 cps, of which

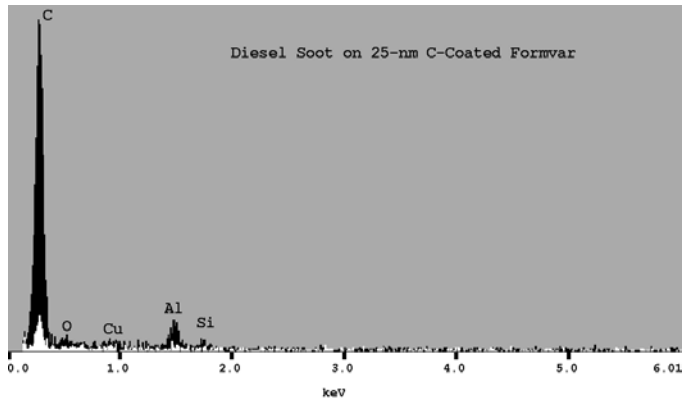

Figure 4-7. EDX spectrum of diesel soot particle plus formvar substrate (black). White spectrum is the formvar blank for the same counting time.

the formvar substrate accounts for about 1.5 cps. For computer-controlled SEM/EDX analyses, a more realistic X-ray acquisition time would be 10 s or less.

Figure 4-8 compares EDX spectra acquired for 10 s on (1) a 0.22-µm aluminum silicate particle (Arizona Road Dust) on standard polycarbonate substrate (top), and (2) a 0.24-um aluminum silicate particle on the formvar film. In the top spectrum, carbon background from the polycarbonate filter, peaking off-scale at 223 counts full scale, dwarfs the signal from the mineral particle. In the bottom spectrum, the signal is generated predominantly by the particle; the small carbon and Cu peaks originate primarily from the substrate and the TEM grid, respectively. Compared to the polycarbonate filter, the formvar film generates much less Bremsstrahlung radiation, which gives rise to the background continuum underlying the discrete, characteristic X-ray peaks. In the bottom spectrum, the Si and Al peak areas are 197 and 96 counts, respectively. The net K and Fe peak areas are only 6 and 25 counts, respectively, but could be used in a qualitative way to assign particles to specific classes. We believe that the probe current could probably be doubled or

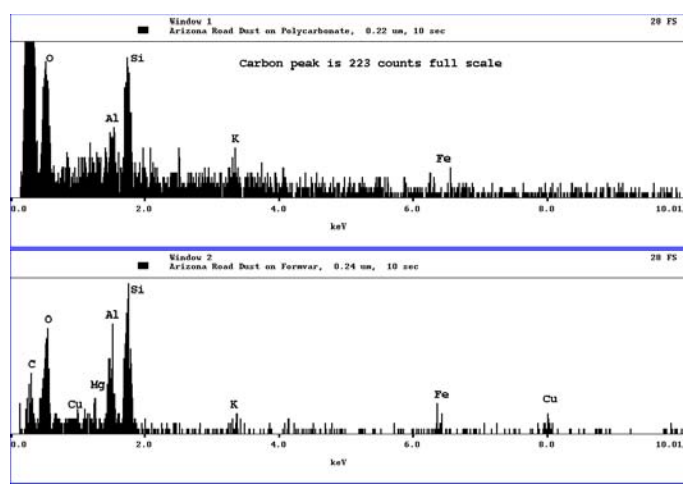

Figure 4-8. Top: 10-s EDX spectrum of a 0.22-µm aluminum silicate particle (Arizona Road Dust) on polycarbonate substrate. Bottom:: 10-s EDX spectrum of a 0.24-µm aluminum silicate particle on the formvar film.

tripled to improve counting statistics without degrading signal-to-noise too much.

The analyses above were painstakingly carried out manually on the LEO/PGT system. It is unlikely that the same data could be acquired with this system in a computer-controlled analysis because of the difficulty of reliably identifying submicrometer, low-Z features automatically due to limited image contrast and image resolution. Laskin and Cowin have the benefit of advanced SEM technology, including a field-emission SEM (roughly 100x brighter than our LaB_6 gun, hence, potentially better image resolution and X-ray count rate) and an in-line secondary electron detector whose signal can be mixed with that of the backscatter detector to optimize feature-to-background contrast. Even if the analysis limitations could be overcome, one must be able to deploy these fragile TEM substrates in the field as active and/or passive aerosol collectors. Laskin and Cowin report to have developed size-selective active and passive sampling devices using TEM grids, so that it appears that the major obstacles can be overcome, enabling the automated, semi-quantitative characterization of particles down to 0.1 μm.

4.6 CCSEM Data Quality and Validity

Studies have been conducted in the NERL SEM Laboratory and elsewhere to assess the quality and validity of CCSEM data. Issues relating to CCSEM data quality and validity include: the stability of unattended CCSEM for multi-hour runs; the precision of CCSEM analyses; the number of particles that must be analyzed in order to yield representative results; the sensitivity of CCSEM results to instrument settings such as video threshold, dwell time, grid point spacing, and X-ray counting time; and errors generated by automated feature analysis software.

Germani (1991) evaluated the effects of critical instrumental parameters on the analysis time and accuracy of automated gunshot residue (GSR) analysis. GSR analysis is similar in many ways to CCSEM analysis of aerosol samples. Germani carried out five experiments, in each of which, one parameter was varied while the others remained the same. The instrumental parameters were: minimum particle size, video threshold, electron beam point spacing, video dwell time, X-ray counting time, and X-ray analysis mode. For each experiment, successive automated analyses were run over the same area of the sample. Results of these experiments are summarized below:

1. Changing the video threshold resulted in different particle types, sizes, and morphologies being selected for analysis. A particle's BSE signal is a function not only of the effective Z of the particle, but also the particle's size and morphology: smaller and flatter or thinner particles generate smaller BSE signals than larger, more spherically shaped particles of the same effective Z.
2. The number of true GSR particles found by wavelength-dispersive analysis (WDX) was always greater than that for EDX analysis, by as much as a factor of 5 at the lowest threshold.
3. Dwell time is the amount of time that the electron beam is stationary at a point while the BSE signal is acquired and averaged. Varying dwell time from 2 to 256 μs with fixed video threshold had no significant effect on the number of GSR particles detected per field. However, dwell time does directly affect the analysis time. Again, the number detected by WDX was 2-3 times greater than that for EDX.
4. Digital point spacing is the distance between grid points in the digital raster used to search for particles. A "coarse" grid reduces analysis time, but at the risk of missing particles whose size is smaller or on the order of the digital point spacing. Germani found that a grid point spacing of about one half the minimum specified particle size was needed. Reducing the grid point spacing by another factor of 2 (to 0.25 μm) increased the number of detected GSR particles per field by 40%, but the analysis time increased by at least a factor of four. Interestingly, the ability of EDX to identify GSR particles improved (using WDX results as the reference) as the grid point spacing increased, indicating that EDX performs better on larger particles.
5. Results of the "point" mode versus "raster" mode of analysis showed no significant difference between the two modes in the ability to detect GSR particles, consistent with a large X-ray emission volume for GSR particles at an accelerating voltage of 20 keV. However, the point mode typically yielded three times the count rate of the raster mode, and so is the better choice for GSR analysis.
6. The effect of X-ray counting time was also tested. The number of GSR particles detected per field doubled with a nine-fold increase in counting time (from 3 s to 27 s), due to the improved signal-to-noise.

Results from Germani's study indicate that trade-offs have to be made between analysis time and accurate particle detection.

Studies were also conducted in the NERL SEM Laboratory to assess the following issues related to the quality and validity of CCSEM data: (1) the stability of unattended CCSEM for multi-hour runs, (2) the number of particles that must be analyzed in order to yield representative results, and (3) errors generated by automated feature analysis software. These studies are described in detail in Mamane et al. (2001). A summary of results is presented below.

Stable operation of the SEM instrument during a multi-hour CCSEM analysis of a sample is an essential requirement. Instrumental drift in key parameters such as magnification, electron probe current, threshold setting, or X-ray energy calibration could seriously compromise the validity of the data.

4.6.1 Precision of CCSEM (Repeat Analyses of Same Sample)

The precision and stability over time of computer controlled SEM was evaluated using an outdoor ambient sample collected from the 1998 Baltimore Retirement Home Study (Conner et al., 2001). The sample, which was originally analyzed by CCSEM on 3/26/99, was re-analyzed in triplicate 21 months (on 12/26/00, 12/27/00, and 12/28/00) after the original CCSEM analysis was conducted. Every effort was made to reproduce the original analysis conditions. The same parameter and other files used in the original CCSEM analysis were used for the replicate analyses. Other conditions were not as straightforward to duplicate exactly. For instance, the filament condition cannot be exactly duplicated. The brightness and contrast of the sample, and thus the analysis thresholds, are dependent on the filament brightness (beam current), which varies at the saturation current depending on the age of the filament and other factors. Hard-copy thermal print images of the original analysis threshold set-up were used as a guide for setting up the replicate analysis thresholds.

Results for each analysis were summarized using the same set of user-defined rules that had been developed for the original study. For the purposes of this analysis, it was assumed that the analyses conducted on the three consecutive days (12/26-28/00) were essentially concurrent. The results of these nearly concurrent analyses were used to calculate the repeatability (precision) of CCSEM for an urban ambient sample. For particle classes assigned 100 or more particles, the CCSEM precision was 10% or less. For most other categories, the precision was 26% or less. However, precision deteriorated significantly for particle classes containing an average of 15 or less particles (the so-called "needle-in-a-haystack" particle types).

Figures 4-9a-d, show the particle summaries for these three analyses plotted as the average, standard error, and standard deviation, compared with the results for the original analysis conducted 21 months earlier. For most particle types, the original analysis was within one standard deviation of the later

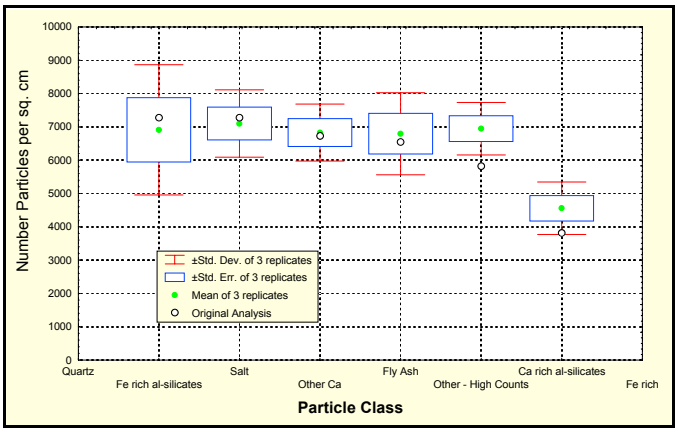

Figure 4-9b. Average number of particles per square cm of filter per particle class for three consecutive analyses, and their distribution, compared with the original analysis conducted 21 months earlier.

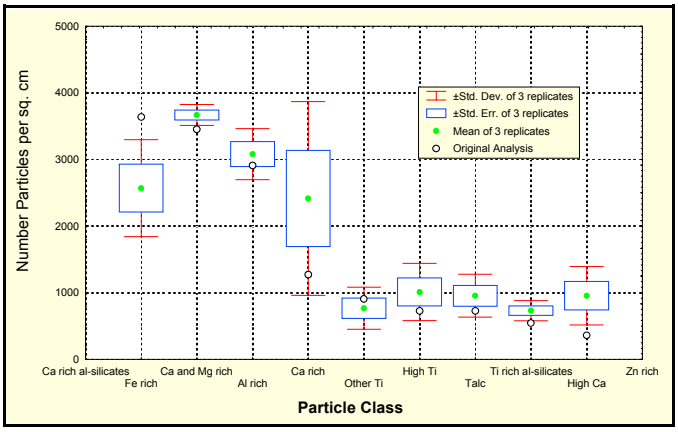

Figure 4-9c. Average number of particles per square cm of filter per particle class for three consecutive analyses, and their distribution, compared with the original analysis conducted 21 months earlier.

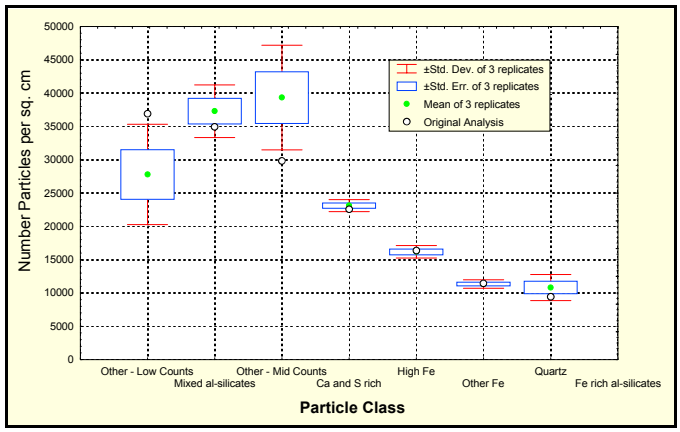

Figure 4-9a. Average number of particles per square cm of filter per particle class for three consecutive analyses, and their distribution, compared with the original analysis conducted 21 months earlier.

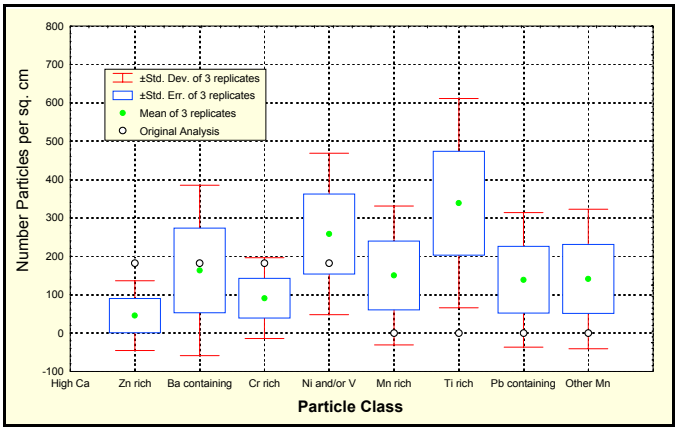

Figure 4-9d. Average number of particles per square cm of filter per particle class for three consecutive analyses, and their distribution, compared with the original analysis conducted 21 months earlier.

replicate analyses. For the higher abundance particle types (Figures 4-9a and b), those whose original analysis did not fall within a standard deviation of the repeat analysis were the generalized particle types characterized only by number of X-ray counts (not by chemistry.)

Germani and Buseck (1991) evaluated the precision and accuracy of mineral classifications by automated SEM. The sample was prepared from particle dispersions of USGS standard rock powders. Mineral types were identified by cluster analysis. Typical precisions of ± 10% for major mineral types and ± 20% for minor mineral types were determined from replicate analyses.

The results of a chemical mass balance between individual particle analyses and bulk chemical compositions of the standard rock powders indicate a precision of better than ± 15% for most elements. The accuracy of the analyses, when normalized to SiO_2, ranged from 1% to more than a factor of 3. Large discrepancies for some elements are due to error in particle volume calculations and problems associated with analyzing minor mineral types.

The precision of CCSEM-determined filter mass loadings was previously discussed in Section 4.3. The sample was a 31μg loading of Arizona Road Dust on a polycarbonate filter. Three repeat analyses of the *same* fields (227 fields, 6000 particles) yielded a relative standard deviation (rsd) in the calculated mass loading of 3.5%. Eight successive analyses of *random* fields (6000 particles, ~ 110 fields) yielded an rsd of 11%.

4.6.2 Representativeness of Data

Sampling error is also a concern for both manual SEM and CCSEM: typically, only a very small fraction (less than 0.1%) of the particles on an ambient filter is characterized by SEM or CCSEM. This leads to the question of how many particles must be analyzed on a sample in order to obtain representative results.

CCSEM was applied to the analysis of a coarse-fraction ($PM_{10-2.5}$) 24-h ambient particle sample collected in Baltimore that was known to be impacted by natural and industrial sources. The sample was collected with a dichotomous sampler on a polycarbonate filter. The sample was fairly typical of ambient urban aerosol samples in terms of the variety of particle types represented. Results show that the number of particles per field of view for this sample stabilized within a few percent of its final value of 36.1 particles per field (based on the analysis of all 78 fields) after the analysis of only 360 particles. Similarly, the cumulative averages for average particle diameter and average particle mass loading show convergence to the final values after about 360 particles.

Cumulative averages for particle composition were examined to determine for what number of particles the average particle composition converges to the final composition of the sample. Comparing chemical properties of particles is more complex than comparing the physical properties discussed above since the composition of each particle is characterized by 20 elemental concentrations plus the total X-ray count. Results for the major and minor elements stabilized only after analyzing about 1000 particles. However, the average particle composition determined from the first few hundred particles approximates the final composition for most purposes.

In the second step of the comparison, particles in each of four nested subsets were independently sorted into 25 particle types or classes according to their elemental concentrations. (The subsets comprised particles 1–360, 1–734, 1–1456, and 1–2819; thus, each smaller subset of particles is contained within the next larger subset.)

Assuming that the full 2819-particle data set is representative of the sample, then deviations in particle classification results of the three smaller subsets from the full data set allow one to estimate the minimum number of particles needed to characterize an urban aerosol sample. For the five major categories, the average relative error decreased from 11.3% (N = 360) to 7.8% (N = 734) to 6.0% (N = 1456), showing a decrease with increasing number of particles analyzed.For all but one of the major categories the abundances converged to within a few percent of the true values for N between 734 and 1456. For many purposes, even 360 particles may adequately characterize major class abundances in the sample.

As the number of particles assigned to a class becomes small, the relative errors become large and variable due to statistical fluctuations. Abundances for three of the minor classes are far from convergence to the true abundances even for N = 1456. However, these classes are populated by only 17, 22, and 3 particles, respectively, in this subset. In the full data set of 2819 particles, the minor classes are populated by only 42, 36, 33, 20, 12, 11, 9, 4, and 2 particles, respectively. Here, the concept of "true" class abundances becomes increasingly untenable, even with 2819 particles. Results show that the average relative error for the minor classes improves from 66.6% (N = 360) to 31.5% (N = 734) to 12.6% (N = 1456). For some PM studies, the classes representing industrial particles (typically minor classes) may be of most interest from the human health perspective. If one needs to accurately quantify the abundance of a minor class, then one must increase the total number of particles analyzed. (Alternatively, the PSEM is able to conduct dedicated searches for specific types of particles. In this mode, particles of no interest are bypassed in the analysis. This greatly enhances the efficiency of searching for rare or exotic particles.) The experiments above show that the *physical* properties of the sample, as represented by the number of particles per field, average particle diameter, and particle mass loading per field, are well characterized by analyzing approximately 360 particles. Little additional information is gained by analyzing more particles. *Chemical* properties of the sample (average elemental composition and major chemical class abundances) converged to within a few percent of their final values after analyzing about 1000 particles. Again, for many purposes several hundred particles may provide adequate characterization. Convergence of minor class (<1.5% by number) abundances was limited by statistical fluctuations as the number of particles populating a class became very small.

4.6.3 Errors Associated with CCSEM

Automated particle recognition algorithms lack the sophistication of the trained human eye; errors can be made by CCSEM that are typically avoided by an experienced operator performing manual analysis. Such errors may include incorrect sizing of complex particles; incorrect X-ray analysis, especially of aggregate particles or organic and carbonaceous particles, leading to particle misclassification; missed particles (e.g., due to poor contrast); and analysis of nonexistent features (contrast artifacts). Errors associated with CCSEM generally fall into two categories: those that result from the use of an automated threshold and those associated with excessive particle loading on the filter. The former are intrinsic to CCSEM and occur because current automated particle recognition algorithms lack the human eye's ability to interpret features in an image. Excessive particle loading results in errors due to overlapping particles, which can be minimized by restricting the mass loading to less than approximately 30 $\mu g/cm^2$ for $PM_{10-2.5}$. Specific types of errors that can be expected when using CCSEM include the following:

- *Missed features.* These are bonafide particles that are not identified by the CCSEM software and are therefore not characterized. Most often these are low-contrast, submicrometer organic or carbonaceous or other low-Z particles such as sulfates that can be identified by eye in the secondary electron mode but are below threshold in the backscatter mode used in most CCSEM analyses. Researchers should be aware that CCSEM analyses may underreport data on small, low-Z particles such as sulfates and carbonaceous particles. This problem is particularly troublesome for $PM_{2.5}$ samples, which are typically dominated by such particles and may require that CCSEM be used in combination with other techniques for an accurate characterization of $PM_{2.5}$.
- *Overlapping particles.* The computer is not able to discriminate touching, overlapping, or agglomerated particles; these will be analyzed as one large particle. Although the X-ray analysis may be valid for one of the overlapping features, that feature will be oversized while the other overlapping particle(s) will not be analyzed at all. A key to minimizing the occurrence of overlapping particles is to avoid overloading the filter during sample collection.
- *Contrast artifacts.* Contiguous pixels whose video level exceeds the threshold setting are assumed to be real features by CCSEM. Occasionally, the substrate produces contrast changes that mimic real particles, and these artifacts will be analyzed as real particles by CCSEM. X-ray analyses of contrast artifacts just yield spectra of the filter substrate, and, in the case of polycarbonate substrates, these may be indistinguishable from the spectra produced by carbonaceous or organic particles. If images have been saved for all features, the contrast artifacts can be identified by reviewing the images of low-count features.
- *Sizing errors.* Particles can be incorrectly sized when particle contrast is at or near the video threshold, as is frequently the case, for example, for low-Z particles such as sulfates, pollens and spores, skin flakes, and carbonaceous particles. Poor contrast may also occur at the edges of a particle where it may be thinner. Sizing errors also occur for particles with complex morphology or with mixed composition. In the case of the latter, differences in composition are reflected in different grayscale values in the backscatter image. If the grayscale of some portion of a feature drops below the threshold, the particle may be undersized.
- *Heterogeneous particles.* Particles of mixed composition cannot be accurately characterized by acquiring a single-spot X-ray analysis at the particle's center of mass. Although the X-ray analysis of a single heterogeneous particle may not be particularly meaningful, the results obtained from analyzing many such particles may provide useful information about the average composition of the sample.

Error rates associated with the Baltimore CCSEM analysis were estimated by reviewing saved images, X-ray spectra, and associated field images for 800 randomly selected particles from the Baltimore data set. In the 22 field images reviewed, we identified 47 particles that were present in the BSE field images but were not processed in the CCSEM analysis. Most of these missing particles were associated with overlapping particles. The remaining particles were inexplicably bypassed during the CCSEM run. This number does not include a small but unknown number of low-Z particles that may have been visible in SE field images but were below the detection threshold in the BSE field images. Review of the particle images also revealed that approximately 23 (2.7%) of the identified "particles" were actually contrast artifacts, leaving a total of 824 real particles in the data set. Of these, approximately 12% were judged during manual review of the images to have been sized incorrectly. Sizing errors were generally the result of overlapping particles or poor contrast (usually small, low-Z or carbonaceous particles). Sizing errors, however, were both positive (oversized) and negative (undersized) and tended to cancel each other out so that the average sizing error computed from all 96 particles was only about 3% (statistically indistinguishable from zero error). Twenty-nine features were analyzed and sized as individual particles, but were actually part of an overlapping pair or multiplet of particles. These contributed both to the sizing and missing-particle errors already counted.

The error rates reported above are sample dependent, being in part a function of particle loading and particle chemistry. Nevertheless, they may reflect typical CCSEM errors for an aerosol sample that is moderately loaded on a polycarbonate filter. Most of the errors (those due to particle sizing, overlapping particles, and contrast artifacts) can be corrected or

eliminated during off-line review of the data. The ZepView software allows the user to review all stored field and particle images and spectra along with particle-by-particle size and chemistry data. Artifacts can be culled from the data set and features can be resized provided that the particle images were saved. As a general practice, we strongly recommend off-line review of CCSEM data both to improve data quality and also because manual review enhances a researcher's understanding of the sample.

The above results need to be qualified by the following remarks. Most air monitoring studies employ Teflon filters for collecting coarse ambient aerosol rather than the polycarbonate filter analyzed in this study. Teflon filters, however, are not well suited for CCSEM. Also, the coarse mass concentration (5.6 $\mu g/m^3$) for the chosen Baltimore sample is roughly half of typical urban coarse mass concentrations; a more typical coarse-fraction urban sample would be expected to show increased CCSEM error rates associated with overlapping particles compared to our sample. Finally, this study was confined to a coarse aerosol sample. Fine PM poses a number of analytical challenges for CCSEM that were beyond the scope of the present study.

In conclusion, although CCSEM makes occasional errors in recognizing features and in sizing and classifying particles, these errors are, in most cases, an acceptable trade-off for the higher throughput, improved particle statistics, and improved objectivity afforded by CCSEM compared to manual SEM analysis. Provided that field and particle images have been saved, most errors can be eliminated during off-line review of the data.

4.6.4 EDX Acquisition Time

The PSEM provides several options for setting the X-ray acquisition time. The simplest option is to terminate EDX acquisition on all particles after a fixed number of seconds (Norm EDX time). A typical value for the Norm EDX time is 3 s. A second option is to terminate EDX acquisition when the net X-ray counts for any single element reaches a target number of counts (Trg Counts). According to the ZepRun Users Manual, "As a general principle, Trg Counts is a better parameter to use to control X-ray time, because it will allow acquisition time to be tailored to the information present in the spectrum—'weak' spectra will be acquired for longer than strong spectra. This helps to effectively trade off speed for precision; more time will be spent where needed to establish spectral statistics; less time where the spectrum is strong and well defined. It also helps by making the statistical content of all spectra more uniform relative to one another." Typical values for Trg Counts may be on the order of 3000 counts. Yet another option for controlling X-ray acquisition is to extend the acquisition time (Max EDX time) for particles of special interest while applying the Trg Counts and Norm EDX limits to all other particles. Specific particle types, defined by the user in a ZepRun Rule File, can be selected to receive the Max EDX time.

The EDX acquisition time impacts the quality of SEM/EDX results. Although very short X-ray acquisition times can boost CCSEM throughput to several thousand particles per hour, the data quality may suffer. For example, repeated analyses of the same particle could show significant variability in the elemental percentages, small peaks could be missed, and noise could be falsely identified as a real peak. These can cause particles to be misclassified when summarizing CCSEM results.

A series of tests were conducted on the PSEM to determine the effect of EDX X-ray collection time on sample composition and particle classification. The X-ray collection time is one of the parameters the user sets in a computer-controlled SEM/EDX analysis. The X-ray collection time is typically a major determinant of the total sample analysis time. Ideally, therefore, the user will choose the minimum X-ray collection time that will still allow accurate determination of each particle's composition. In aerosol sample analyses conducted at the NERL SEM/EDX laboratory, EDX analyses are not meant to be quantitative on an absolute concentration basis. Instead, samples are generally characterized in terms of number or weight percent of particle classes (e.g., aluminum silicate, quartz, etc.,), which are derived from the qualitative EDX analysis of a representative number of particles in the sample. We repeatedly analyzed identical fields of particles using different EDX collection times in an attempt to determine the minimum EDX time in which the resulting particle classes are not significantly different from the "true" particle classes of the sample. "Truth" in these studies was assumed to be determined by the results based on an EDX collection time of 25 seconds.

The test sample for these tests was NIST Standard Reference Material 2710 (Montana Soil, Highly Elevated Traces). SRM material was suspended in acetone and deposited by vacuum filtration onto a polycarbonate filter (12-μm pore). Three repeat analyses of the same fields were conducted at each of five different EDX collection times (Norm EDX = 25, 15, 8, 3, and 1 s). The Trg Counts parameter and the Max EDX parameter were not used in the following tests. Instrumental parameters for the 15 CCSEM analyses were set up to ideally analyze the same particles in each run, although this was only partially successful. Only particles in the size range of 10–40 μm were analyzed. X-ray analyses were carried out in the raster mode (X-rays collected by rastering the electron beam over the projected area of each particle). In addition to X-ray analysis, photomicrographs were collected for each particle. The total CCSEM analysis time is dominated by the X-ray counting time for collection times of 3 s or greater, but at shorter EDX times other tasks such as moving the stage and collecting micrographs, assume competing importance in determining overall sample analysis time. The number of particles analyzed in each of the 15 repeat runs ranged from 522 to 590, and the total analysis times ranged from 0.47 h to 4.49 h. The probe spot size was set to the standard 30% used in EDX analysis, and the X-ray count rates were typically on the order of 600 cps.

The 15 repeat analyses provide an opportunity to assess the precision of CCSEM analysis as a "bulk" analytical tool for determining sample mass. For each run, the SEM-determined masses of all particles analyzed were summed. The mean and

standard deviation for the sample mass was calculated from these 15 sums. The one-sigma relative standard deviation for the 15 analyses was excellent: 5.8%, even though the particles analyzed in each run were not entirely identical. These results reflect the *precision* of CCSEM in measuring particle size and estimating particle density (from the EDX analysis). As other studies have shown, however, the *accuracy* of determining sample mass by CCSEM is relatively poor because of the inability to accurately measure particle volume and density (see Sections 4.2 and 4.3). Of the particles analyzed in each run, 372 were found in all 15 analyses (based on examination of the individual micrographs). The precision of individual particle mass measurements was determined for each of these 372 particles. The average relative standard deviation (RSD) in individual particle mass was 16%. Variability in particle mass is primarily due to variability in the measured volume. Examination of the micrographs of particles having very large standard deviations (>100%) in mass do not reveal anything unusual.

The effect of EDX collection time on particle chemistry is shown in Table 4-2. Starting with the 372 particles found in all analyses, N is the number of particles for which the given element was detected in all three 25-s analyses. These N particles were subsequently analyzed (three repeat analyses each) at EDX times of 15, 8, 3, and 1 s to generate the results presented in Table 4-2. For example, 19 particles were Na-bearing in all three 25-s analyses. The average measured Na concentration in these 19 particles is 2.6 ± 0.26 wt%. The concentrations reported in Table 4-2 are not quantitative on an absolute basis and are not comparable to the NIST-certified "bulk" concentrations. For a single analysis, an element's wt% value is calculated by estimating the element's mass in each of the N particles, summing these individual particle contributions, and dividing by the total mass of all N particles. [The mass of each particle is estimated by the product of the particle's volume and density (density is calculated from the X-ray spectrum), and the mass of a specific element in a particle is the particle mass times the element's fractional contribution to the particle's X-ray spectrum; no corrections are made for detector efficiency, X-ray fluorescence yields, or size-dependent X-ray absorption effects]. The Avg wt% values in Table 4-2 are the wt% values averaged

Table 4-2. EDX Collection Time versus CCSEM Particle Composition (in weight percent concentration)

		25 s		15 s		8 s		3 s		1 s	
	N	Avg wt%	Std. dev	Avg wt%	Std. dev	Avg wt%	Std. dev	Avg wt%	Std. dev	Avg wt%	Std. dev
Na	19	2.6	0.26	2.2	0.41	2.0	0.38	2.1	0.22	2.2	0.07
Mg	84	5.0	0.08	4.9	0.05	4.7	0.38	4.8	0.39	4.6	0.69
Al	369	22.6	0.39	22.7	0.47	22.8	0.42	22.4	0.63	21.8	1.48
Si	372	53.6	0.42	53.1	0.48	53.1	0.04	52.0	1.00	50.8	1.04
P	4	1.8	0.03	1.6	0.57	1.6	0.48	1.2	0.75	1.5	1.25
S	33	1.8	0.07	1.3	0.29	1.5	0.13	1.2	0.04	2.0	0.41
Cl	7	12.5	0.63	12.2	0.62	12.2	1.50	11.9	0.82	11.2	1.66
K	308	10.1	0.08	10.2	0.18	9.7	0.20	9.9	0.46	9.3	0.32
Ca	211	2.7	0.11	2.5	0.17	2.6	0.13	2.4	0.15	2.6	0.17
Ti	87	2.8	0.07	2.6	0.01	2.8	0.13	2.7	0.34	2.9	0.26
Cr	1	21.0	0.00	21.0	2.00	21.7	0.58	21.0	2.65	19.0	4.00
Mn	68	3.2	0.09	2.8	0.08	2.9	0.21	2.8	0.34	2.7	0.20
Fe	301	8.1	0.08	8.0	0.12	7.9	0.20	7.8	0.33	7.9	0.55
Cu	73	1.7	0.11	1.5	0.19	1.5	0.16	1.2	0.17	1.6	0.20
Zn	28	1.3	0.01	1.0	0.43	1.4	0.38	1.2	0.11	1.0	0.53
As	200	1.5	0.07	1.5	0.24	1.7	0.11	1.6	0.35	2.1	0.40

N = number of particles for which the given element was detected in all three 25-s analyses. Only these N particles were analyzed at shorter EDX times.

Avg wt%: Elemental weight concentrations were calculated for each individual particle and averaged over N particles to get an average wt%. The average weight percents from three repeat analyses of the same N particles were averaged to get the Avg wt% shown in the table.

Std. dev = percent standard deviation in the Avg wt% for 3 repeat analyses.

over three repeat analyses of the same N particles. We assume that the Avg wt% listed for the 25-s analysis represents the "true" average concentration, and we are interested in looking for significant deviations from the truth as the EDX collection time is decreased. The results in Table 4-2 indicate that the effect of reducing EDX collection time is minimal for most of the listed species, even for X-ray analysis times as short as 1 s.

In general, variability in the measured elemental concentrations increases as the X-ray collection time is reduced, and the variability among the three repeat analyses at a given EDX collection time approximately equals any changes in the average measured concentration due to reducing the EDX time. For the most robust species (e.g., K and Si), reducing the EDX time may result in slightly lower measured concentrations. For example, measured Si and K concentrations drop by 5.4% and 8.6%, respectively, when the EDX time is reduced from 25 s to 1 s. Table 4-2 suggests a possible increase in the "As" concentration for the shortest EDX time. The arsenic signal is actually a noise artifact due to inadequate noise suppression in the CCSEM setup file. (A better element setup file for As would have included the requirement that the secondary As K_α and K_β peaks be present above noise as a condition for As to be detected). The As results may indicate the need for careful noise suppression for species that are typically present near the minimum detection limits.

As mentioned above, samples are typically not characterized in terms of absolute elemental weight percents, but in terms of particle classes. Particles in the 25-s data sets were sorted, somewhat arbitrarily, into 13 particle classes, which were suggested by cluster analysis of the particle EDX data. (The Montana soil sample used for this test was not ideal for particle classification because the sample did not show a large diversity of particle classes. The great majority of the particles were either aluminosilicates or quartz.) A set of rules were developed using the Zeppelin Feature Rule Editor (Aspex Instruments) to sort the particles hierarchically into the 13 classes. The identical set of 372 particles was classified using this fixed set of rules for each of the 5 EDX times (15 analyses in all). Figure 4-10 shows the resulting average class populations relative to the average "true" populations measured at EDX times of 25 s. The figure displays results for only those classes having "true" populations of seven or more particles. Classes are arranged in order of decreasing population, with the AlSi class being the most populated (average "true" N = 153) and the CaAlSi class being the least populated (average "true" N = 7). Each data bar shows the average ± standard deviation of three repeat analyses. Classification results at EDX times of 3 s and 1 s show increasing divergence from the "true" populations, which is attributed to a systematic increase in the population of the NaAlSi class as EDX time is reduced. Because each particle in all 15 data sets must be sorted into one and only one of the same 13 classes, any growth in the population of one class must be accompanied by a decrease in the population of another class or classes. The increase in the NaAlSi class is thus accompanied by decreasing populations in the High Al, K, Fe-Mg Al, and High Si classes. Examination of the EDX data shows that the number of Na-bearing particles (Na X-ray count >1% of total X-ray count) increases substantially as EDX time is reduced. We believe that noise in the EDX spectrum is responsible for the apparent increase in the number of Na-bearing particles at reduced EDX times. If an element threshold of 3% (percentage of total X-ray counts needed for the given element to be considered as present in the particle) had been assumed in the run parameter file rather than 1%, the classification results would be expected to be more consistent across EDX times.

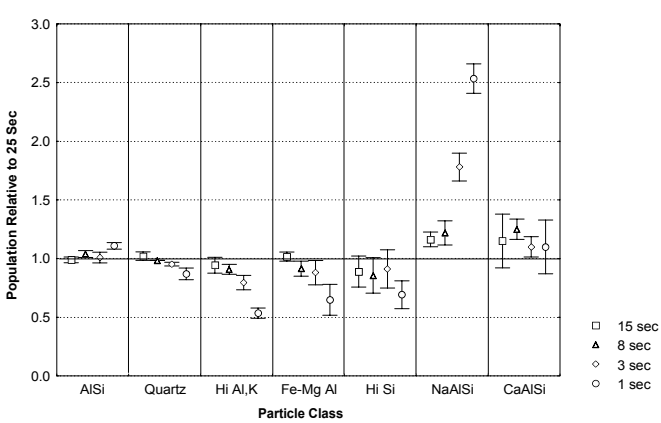

Figure 4-10. Particle classification results on repeat CCSEM analyses of Montana Soil SRM at five different X-ray collection times. Each data point represents the number of particles in the given particle class relative to the class population for the 25-sec data.

The tests above need to be repeated for a sample that is truly heterogeneous in particle types. These preliminary results, however, suggest that if only the major elements are considered, particle composition and classification results are remarkably constant and independent of X-ray counting time for EDX times as short as 1 s. For elements whose concentrations in particles are near the EDX detection limit (roughly 1 wt %), the need for careful noise suppression becomes increasingly important as the X-ray counting time is reduced. If a minor species is critically important to the analytical results, the user should confirm the results obtained at short EDX times by repeating the analyses of a subset of particles at long X-ray counting times.

In conclusion it should be mentioned that EDX detector technology continues to improve. New pulse-processors with significantly higher count rate capability combined with large area detectors, have the potential to reduce X-ray counting times and significantly boost particle throughput such that 10,000 particles per hour may become routine with state-of-the-art technology.

Chapter 5
Examples of Research Applications

5.1 Examples from the Literature

Numerous applications of SEM/EDX to environmental problems have appeared in the literature. For convenience, these examples are sorted into papers focusing on: (1) aerosol characterization, (2) source apportionment, or (3) SEM/EDX methodology.

5.1.1 Aerosol Characterization

In response to growing concern over potential health effects and air quality impacts of aerosols associated with anthropogenic activities, numerous articles have appeared in the literature during the past three decades focusing on characterization of several important classes of anthropogenic aerosols: fly ash, soot, and sulfate. Buseck and Bradley (1982) discuss electron beam studies of natural and anthropogenic microparticles and offer the following statement: "The range of particle sizes and compositions in aerosols is extremely wide, as is the number of possible mineral types and synthetic compounds. . . .Although the majority of airborne particles are minerals, a significant fraction in urban areas is anthropogenic. Furthermore, in these urban regions even the natural particles carry surficial deposits of an anthropogenic character, clearly the result of the efficient scavenging ability of fine-grained dusts."

5.1.1.1 Fly Ash

Numerous papers describe SEM characterization of fly ash from coal- and/or oil-fired power plants. Studies consistently show selective accumulation of volatile species on the surface of refractory metal oxide cores and enrichment of the fine fraction, especially submicrometer particles, by toxic elements and compounds (Pueschel, 1976; Rothenberg et al., 1980; Mamane, 1984, Mamane et al. 1986; Hock and Lichtman, 1983). Linton et al. (1977), using ion microprobe mass spectrometry and Auger electron spectrometry demonstrated surface predominance of S, Fe, K, Na, Li, Pb, Tl, Mn, Cr, and V in coal fly ash. This was explained in terms of a volatilization-condensation mechanism. In addition, the last five of these elements were found to be highly leachable and therefore of particular environmental and health significance. The general consensus appears to be that particles formed at high temperatures act as substrates for the condensation of other materials during cooling. Coal and oil fly ash can be quite heterogeneous in both morphology and elemental content, greatly complicating the application of SEM/EDX to quantitative receptor modeling. Morphological analysis of a coal fly ash sample by Fisher et al. (1978) indicated 11 major classes of fly ash particles. Mamane et al. (1986) analyzed fly ash from both coal-fired and oil-fired power plants by SEM/EDX and examined the potential for SEM/EDX as a tool for receptor modeling. They found that potentially useful bulk elemental tracers such as As and Se in coal fly ash and V and Ni in oil fly ash were not reliably detected in individual particles by EDX. (As and Se were not detected while V and Ni were detected in only 50–60% of the oil fly ash particles.) In addition, most fine-fraction oil fly ash particles resembled the mineral-rich spheres that are typically associated with coal-fired power plants, making it difficult for SEM/EDX to reliably distinguish these two source types. Obrusnik et al. (1989) used SEM and neutron activation analysis to examine differences in trace element composition and morphology between coal fly ash and oil fly ash. These authors observed enrichment factors (EFs) in oil fly ash > 500 for V, Ni, Cu, Zn, Sb, Hg, Cl, Ta, and Co, and EFs in coal fly ash > 60 for Se, Hg, As, Cu, and Sb. (The particle size in these studies was apparently not directly determined, but the authors suggest that the geometric mean particle size was between 1 and 30 μm for the coal fly ash and between 15 and 82 μm for the oil fly ash). Buseck and Bradley (1982), Germani et al. (1981), and Small et al. (1981) discuss bulk and individual particle analyses of copper smelter fly ash. Buseck and Bradley (1982) directly observed condensates of volatile elements on the outer surfaces of smelter fly-ash spheres.

5.1.1.2 Carbonaceous Particles

Carbonaceous particles typically comprise one-third or more of the total PM_{10} mass. However, these particles, including soot and biological particles, are traditionally problematic for CCSEM because of poor contrast in the backscatter image, making it difficult or impossible for feature analysis software to reliably identify and size such particles, especially submicrometer particles. Martello et al. (2001) and Casuccio et al. (2002) have developed a procedure that optimizes CCSEM analysis of carbonaceous particles. The sample is collected on a Pd-coated

polycarbonate filter. The Pd coating (~0.17 μm) attenuates the carbon signal from the filter substrate, thereby improving the carbon signal-to-noise for particles. No carbon or metal conductive coating is applied to the sample in order to avoid confounding the EDX analysis. A section of the filter is fixed to a stub with double-sided silver tape for maximum conductivity. Sample charging problems were evidently minimal, enabling the analysis to be carried out in the high-resolution SE mode in which carbonaceous particles are more reliably detected and sized. The sample was analyzed at 15 kV accelerating voltage, which yields adequate image and EDX information while minimizing electron beam penetration into the filter substrate. The C:Pd X-ray ratio for particle-free areas of the sample is used as a baseline for quantifying the carbon in particles.

Soot is primary combustion-generated carbonaceous aerosol. Chemically and structurally, soot is a complex mixture of amorphous polymerized organic material plus graphitic elemental carbon. Soot emissions from gas turbines, diesel engines, and other combustion sources are major contributors to air contamination in industrial and urban environments, typically accounting for 1–4 $\mu g/m^3$ of atmospheric inhalable particulate matter (Palotás et al., 1998). Pósfai et al. (1999) used TEM to show that a significant fraction of sulfate particles occurs internally mixed with soot. With a graphite-like structure possessing extremely high surface area, soot is an efficient catalyst: Soot-catalyzed reactions may be a major factor in the oxidation of SO_2 to sulfate in polluted atmospheres (Novakov et al., 1974). In addition, soot may act as a carrier of carcinogenic polycyclic aromatic hydrocarbons into the lungs (Palotás et al., 1998). Most studies of soot have employed methods such as TEM to characterize the microstructure of soot (Katrinak et al. 1992). These studies show that the structure and composition of soot particles vary from different sources because of fuel compositions and combustion conditions. The microstructure of soot can therefore potentially be used to infer the emission source.

5.1.1.3 Sulfates

On a global scale, sulfur-containing particles are perhaps the most important class of particles in the submicrometer size range, and the great majority of these particles are in the form of sulfate. Several papers have reported evidence of S-enrichment in minerals and spores. Mamane et al. (1992) showed that ambient particles in the size range of 0.5–10 μm were enriched in sulfur and attributed the S-enrichment to reactions that occur in the atmosphere while particles are airborne. Microscopists should be aware that volatile particles such as sulfates may be sublimed during the carbon-coating process and/or during SEM analysis. Parungo et al. (1986) reported that sulfate particle counts by EDX were consistently lower than those obtained on the same sample using the $BaCl_2$ reaction test (discussed below), and attributed the difference to sublimation losses. Thus, in general, one should be aware that the particles characterized in conventional, high-vacuum SEM/EDX analysis may represent only the non-volatile fraction of the sample.

Sulfate particles are often difficult to identify in CCSEM analyses because of their low contrast and are, therefore, easy to undercount. A simple chemical test to quantify the fraction of sulfate particles in a sample is described by Bigg et al. (1974), Mamane and de Pena (1978), and Ayers (1978). For the detection of sulfates, a thin-film (~300 Å) of $BaCl_2$ may be applied to the filter collection surface before or after the aerosol is sampled. Particles containing sulfate react with the $BaCl_2$ coating and form distinctive reaction rings that can be examined with an electron microscope. This method is applicable primarily for particles smaller than 1 μm.

5.1.1.4 Marine Aerosol

The world's oceans are a major source for both primary and secondary aerosols. In our laboratory, sea salt has been observed in ambient samples from Phoenix, AZ, Baltimore, MD, and Brownsville, TX. It is important from the point of view of source attribution to recognize the morphology and chemistry of marine aerosols. Mészáros and Vissy (1974) employed SEM in an attempt to identify the chemical composition of marine aerosol by particle morphology. They identified four types of particles (sodium chloride, sulfuric acid, ammonium sulfate, and mixed sodium chloride and ammonium sulfate) and measured their size distributions. Parungo et al. (1986) carried out SEM/EDX analyses of marine aerosol collected over the Pacific Ocean and showed that larger particles (d > 0.5 μm) comprised a wide variety of morphologies and combinations of NaCl, $CaSO_4$, $MgSO_4$, and KCl. A large fraction of these particles contained sulfate. Nitrate appeared to attach preferentially to sea-salt particles in this larger size range. The great majority of particles < 0.5 μm were sulfate. This size range was more difficult to characterize because many particles sublimed under the electron beam. This study also reported excess (non-sea salt) sulfate, nitrate, and ammonium particles. The authors attribute these secondary particles to photochemically assisted, gas-to-particle conversion of biogenic precursor gases. Pósfai et al. (1994) studied marine aerosol from the Equatorial Pacific using TEM, EDX, and selected-area electron diffraction (SAED). Sea-salt aggregates consisted largely of NaCl and Na-Ca sulfate crystals. Sulfates of Na and Ca with minor K and Mg form on NaCl crystals. In addition, several species of submicrometer (typically 0.2 μm) S-bearing particles were observed, presumably including ammonium sulfate and acid sulfates. The presumed ammonium sulfate particles were rapidly volatilized in the electron beam. Diatom fragments were common, and there was a sparse crustal component consisting mostly of kaolinite and rutile. The authors report that volatile elements were lost during EDX analysis. Results provided evidence of gas-phase HCl released from sea-salt. Parungo et al. (1990) also reported a deficiency of chloride ion relative to seawater composition in aerosol collected in the Gulf of Mexico and hypothesized the release of HCl as SO_2 and NO_x replace chloride ion in sea salt particles. Using laser microprobe mass analysis, Bruynseels and Van Grieken (1985) proved the existence of sulfate and nitrate layers on the

surface of sampled marine aerosol, although it could not be established whether the surface layers existed in the atmosphere or were created after collection by differential crystallization from homogeneous liquid-phase particles. Andreae et al. (1986) examined individual aerosol particles from the remote marine atmosphere and found that a very large fraction of the silicate mineral component of the aerosol was internally mixed with sea-salt particles. They proposed cloud processing as a mechanism and suggested that this could also explain excess sulfate (non-sea salt) enrichment of sea-salt particles.

5.1.1.5 Miscellaneous

CCSEM has been used to characterize and identify sources of lead-rich particles in the environment (Mamane et al., 1995; Johnson and Hunt, 1995; and Vander Wood and Brown, 1992). Mamane (1988) used manual SEM to characterize particles emitted from a municipal waste incinerator. The results were then used in combination with conventional bulk analysis of ambient filters to apportion the fraction of Philadelphia aerosol contributed by municipal waste incineration (Mamane, 1990). Germani and Zoller (1994) characterized particulate emissions from a municipal waste incinerator using SEM/EDX. They found that small incinerator particles are composed of a rather homogeneous mixture of chloride salts of Na, K, Zn, and Pb, and that, like coal-fired power plants, incinerators enrich volatile elements via a vaporization-condensation mechanism. Their data suggest that small incinerator particles are coated with a thick, soluble chloride salt coating. Waste incineration appears to be the major source of Zn, Cd, Sb, and possibly Ag, Sn, In, and Pb in urban atmospheres.

5.1.2 Source Apportionment

Individual particle analysis, combined with bulk chemical analysis or as an alternative to bulk techniques, can potentially improve source resolution in source apportionment studies (Kim and Hopke, 1988b; Mamane, 1990). Dzubay and Mamane (1989) explored the feasibility of increasing the source resolution of the CMB method by using SEM/EDX data with bulk XRF results. In this way, the authors were able to determine two additional components (coal fly-ash and botanical matter) that could not be determined by XRF data alone. SEM provided estimates for other components as well including municipal incinerators. SEM generally confirmed CMB source contribution estimates, but in some cases CMB results predicted a contribution from municipal incinerators, but SEM results were not able to support a contribution.

Casuccio et al. (1988) compared upwind, stack, diluted stack, and plume samples from a coal-fired power plant, demonstrating the ability of CCSEM to provide information on source/receptor relationships. Kim and Hopke (1988b) used CCSEM data in a particle class balance (PCB) analysis to apportion sources of PM in El Paso. The authors conclude that the large number of particle classes typically identified by CCSEM reduces collinearity problems and enables greater resolution of sources compared with conventional bulk analysis. Hopke and Mi (1990) classified CCSEM particle data from a power plant and were able to distinguish in-plume particles from in-stack and ambient particles. Anderson et al. (1992) determined the size distribution of ~ 30,000 fine (0.1 to ~ 2 μm) arctic aerosol particles and attempted to identify their sources. The ability to reliably detect low-Z particles as small as 0.1 μm distinguishes this work from many others. Katrinak et al. (1995) used CCSEM to identify individual particle types in the Phoenix aerosol. Jambers and Van Grieken (1997) combined CCSEM analysis of riverine suspension particles with hierarchical cluster analysis to shed light on sources of pollution in Lake Baikal. Xhoffer et al. (1992) apportioned particles collected in the North Sea surface microlayer and in underlying bulk waters to atmospheric or riverine suspension sources.

5.1.3 SEM/EDX Methodology

Researchers have had mixed success in efforts to establish a quantitative link between individual particle analysis and bulk chemical analysis of a sample. Johnson et al. (1981) compared bulk XRF results and (summed) individual particle results on the same filter samples. The authors were unable to resolve differences between the elemental mass accounted for by the two approaches and concluded that accurate calculation of bulk elemental weight percents based on individual particle analysis was not quite feasible. Nevertheless, CCSEM can provide an internally consistent bulk chemical analysis, which is useful in comparing samples. Potential sources of error associated with CCSEM are discussed including particle volume and density calculations, assumptions about particle stoichiometry, and particle classification. Casuccio et al. (1983b) compared bulk and microscopic analyses of ambient High Volume (Hi Vol) filters. Mamane (1988 and 1990) showed excellent agreement between mass concentrations derived from bulk and manual individual particle analysis (regression line slope of almost 1.0 and correlation coefficient of 0.9).

A major issue with CCSEM data is how to classify particles in order to facilitate interpretation of the data. In the decades since the introduction of CCSEM, particle classification schemes have grown in number and sophistication. Johnson and Twist (1982) discuss approaches to sorting and classifying individual particle data for use in microscopy-based receptor models. Johnson et al. (1981) classified particles into environmentally recognizable classes, which were based on a variety of source standards (coal and oil fly ash, wood combustion, high temperature industrial emissions, clay mineral classes, etc). Johnson et al. (1984b) and Dzubay et al. (1984) describe the use of SAX (scanning electron microscopy with automated image analysis and X-ray energy spectroscopy) to classify particles in Houston aerosol. Aerosol samples were described in terms of 25 fixed particle types making up the mass on each filter. The 25 particle classes were developed from a combined set of 18 ambient and 30 source signatures subjected to factor analysis.

The statistical technique of cluster analysis (including hierarchical and non-hierarchical cluster analysis) has proven

successful in discerning particle groupings in large data sets with no prior knowledge of the group characteristics (Kim et al., 1987; Kim and Hopke, 1988a; Hopke and Mi, 1990; Anderson et al., 1992; Saucy et al., 1987, 1991; Shattuck et al., 1991; Germani and Buseck, 1991; Van Borm et al., 1989; Katrinak et al., 1995). Shattuck et al. (1991) applied non-hierarchical cluster analysis to a complex Phoenix aerosol sample that was about 75% crustal in origin. The authors concluded that cluster analysis was effective for determining the types of particles that occurred in the Phoenix aerosol. This paper presents a particularly detailed multistep recipe for applying cluster analysis, assessing the validity of the clusters, and interpreting relationships and trends among multiple samples. There appears to be some disagreement among researchers as to the need for pretreating CCSEM data prior to performing cluster analysis. However, Shattuck et al. (1991) argue that data normalization gives artificially low values for the standard deviations of such variables and correspondingly too great a weight after normalization. Hopke and Mi (1990), on the other hand, found that cluster analysis results were more reasonable when the raw CCSEM data were pretreated as follows: (1) Any X-ray peaks containing fewer than N_c counts, where $N_c = 2N_T^{1/2}$ and N_T is the total X-ray count in the spectrum, were considered to be noise and set to zero. (2) The noise-reduced data were log-transformed after adding 1 to all X-ray intensities; thus, $X_{ij} = log_{10}(1+x_{ij})$, where x_{ij} is the ith variable of the jth particle and X_{ij} is the transformed value of x_{ij}. (3) Finally, the data are transformed to have zero means and unit variance (z-transformation).

Routine quantitative analysis of individual particles has generally been considered to be an intractable problem because of the difficulty of relating X-ray intensities to a particle's element concentrations. Armstrong and Buseck (1975) derived theoretical correction factors specific for a variety of particle shapes. The correction procedures were applied to particles of known composition, and the results demonstrated that routine, *manual* quantitative analysis of microparticles is both feasible and straightforward. Successful application of these correction procedures, however, assumes that each particle's thickness and shape can be approximated during the time of analysis; it is not clear whether the particle shape parameters typically acquired during a CCSEM analysis are sufficient for approximating particle shape and thickness.

5.2 Phoenix $PM_{2.5}$ Samples

A 3-yr campaign of $PM_{2.5}$ air sampling beginning in 1995 provided a database of sample chemical analyses of sufficient size to be well-suited to the large data quantity requirements of multivariate analysis. A study was conducted to demonstrate the multivariate receptor model Unmix (Henry, 1997, 2001) on a typical urban aerosol data set. Using only ambient concentration data for $PM_{2.5}$ mass and various chemical species the Unmix software estimates the number of contributing sources, their compositions (with uncertainties), their $PM_{2.5}$ mass contributions to each sample, and their average $PM_{2.5}$ mass contributions (with uncertainties). Unmix is a type of factor analysis, but geometrically constrained to generate source contributions and profiles with the physically meaningful attribute of non-negativity. The Unmix analysis was supplemented with SEM/EDX of a limited number of filter samples. These results provided information about additional low-strength sources that Unmix did not quantify. Details of this study are reported in Lewis et al. (in press). The application of SEM/EDX in the study is featured here as a demonstration of an SEM/EDX application.

5.2.1 Unmix Receptor Model Findings

The multivariate receptor model Unmix has been used to analyze a 3-yr $PM_{2.5}$ ambient aerosol data set collected in Phoenix AZ beginning in 1995. The analysis generated source profiles and overall percentage source contribution estimates (SCE) for five source categories: gasoline engines (33±4%), diesel engines (16±2%), secondary sulfate (19±2%), crustal/soil (22±2%), and vegetative burning (10±2%). Unmix results show the element Mn playing an unexpectedly large role in the diesel source. Except for the diesel engine source category the Unmix SCE's were generally consistent with an earlier multivariate receptor analysis of essentially the same data using the Positive Matrix Factorization (PMF) model (Paatero and Tapper, 1994; Paatero, 1997).

5.2.2 SEM/EDX Findings

SEM/EDX was used to obtain information about additional low-strength sources that Unmix did not quantify, and to investigate the association of Mn with the diesel source. The Personal SEM® (PSEM) (formerly R. J. Lee Instruments, Ltd., now Aspex Instruments, Trafford, PA) was used to conduct manual single-particle analyses of a limited number of samples.

Sea salt. Because of the inland location of Phoenix it is not intuitive that its aerosol would have a measurable marine component. In fact, however, particles such as the one shown in Photo 1 of Figure 5-1, consisting only of Na and Cl and having a cubic structure, were quite easy to find in Phoenix samples having measurable amounts of Na. The Hybrid Single-Particle Lagrangian Integrated Trajectory Model version 4.3 (Draxler, 1999) was used to compute back-trajectories for eleven samples having the highest Na concentrations. Virtually all of the trajectories originated from a westerly direction, with most having passed over the Pacific Ocean less than 48 h earlier, clearly suggesting a marine impact. Previous SEM work (Saucy et al., 1991; Katrinak et al., 1995) has identified possible sea salt particles in the Phoenix area.

Fly Ash particles. Fly ash particles (spherical alumino-silicates with minor amounts of Fe and Ca) were observed in most samples examined by SEM/EDX. A typical fly ash particle is shown in Photo 2 of Figure 5-1. A spherical particle shape is indicative of any high-temperature process, including combustion or smelting. Fly ash particles have been previously

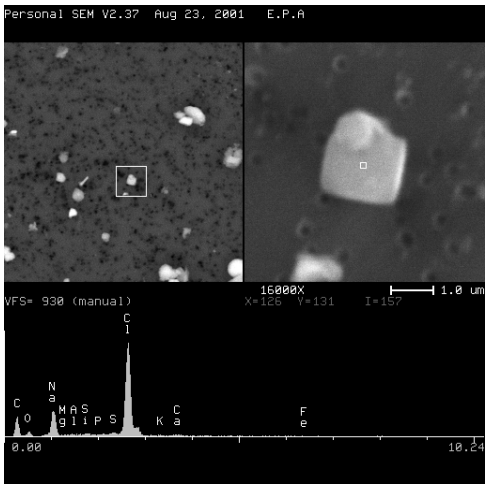

Photo 1

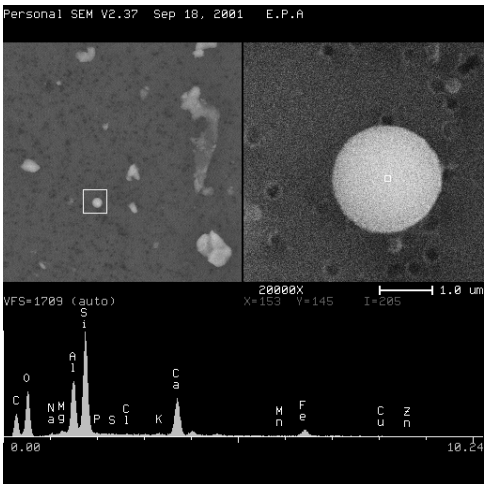

Photo 2

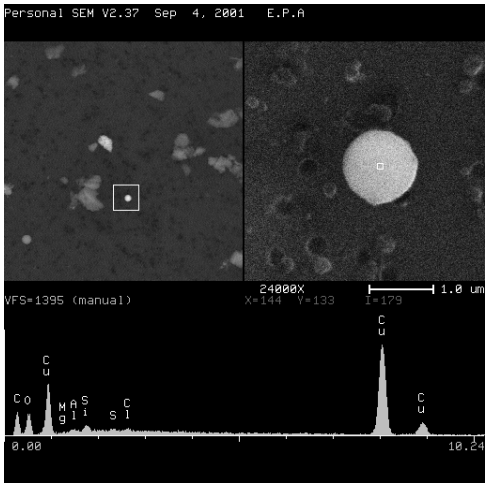

Photo 3

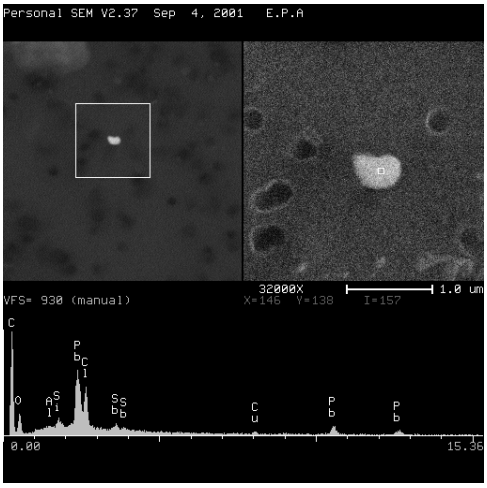

Photo 4

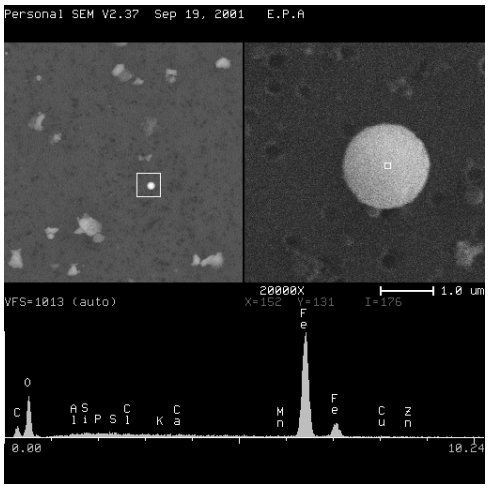

Photo 5

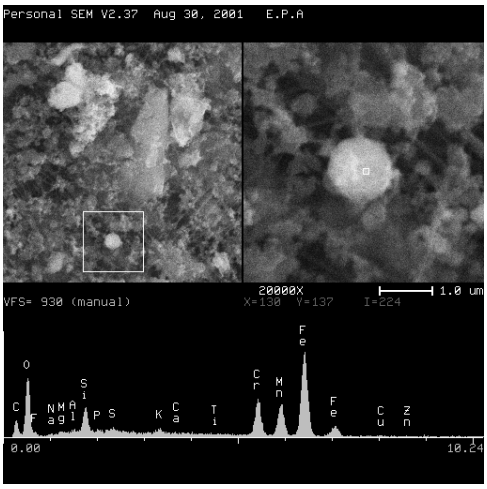

Photo 6

Figure 5-1. Examples of particles identified by SEM/EDX (Photos 1- 6). The upper-left quadrant of each photomicrograph shows a field of view with the particle of interest within the smaller square in that field. The upper-right quadrant shows a zoomed-in view of the feature (the area from within the square in the upper-left quadrant), and the lower half shows the elemental spectrum acquired with the electron beam centered on the small square in the zoomed-in view. A 1-µm scale appears just below the upper-right quadrant.

observed in Phoenix and attributed to coal-fired power plant emissions (Post and Buseck, 1984).

Cu-, Pb-, and Zn-bearing particles. Various studies of the Phoenix aerosol have identified (Saucy et al., 1991) and sought to quantify (Chow et al., 1991; Ramadan et al., 2000) emissions from copper smelters, the nearest of which are located about 100 km to the southeast. Source measurements have shown (Small et al., 1981) that copper smelter plumes in this region are highly enriched in the elements Cu, Zn, and Pb compared with crustal abundances. Other sources such as municipal incinerators or industries making or using bronze may also be strongly enriched in one or more of these elements. Particles from a sample associated with a southeasterly back-trajectory (the general direction of the copper smelters in the area) were examined by SEM/EDX. On an individual particle basis, Cu-bearing particles were most often seen as spheres in their pure oxide form (Photo 3 of Figure 5-1), while Pb-bearing particles were most often seen combined with Cl (Photo 4 of Figure 5-1). These two elements were not generally found in combination with each other (although Photo 4 does show a small amount of Cu in the Pb-Cl particle). Zn-bearing particles were observed less frequently than Pb- or Cu-bearing particles and were typically combined with Pb, Cu, or other metals. Collectively, this evidence suggests that any high-temperature or other process employing Cu, Pb, and/or Zn may be contributing to particles composed of these elements measured in the Phoenix area.

Spherical Fe particles. Numerous iron oxide or Fe-bearing particles were observed on the samples examined by SEM/EDX. Among these were spherical iron oxide particles (Photo 5 of Figure 5-1), again indicating a high-temperature process was involved in their formation. Researchers have previously reported iron oxides as being one of the main types of particles produced by iron foundries (Post and Buseck, 1984). Two such facilities were operating near Phoenix during the time of this field study (U.S. EPA, 1996). Additional SEM/EDX work has identified iron microspheres in foundry emissions (Michaud et al, 1993). Iron foundry operations were not identified by the Unmix calculation, most likely because of their low impact on the overall fine mass loading.

Mn-bearing particles. These particles were investigated by SEM because of their unexpected association with the Unmix-generated source that was attributed to diesel emissions. Photo 6 of Figure 5-1 shows a typical Mn-bearing fine particle located on a Teflon® membrane sample filter identified as having a relatively high diesel source contribution. The particle shown is composed principally of Fe, Mn, Cr and Si, with Fe being the largest component. Its spherical shape is indicative of a high-temperature process, such as combustion or smelting.

Researchers using SEM (Zayed et al., 1999) have shown that for *automobiles* using the *gasoline* additive methylcyclopentadienyl manganese tricarbonyl (MMT), Mn-bearing particles sampled from the tailpipe also contained phosphorus and sulfur. Iron or other metals were not typically found. These do not appear to be similar to the Mn-bearing particles observed on the samples reported here, which are primarily iron-oxides, with lesser amounts of Mn and other metals but no phosphorus and/or sulfur. While this argues against the possibility that Mn in Phoenix aerosol may originate from the combustion of gasoline containing MMT, as has been speculated (Ramadan et al.), it does not clearly demonstrate that Mn is associated with diesel emissions.

An earlier study conducted in Phoenix (Post and Buseck, 1984) identified particles containing oxides of Fe or Zn, with smaller amounts of Mn, Cr, Si, Al, Cl, K, or Ca and suggested that these particles originate from iron foundries located SE of Phoenix. The Mn-bearing particles identified in the present study are consistent with the type of particles that may be emitted by iron foundries.

5.2.3 Summary of Results

Application of the Unmix receptor model to the 1995-1998 Phoenix $PM_{2.5}$ data set has resulted in a 5-source apportionment. Limited SEM examination of filter samples from the field study indicated the presence of additional sources (sea salt, copper smelter, iron foundry, fly ash), but their presumably small impacts on $PM_{2.5}$ were not quantified by Unmix.

5.3 Fort Hall Source Apportionment Study

The objective of the Fort Hall Source Apportionment Study (Willis et al., 2001) was to identify and quantify individual sources within the Astaris (formerly FMC) elemental phosphorus plant that contribute to exceedances of the NAAQS for 24-h PM_{10}. The Astaris plant is located on the Fort Hall Indian Reservation near Pocatello, ID. The source apportionment effort relied heavily on XRF analysis of ambient 24-h $PM_{2.5}$ and $PM_{10-2.5}$ data collected at three monitoring sites. Wind-directional analysis was also critical in locating major emission sources. The major conclusion of the study was that fine-fraction phosphate was the dominant species contributing to PM_{10} exceedances, though in general, resuspended coarse dusts from raw and processed materials at the plant were also needed to create an exceedance. Major sources that were identified included the calciners, the CO flares, process-related dust, and electric-arc furnace operations.

SEM/EDX analyses of source and ambient samples played an important supporting role in the study by complementing and confirming results obtained by bulk XRF analysis, by providing visual and chemical confirmation that combustion-related phosphate particles dominate the ambient fine fraction downwind of the Astaris facility, and by helping in the identification of potential sources. Examples are discussed below.

Figure 5-2a is a micrograph of a fine-fraction dichot filter collected at the Primary site on August 26, 1997. The 24-h PM_{10} concentration was 86 $\mu g/m^3$. Particles are on the order of 1 μm in size and nearly all are P-rich. Many of the P-rich particles have a "wet" appearance and cling to the filter's Teflon fibers

like dewdrops. During exceedances, the concentration of P-rich particles on the filter can be so great that the particles begin to coalesce on the filter, forming P-rich islands as shown in Figure 5-3, collected during a PM_{10} exceedance when the 24-h PM_{10} concentration was 206 $\mu g/m^3$. Manual SEM/EDX analyses of ambient filters like these provided evidence early in the study for a major combustion source or sources emitting fine-fraction P-rich particles. A comparison of ambient particles with source particles collected in the ground flare (see Figure 5-4) and at the phos dock (see Figure 5-5) showed that the particle chemistry and morphology were very similar. Receptor model results, in fact, attribute on average about one-third of the PM_{10} during exceedances to flaring operations (the ground flare and the elevated flare) and fugitive emissions from the furnace building.

Particles in the coarse fraction show a distinctly different chemistry and morphology. Figure 5-2b shows the coarse-fraction mate to Figure 5-2a. Most coarse particles have the rough, irregular surface morphology characteristic of crustal dust or soil particles. Particle chemistry is dominated by Ca and Si, which are the major species in the phosphate ore used at Astaris. Ambient particle morphology and particle chemistry indicate a strong contribution to the coarse fraction from re-entrained dust related to raw or processed phosphate ore. Occasional fly ash spheres from combustion processes are observed such as the large Ca-Si-rich sphere in the upper center of the field. Similar combustion spheres were observed in dust and air samples collected in the furnace building (see Figure 5-6), suggesting the furnace as a probable source. The fine-fraction component collected on this coarse filter can be seen in the background as small, submicrometer phosphate particles clinging to the filter fibers.

SEM/EDX analyses can elucidate elemental associations in particle chemistry. For example, particle-bound mercury (HgP) was detected by bulk XRF in a few ambient fine-fraction samples at the level of about 0.2% of the total fine mass. A dedicated CCSEM search for Hg-rich particles yielded a number of Hg-rich particles embedded in P-rich matrix (see Section 3.3.5). The EDX spectra for these particles indicate that Hg and Se are present in most Hg-rich particles in a fairly constant ratio, perhaps as mercury selenide (tiemmanite). In addition, several Hg-rich particles also contained silver, although silver was below XRF detection limits in the bulk filter analysis.

Particles originating from different sources or processes often have distinctive chemistry and/or morphologies that can be used to identify and quantify the impact of these sources in ambient samples. Examples include the droplet-like P-rich particles from the flares or emissions from the furnace building; the Fe-P-V-rich ferrophos particles, which exhibit chonchoidal, glass-like fractures; and the P-K-rich particles from the hot slag tapping area.

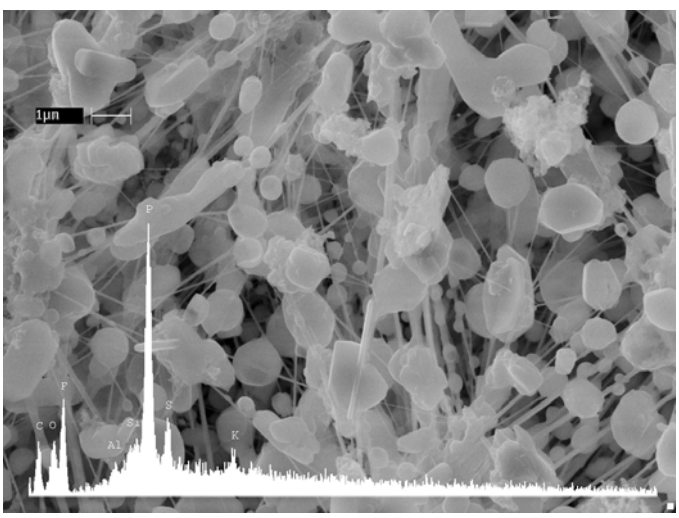

Figure 5-2a. Fine dichot sample collected at the Primary site (8/26/97). The superimposed X-ray spectrum shows that nearly all particles are phosphorus-rich. (The fluorine and carbon peaks are generated by the Teflon filter).

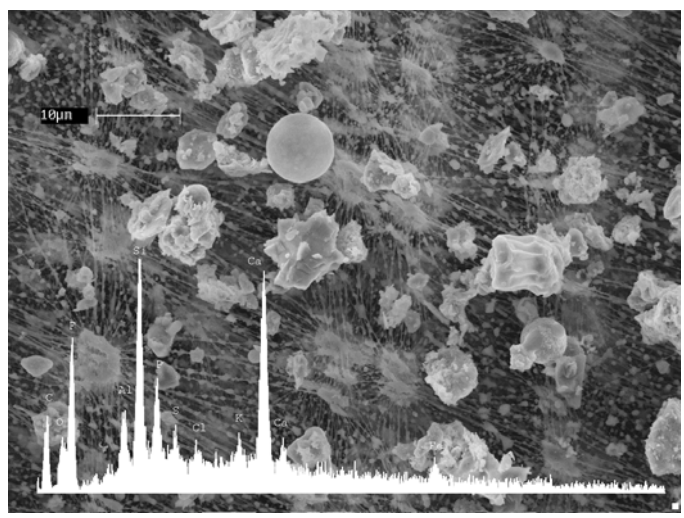

Figure 5-2b. Coarse dichot sample collected at the Primary site (8/26/97). Coarse particle chemistry is dominated by Ca and Si. Spherical particles such as the large Ca-Si-rich sphere in the upper center of the field are produced in combustion processes.

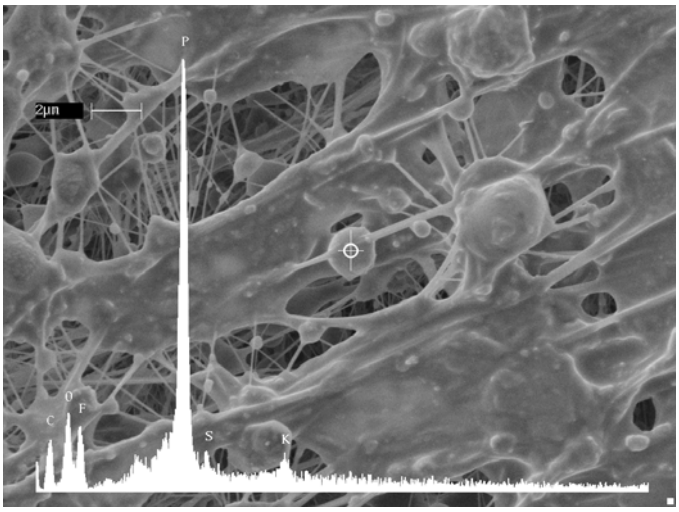

Figure 5-3. Ambient sample 57f, Primary site, 3/11/97. PM10 concentration for this day was 206 µg/m^3. Liquid-like phosphorus-rich particles coalesce on the heavily-loaded filter to form a quasi-continuous layer of phosphorus-rich material. The X-ray spectrum was acquired from the point shown by the cross hairs.

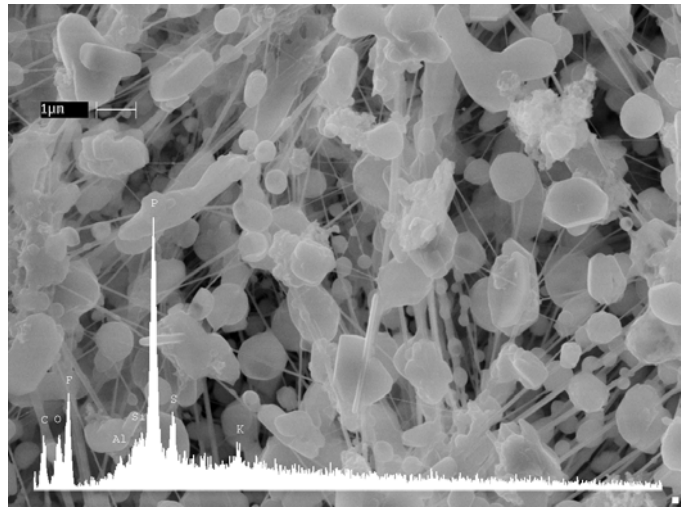

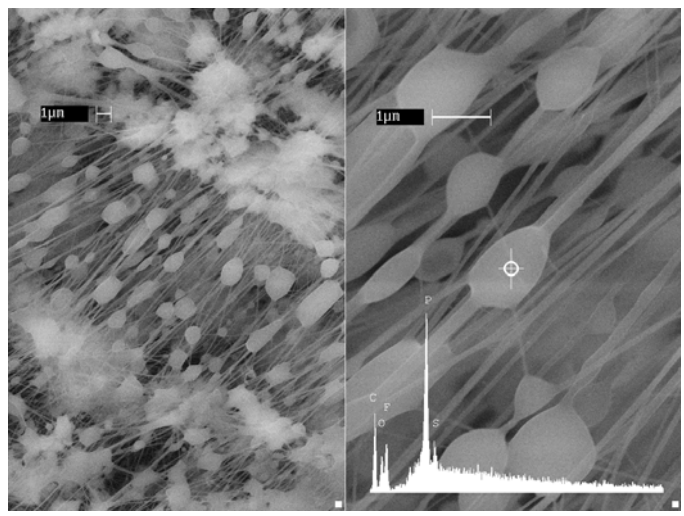

Figure 5-4. Top photo: Fine dichot sample collected at the Primary site (8/26/97). Bottom photo: Personal air sample collected from the ground flare plume during a miniflush. Particles are approximately 1 micrometer in size and cling to fine Teflon fibers comprising the filter. Nearly all particles are droplet-like P-rich particles similar to the one centered in the magnified image on the right, and similar in size, morphology and chemistry to the particles dominating the ambient fine-fraction sample in the top photo.

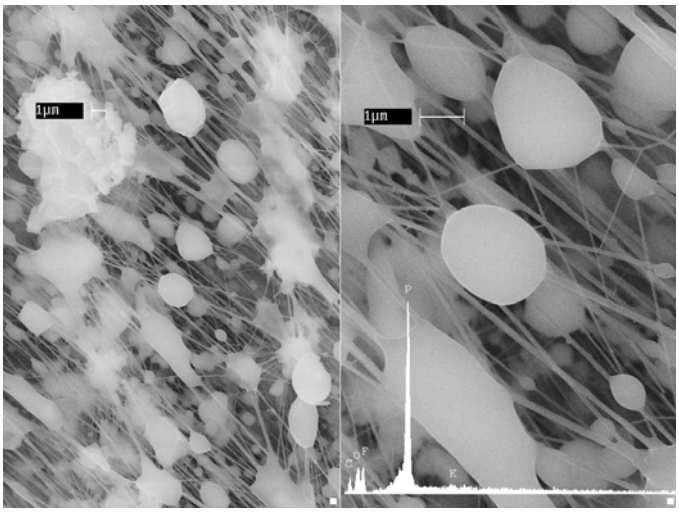

Figure 5-5. Personal air sample collected on the phos-dock. P-rich particles dominate the sample.

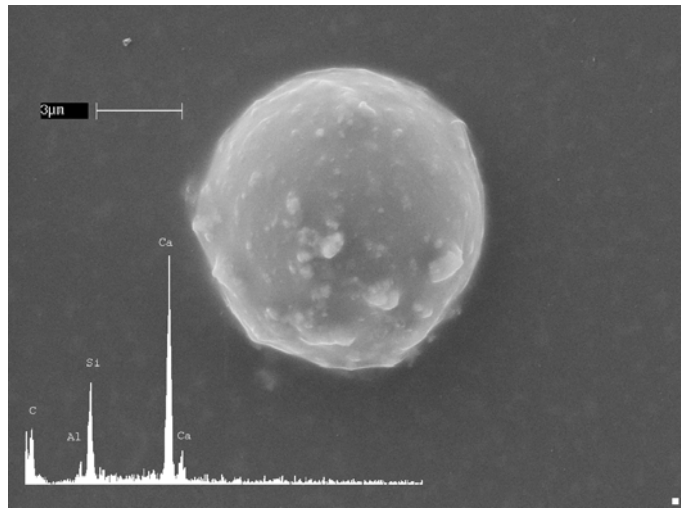

Figure 5-6. Calcium silicate fly ash from the burden level of the furnace building.

5.4 Baltimore Retirement Home Study

The United States Environmental Protection Agency (U.S. EPA) recently conducted the 1998 Baltimore Particulate Matter (PM) Epidemiology-Exposure Study of the Elderly. The primary goal of that study was to establish the relationship between outdoor PM concentrations and actual human PM exposures within a susceptible (elderly) sub-population. The overall study design has been described by Williams et al., 2000a, and Williams et al., 2000b. The study was conducted over a four-week period during July and August 1998. Personal, indoor, and outdoor sampling of particulate matter was conducted at a retirement center in the Towson area of northern Baltimore County. Concurrent sampling was conducted at a central community site 10 km from the retirement facility and four km from the Baltimore harbor area. The main objective of this work was to use computer-controlled scanning electron microscopy with individual-particle X-ray analysis (CCSEM) to measure the chemical and physical characteristics of geological and trace element particles collected at the various sampling locations in and around the retirement facility. The CCSEM work is described in detail in Conner et al. (2001) and is synopsized here. This work provides a preliminary model for how to conduct CCSEM analyses of ambient PM samples and how to present the results.

5.4.1 Methods

Three sets of samples were selected for CCSEM analysis based on mass loading on the filter and meteorological air mass transport during the sampling period (Sampson and Moody, 1981, Draxler, 1999). Each set consisted of the concurrently collected community, residential outdoor, and residential indoor coarse-fraction VAPS samples. Day 13 (8/7/98) of the sampling campaign was influenced by easterly transport and was selected to represent a primarily marine air mass. Day 20 (8/14/98) was influenced by southeasterly transport and represents industrial emissions, but was also impacted by marine air. Day 18 (8/12/98) was influenced by northerly transport and was selected to represent the background air with minimal influence of Baltimore industrial emissions and marine air masses. These sampling days will be referred to as “marine”, “industrial”, and “background”, respectively, in subsequent text, tables, and figures.

The PERSONAL SEM® (PSEM) (formerly R. J. Lee Instruments, Ltd., now Aspex Instruments, Trafford, PA) was used to conduct the manual SEM/EDX and computer-controlled (CCSEM) analyses. The PSEM features software that enables the user to review and summarize the data off-line. Particle classes can be developed by the analyst and are based on particle size, shape, image brightness, X-ray counts and/or chemical composition criteria. Particle classes provide a convenient way of summarizing the very large data sets acquired through computer-controlled analysis, and help to interpret the possible sources.

For the computer-controlled analyses, the PSEM was operated with a 20-kV, 30% spot size electron beam. (For the PSEM, spot size corresponds to beam current.) The working distance was set at 18-19 mm, which is the optimum distance for X-ray acquisition for the PSEM. A lens degaussing procedure was performed prior to each analysis to correct for lens hysteresis which may occur when operating conditions are changed between analyses. The backscattered electron mode was used for particle location, measurement, and analysis. A magnification of 1000x was used for the coarse particle analysis; fine particles were analyzed at a magnification of 1800x. Secondary electron images for each particle and analysis field were acquired. The

magnification for the individual particle images varied based on the size of the particle. Acquired images played a key role in the development of rules for particle classification.

The minimum *physical* diameter for the coarse particles was set at 1 μm in anticipation of some of those particles being greater than 2.5 μm *aerodynamic* diameter. The maximum physical diameter was set at 12 μm. The fine particle analysis was set up to look for particles with a physical diameter between 0.1 and 2.5 μm. The overlap was intentional to ensure that no particles were missed. The post-analysis classification rules eliminated any duplication.

X-ray counts for 26 elements (coarse fraction) ranging in atomic number from Na to Bi were acquired for each particle and saved along with other measured parameters. Bromine and Sr were also included in the fine particle analysis for a total of 28 elements. A few elements included are not typically measured in outdoor ambient particles but were found in the preliminary examination of the filters. Some might be found in the indoor environment (e.g., Zr, Bi), while others could be found in the industrial emissions in the Baltimore airshed (e.g., Sb, Cd).

A minimum number of X-ray counts was specified to adequately characterize each particle and to minimize the amount of data acquired for non-particle features (e.g., filter pores), or incomplete particle features (e.g., small portions of large, light-element particles such as skin flakes). The post-analysis summary applied an additional low counts rule to all samples to separate the low count particles from the rest of the data set.

Approximately 500 to 1000 particles need to be characterized to get a representative sample (Mamane et al., 2001), depending on the complexity of the sample and the overall research objectives. The Baltimore airshed contains a complex mixture of particles from a variety of natural and industrial sources, with the coarse fraction having more variety than the fine fraction. An adequate number of particles must be specified in the analysis routine to compensate for the later exclusion of some of the particles which fall outside of the size range of interest, or which will be excluded based on chemical composition (e.g., salt). Thus, up to 2000 particles were measured for each analysis, and two analyses (one for coarse particles and one for fine particles) were conducted per sample. The actual filter area covered in any given analysis depends on the loading of the particles meeting the analysis specifications.

The threshold is the brightness (grayscale) value in the digital imaging system which is chosen by the operator to discriminate between particles and filter background. The thresholds for particle detection and measurement were selected to acquire data for as many features as possible while avoiding excess detection of non-particle features. The threshold was self-correcting to account for the slight variation in image brightness from one analysis field to another. In addition, the threshold stability was manually verified at least once per analysis.

The CCSEM analysis results should be considered a lower-limit estimate of the numbers of carbonaceous, sulfate, ammonium salts, or other light-element particles. Such particles do not produce a significant backscattered electron signal, resulting in poor contrast with the filter medium, and are typically smaller than 1 μm.

5.4.2 Summary of Manual SEM/EDX Analysis Results

Each sample was surveyed manually by SEM/EDX to assess their suitability for computer-controlled analyses. Particle loading must be light enough to have adequate separation of the particles for the computer-controlled analysis. The preliminary manual survey also provides information on particle size and chemistry, which is used to set up the CCSEM analysis parameter files and familiarize the analyst with the sample.

Manual examinations indicated that the selected samples had adequately spaced particles. Both residential outdoor and community samples were loaded with particles of geological and industrial origin. The indoor samples were lightly loaded. Most samples collected at the outdoor and community sites on the marine air and industrial air days were covered with large amounts of both fine and coarse salt (NaCl). The overwhelming numbers of salt particles on samples impacted by a marine air mass would have required a prohibitive amount of time to acquire data for a representative number of non-salt particles, the particles of primary interest. Thus, an analysis rule was written to reject most of the salt particles. In addition, a post-analysis rule was developed as part of the particle classification system (see Section 5.4.3) to separate the remaining salt particles that were not screened out by the analysis rule.

5.4.3 Summary of CCSEM Analysis Results

Following the analysis, particle classification rules (see Appendix C) were developed to summarize the CCSEM data. These particle classification rules were designed to classify particles based on size, shape (aspect ratio), elemental composition, X-ray counts, and/or video (grayscale brightness) level (reported as a numeric value) of the particle image. The rules were applied to each sample, and results evaluated by examining both measured parameters and particle images. Rules were changed or added based on these evaluations, and the process continued in an iterative manner until the particle classifications were judged to be satisfactory, based on the uniformity of chemical and physical characteristics within a particle class. The rules were applied to other samples to make minor adjustments and to test the robustness of the classification scheme, based on the uniformity of particle characteristics within each particle class both within a single sample and across all samples. For all particles reported to contain Pb or other trace metals, the X-ray spectrum was reviewed to verify the identification of such elements.

The CCSEM coarse particle classifications are compared in Figures 5-7. The CCSEM fine particle classifications are compared in Figures 5-8. Data are reported as number of particles per unit filter area for each particle class. Unit filter area was used as a surrogate for volume of air sampled because approximately the same volume of air (maximum and minimum

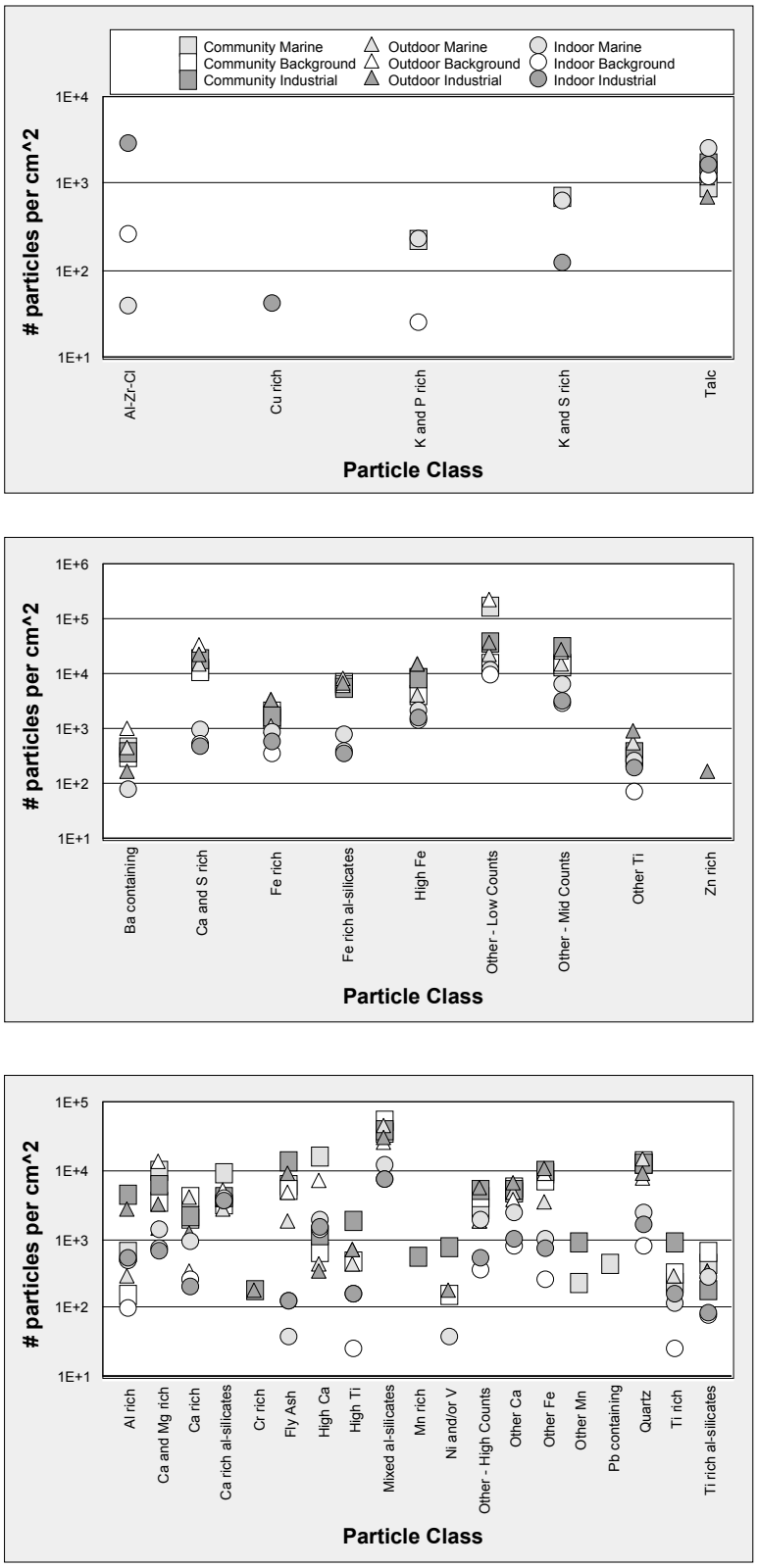

Figure 5-7. Comparison of CCSEM particle classifications for $PM_{10-2.5}$ (coarse) particle classes (a) dominant at the residential indoor site, (b) dominant at the residential outdoor site, (c) dominant at the ambient community site.

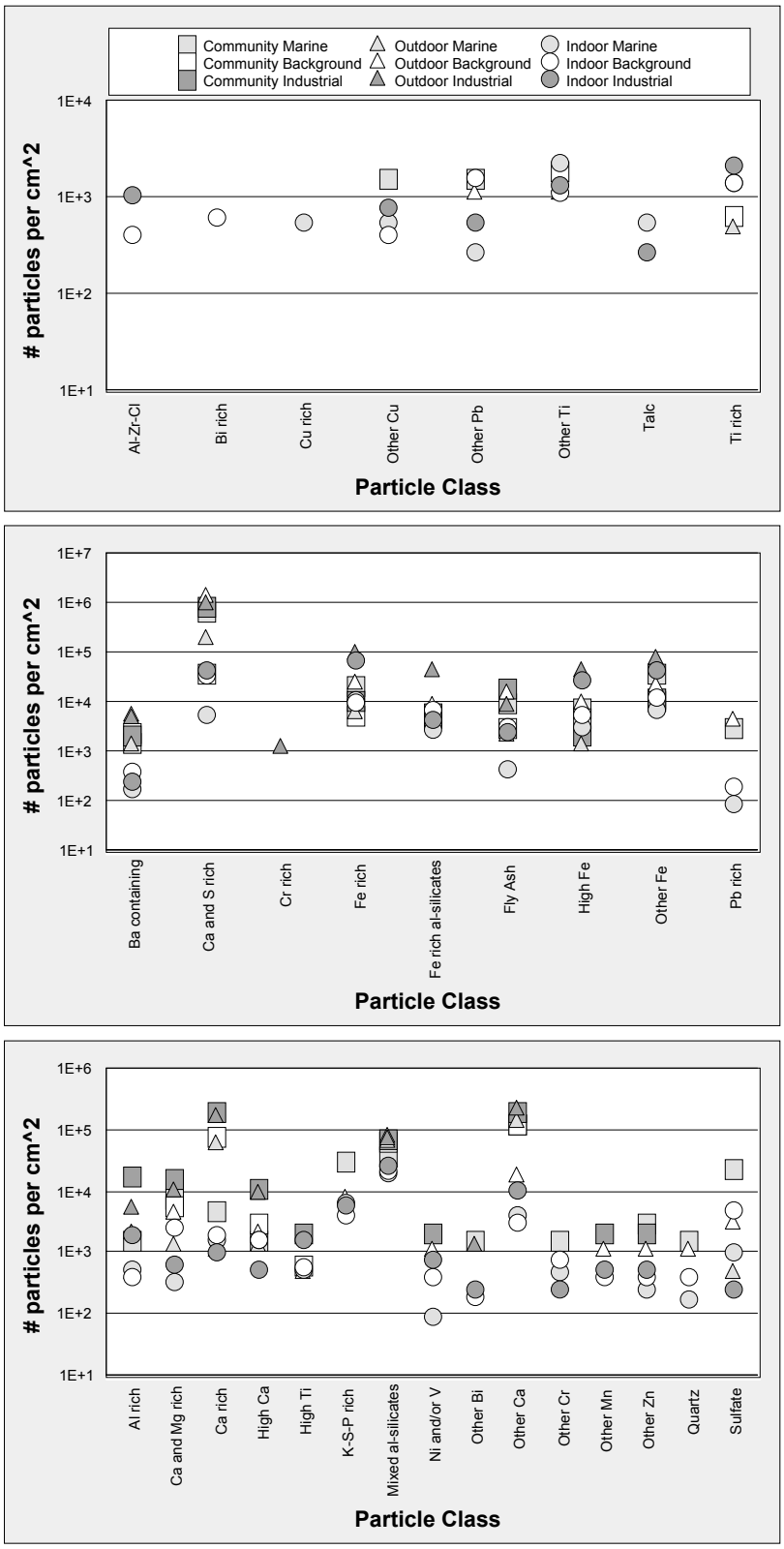

Figure 5-8. Comparison of CCSEM particle classifications for $PM_{2.5}$ (fine) particle classes (a) dominant at the residential indoor site, (b) dominant at the residential outdoor site, (c) dominant at the ambient community site.

volumes differed by less than 9%) was drawn through each filter. Reporting data in this way provided a satisfactory means of comparing particle number concentrations among samples.

The following are the principal findings of this analysis:

1. At both the community and outdoor sites, particle types associated with industrial activities (e.g., Al rich, Cr rich, Ni and/or V, Fly Ash) were measured at their highest concentrations on the industrial air mass trajectory day. These were found at much lower concentrations, or not at all, at the indoor site on this day, as expected for coarse particles of industrial origin.
2. Coarse particles characterized by high concentrations of Ca, Mg, and K (components of sea salt) were measured at their highest concentrations on the marine air mass trajectory day at the community site. The outdoor site appeared to be less impacted by marine air on that day.
3. Several particle classes were observed predominantly or exclusively at the indoor sampling location. The most prominent is the Al-Zr-Cl particle class, found exclusively indoors in both the fine and coarse fractions. Source images and spectra (Conner et al., 2001) support the hypothesis that Al-Zr-Cl particles originated from a personal antiperspirant product.
4. Evidence was found to support the hypothesis that cosmetic products may be a source of particulate matter indoors among this unique study population (Conner et al., 2001). However, this population may not be considered fully representative of the general elderly population.
5. Review of acquired images demonstrated the capability of the CCSEM technique to identify spherical particles, which are generally indicative of combustion or other high temperature processes characteristic of industrial activities. These spherical particles were found in the coarse fraction almost exclusively at the outdoor and community sites.
6. Review of acquired images demonstrated the capability of the CCSEM technique to identify pollens and spores. The highest concentration of these particles was found at the outdoor site on the background air day.

5.4.4 Conclusions

The CCSEM results show that the relative abundances of some geological and trace element particle classes identified at the outdoor and community locations differ from each other and from the indoor location. Particle images acquired during the computer-controlled analyses played a key role in the identification of certain particle types. Review of these images was particularly useful in distinguishing spherical particles (usually indicative of combustion) from non-spherical particles of similar chemical composition. Pollens and spores were also identified through a manual review of the particle images. Overall, this work shows that CCSEM and manual SEM/EDX can contribute to the understanding of the sources of particulate matter in different micro-environments in a way that is complementary to bulk elemental analysis techniques.

5.5 World Trade Center Study

The potential health implications of exposure to dust from the collapse of the World Trade Center (WTC) motivated a study of samples collected on and near the WTC site. SEM/EDX was used to obtain chemical and physical characteristics of particles and fibers found in hand-collected bulk material and in filter-based air monitoring samples.

5.5.1 Verification of XRF Results

Figure 5-9 shows a gold particle identified in a hand-collected dust sample. X-ray fluorescence analysis of this dust had shown detectable levels of gold which is unusual. The size of the gold particle (~1 μm) and the roughly spherical shape suggest that the particle was formed in a high-temperature combustion process.

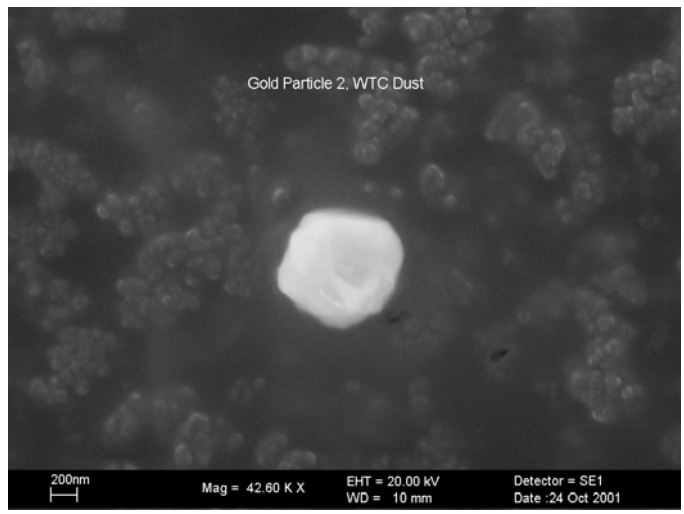

Figure 5-9. Micrometer-sized gold particle in World Trade Center dust sample.

5.5.2 Analysis of Bulk Sample

Bulk material was collected from a car windshield located in a parking garage about 3 blocks from the WTC site. This sample is thought to represent the initial light-colored cloud that emanated from the tower collapse. The covered garage location provided some protection from rains which had fallen since the initial deposit of the material.

A small amount of the bulk material was sprinkled onto sticky carbon tabs affixed to aluminum SEM stubs. Images and X-ray spectra of representative features were manually acquired. Images were created using the backscattered electron mode to avoid distortion of the image due to charging of the specimen surface. Each image and spectrum was saved electronically to a Zip Disk.

In general, this bulk material was quite fibrous and tended to aggregate into large clumps. Evidence of the fibrous nature of

the particles is presented in Figure 5-10, which shows three randomly selected fields of view taken at low magnification. Examples of individual fibers are shown in Figure 5-11. Note that though SEM is not the definitive or sole method for identifying asbestos, it is unlikely that the fibers found in this particular sample are asbestos fibers, based on their variable size and chemical composition. Most of the individual particles or fibers had a Ca-Si-Al-Mg-S composition and ranged in diameter between approximately 1 and 10 μm. The size and composition of these fibers suggests insulation materials as the source. Some carbonaceous fibers were also found, as depicted in one of the micrographs in Figure 5-11. There are numerous possible sources for carbonaceous fibers, including any type of fabric or textile which may have been used in the buildings' interior structure or furnishings.

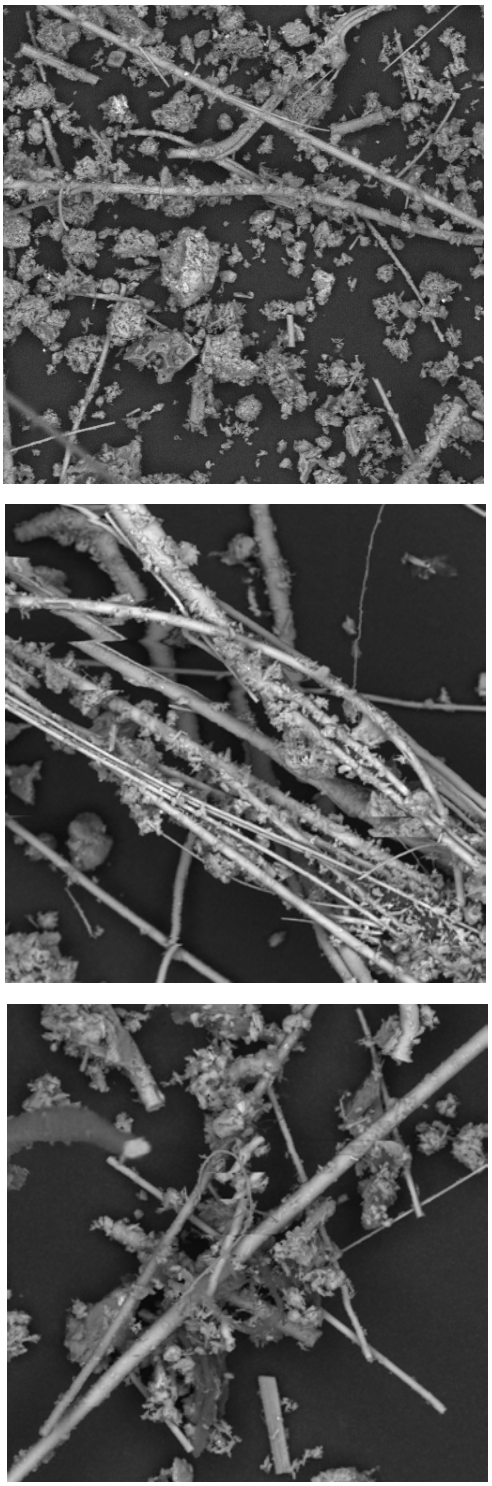

Figure 5-10. Three randomly selected fields of view of a fibrous bulk material collected in a parking garage near the WTC site.

Examples of particles less than 10 μm in diameter are presented in Figure 5-12. Most of these were composed primarily of Ca and S (gypsum) with wallboard and plaster materials being the likely source. Some metals including Fe and Zn, were also found.

5.5.3 Analysis of Ambient Air Sample

A coarse fraction VAPS sample was collected in NYC in September 2001. The coarse fraction of a VAPS filter also contains a small fraction of the fine particles, enabling simultaneous examination of both the coarse and fine particulate matter.

A small (less than 1 cm^2) piece of filter material was affixed to aluminum SEM stubs using a carbonaceous suspension. Images and X-ray spectra of representative features were manually acquired. Images were created using both the backscattered and secondary electron modes. Each image and spectrum was saved electronically.

SEM/EDX data is best presented in image format. A randomly selected field of view is depicted in Figure 5-13. This figure clearly shows the "honeycomb" particle distribution typical of samples collected on polycarbonate filters with no additional filter backing to act as a diffuser.

Images of 44 representative particles, with emphasis on metal-containing particles, were acquired and are presented in Appendix D. Most of the particles were either Ca-S, Fe or Fe-containing Pb-Cl or other Pb-containing, Zn-S, Na-Cl, carbonaceous, aluminosilicates, carbonaceaous, or spheres of various compositions. Such a variety of composition is typical of urban ambient air samples. The prevalence of the Ca-S particles probably indicates some impact from the WTC collapse (see previous section on analysis of bulk sample).

5.6 Source Particle SEM/EDX Data

The NERL SEM Laboratory has an on-going project to create an atlas of various source particulates. The goal of the NERL Particle Atlas is to provide a reference tool to assist microscopists in identifying particles and possible sources in ambient air samples. Each entry in the atlas includes a photomicrograph and an X-ray spectrum of a particle (or particles) considered to be representative of the source type. A description of the sample and details about the sample's collection and preparation are also provided. Selections from the particle atlas are presented in Appendix E.

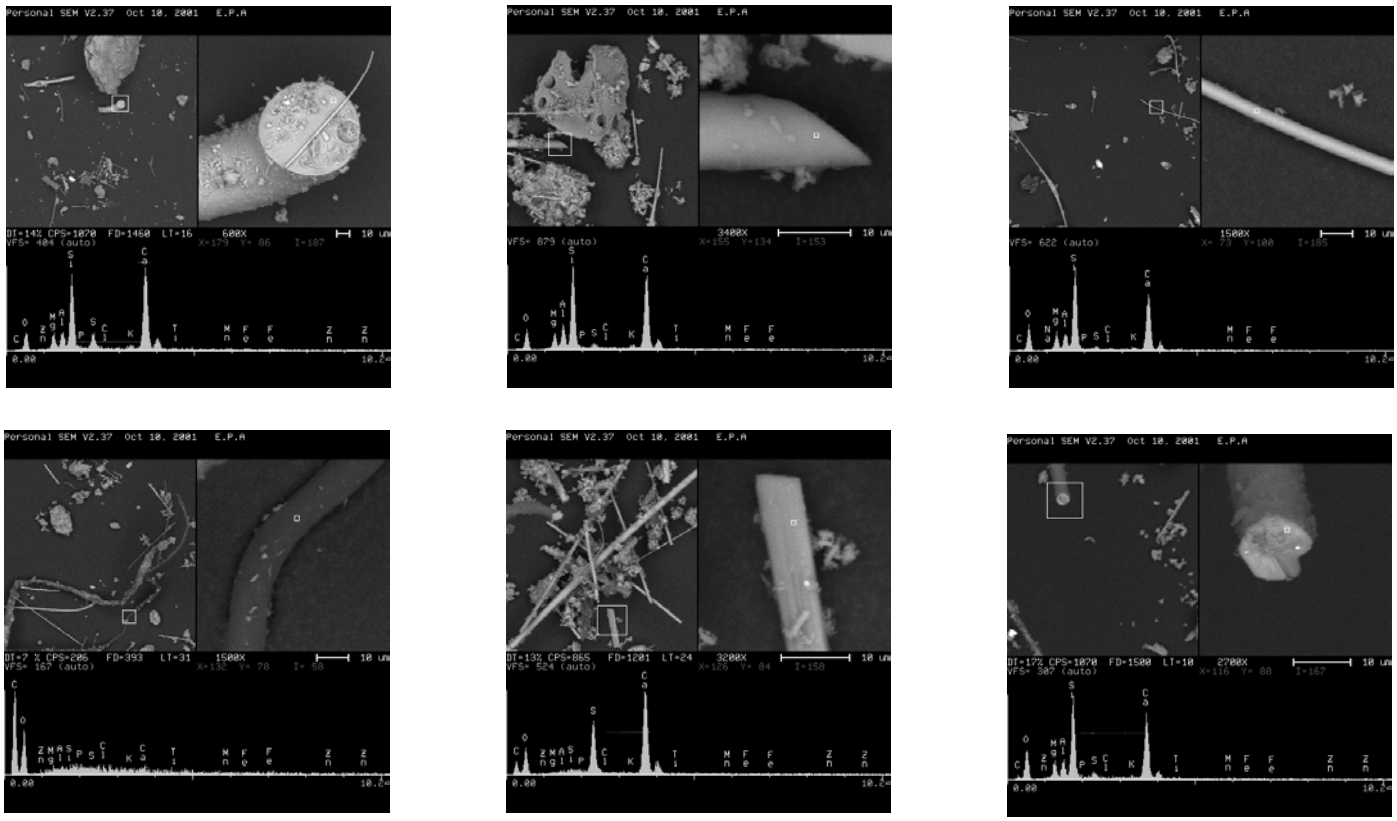

Figure 5-11. Examples of individual fibers from a fibrous bulk material collected in a parking garage near the WTC site. The upper-left quadrant of each photomicrograph shows a field of view with the particle of interest within the smaller square in that field. The upper-right quadrant shows a zoomed-in view of the feature (the area from within the square in the upper-left quadrant), and the lower half shows the elemental spectrum acquired with the electron beam centered on the small square in the zoomed-in view.

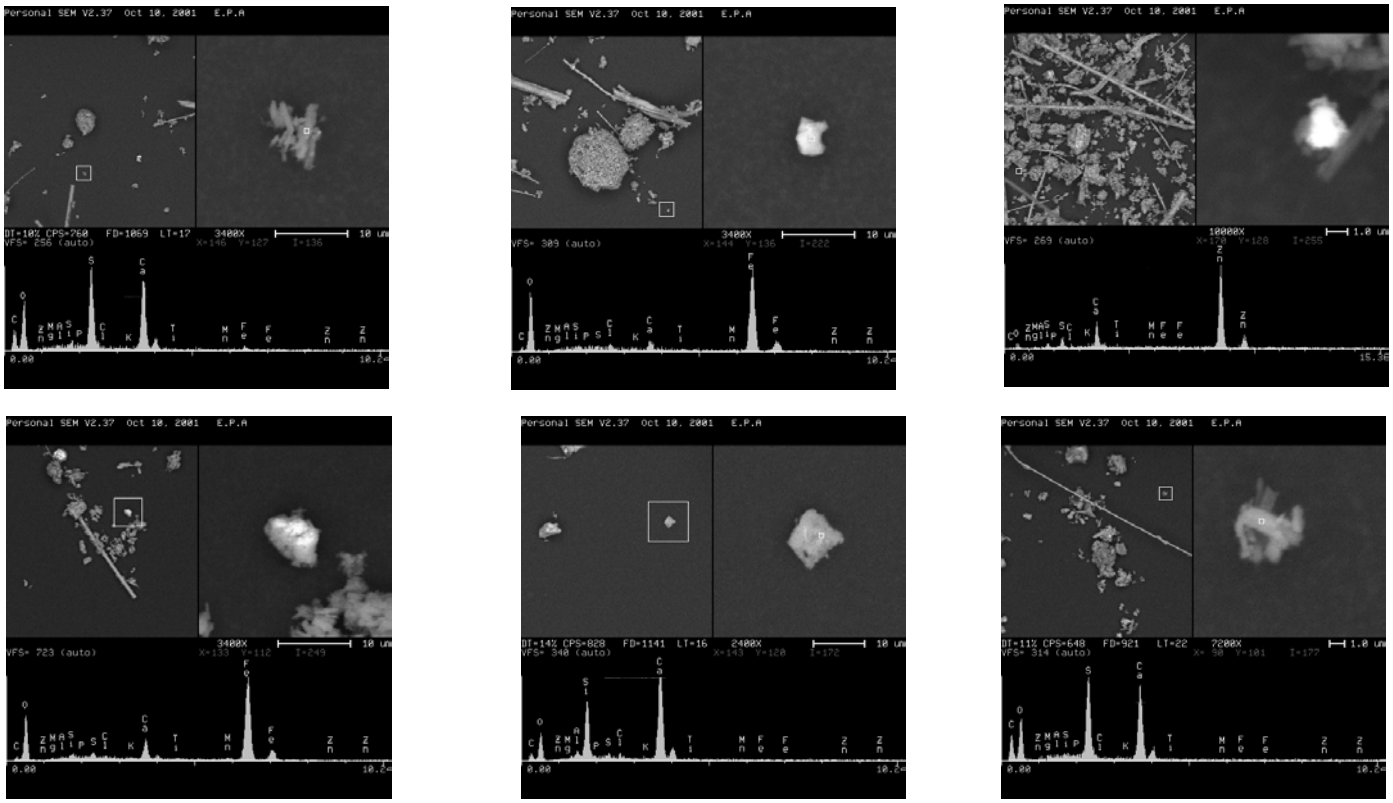

Figure 5-12. Examples of individual particles (<10 µm) from bulk material collected in a parking garage near the WTC site. The upper-left quadrant of each photomicrograph shows a field of view with the particle of interest within the smaller square in that field. The upper-right quadrant shows a zoomed-in view of the feature (the area from within the square in the upper-left quadrant), and the lower half shows the elemental spectrum acquired with the electron beam centered on the small square in the zoomed-in view.

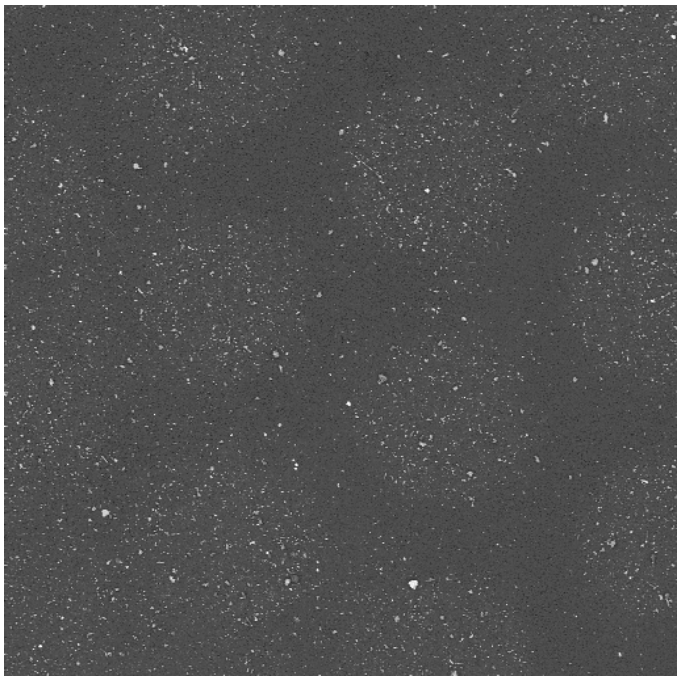

Figure 5-13. Randomly selected field of view of VAPS-collected coarse fraction filter showing “honeycomb” particle distribution.

Chapter 6
References

Anderson, J.R.; Buseck, P.R.; Saucy, D.A. (1992). Characterization of Individual Fine-Fraction Particles from the Arctic Aerosol at Spitsbergen, May-June 1987. ***Atmos. Environ.*** 26A:1747–1762.

Anderson, C.A.; Hasler, M.F. (1966). In *Proc. 4th Intl. Conf. On X-ray Optics and Microanalysis* (R. Castaing, P. Deschamps and J. Philibert, eds.) Hermann: Paris, p. 310.

Anderson, J.R.; Aggett, F.J.; Buseck, P.R.; Germani, M.S.; Shattuck, T.W. (1988). Chemistry of Individual Aerosol Particles from Chandler, Arizona, an Arid Urban Environment. ***Environ. Sci. Technol.*** 22:811–818.

Andreae, M.O.; Charlson, R.J.; Bruynseels, F.; Storms, H.; Van Grieken, R.; Maenhut, W. (1986). Internal Mixture of Sea Salt, Silicates, and Excess Sulfate in Marine Aerosols. ***Science*** 232:1620–1624.

Armstrong, J.T.; Buseck, P.R. (1975). Quantitative Chemical Analysis of Individual Microparticles Using the Electron Microprobe. ***Theoretical Anal. Chem.*** 47: 2178-2192.

Ayers, G.P. (1978). Quantitative Determination of Sulphate in Individual Aerosol Particles. ***Atmos. Environ.*** 12:1613–1621.

Bernard, P.C.; Van Grieken, R.E.; Eisma, D. (1986). Classification of Estuarine Particles Using Electron Microprobe Analysis and Multivariate Methods. ***Environ. Sci. Technol.*** 20:467–473.

Bigg, E.K.; Ono, A.; Williams, J.A. (1974). Chemical Tests for Individual Submicron Aerosol Particles. ***Atmos. Environ.*** 8:1–13.

Bruynseels, O.F.; Van Grieken, R. (1987). Study of Inorganic Ammonium Compounds in individual Marine Aerosol Particles by Laser Microprobe Mass Spectrometry. ***Analytica Chimica Acta*** 195:117-124.

Buseck, P.R.; Bradley, J.P. (1982). Electron Beam Studies of Individual Natural and Anthropogenic Microparticles: Compositions, Structures, and Surface Reactions. In *Heterogeneous Atmospheric Chemistry, Geophysical Monograph 26,* D.R. Schryer, ed., American Geophysical Union, Washington, DC, pp 57–76.

Buseck, P.R.; Bradley, J.P. (1982). Electron Beam Studies of Individual Natural and Anthropogenic Microparticles: Compositions, Structures, and Surface Reactions. In *Heterogeneous Atmospheric Chemistry, Geophysical Monograph 26,* D.R. Schryer, ed., American Geophysical Union, Washington, DC, pp 57-76.

Carpenter, G.A.; Grossberg, S.; Rosen, D.B. (1991). ART2-A: An Adaptive Resonance Algorithm for Rapid Category Learning and Recognition. ***Neural Networks***, 4:493-504.

Casuccio, G.S.; Janocko, P.B.; Lee, R.J.; Kelly, J.F.; Dattner, S.L.; Mgebroff, J.S. (1983a). The Use of Computer Controlled Scanning Electron Microscopy in Environmental Studies. ***J. Air Pollut. Control Assoc.*** 33:937.

Casuccio, G.S.; Janocko, P.B.; Dattner, S.L.; Mgebroff, J.S.; Zalar, J.L. (1983b). Measurement of Ambient Hi-Vol Filters by Microscopic and Bulk Chemistry Methods. Presented at the 76th Annual Meeting of the Air Pollution Control Association, Atlanta, GA, June 1983.

Casuccio, G.S.; Schwoeble, A.J.; Henderson, B.C.; Lee, R.J.; Hopke, P.K.; Sverdrup, G.M. (1988). The Use of CCSEM and Microimaging to Study Source/Receptor Relationships. In *Receptor Models in Air Resources Management*, J.G. Watson, ed., Air Pollution Control Association Specialty Conference, San Francisco, CA, February 1988.

Casuccio, G.S. (2002). Personal communication.

Casuccio, G.S.; Lersch, T.L.; Schlaegle, S.F.; Martello, D.V. (2002). Characterization of Ambient Carbonaceous Particles Using Electron Microscopy Techniques. American Chemical Society, Fuel Chemistry Division Preprints 47(1).

Chow, J.C.; Watson, J.G.; Richards, L.W.; Haase, D.L.; McDade, C.; Dietrich, D.L.; Moon, D.; Sloane, C. The 1989-1990 Phoenix PM_{10} Study, Volume II: Source Apportionment; DRI Document No. 8931.6F1, Desert Research Institute, Reno, NV, 1991.

Conner, T.L., Norris, G.A., Landis, M.S., and Williams, R.W. Individual particle analysis of indoor, outdoor, and community samples from the 1998 Baltimore particulate matter study. Atmospheric Environment 35 (23):3935-3946 (2001).

Costantino, J.P.; Janocko, P.B.; Casuccio, G.S. (1983). Assessment of Thoracic Particulate Levels at Surface-Mining Operations. Bituminous Coal Research, Report No. BCR L-1355, March.

Dockery, D.W.; Pope, C.A.; Xu, X.; Spengler, J.D.; Ware, J.H.; Fay, M.E.; Ferris, B.G.; Speizer, F.E. (1993). An Association between Air Pollution and Mortality in Six U.S. Cities. ***N. Engl. J. Med.*** 329:1753–1759.

Dockery, D.W.; Pope III, C.A. (1994). Acute Respiratory Effects of Particulate Air Pollution. ***Ann. Rev. Public Health*** 15:107–132.

Draxler, R.D., 1999. Hysplit_4 User's Guide, Draft NOAA Technical Memorandum, Air Resources Laboratory, Silver Springs, MD.

Dzubay, T.G.; Mamane, Y. (1989). Use of Electron Microscopy Data in Receptor Models for PM-10. ***Atmos. Environ.*** 23:467–476.

Dzubay, T.G.; Stevens, R.K.; Balfour, W.D.; Williamson, H.J.; Cooper, J.A.; Core, J.E.; De Cesar, R.T.; Crutcher, E.R.; Dattner, S.L.; Davis, B.L.; Heisler, S.L.; Shah, J.J.; Hopke, P.K.; Johnson, D.L. (1984). ***Atmos. Environ.*** 18:1555–1566.

Fisher, G.L.; Prentice, B.A.; Iberman, D.S.; Ondov, J.M.; Bierman, A.H.; Ragaini, R.C.; McFarland, A.R. (1978). Physical and Morphological Studies of Size-Classified Coal Fly-Ash. ***Environ. Sci. Technol.*** 12:447-451.

Germani, M.S.; Zoller, W.H. (1994). Solubilities of In-Stack Suspended Particles from a Municipal Incinerator. ***Atmos. Environ.*** 28:1393–1400.

Germani, M.S.; Small, M.; Zoller, W.H.; Moyers, J.L. (1981). Fractionation of Elements During Copper Smelting. ***Environ. Sci. Technol.*** 15:299–305.

Germani, M.S.; Buseck, P.R. (1991). Automated Scanning Electron Microscopy for Atmospheric Particle Analysis. ***Anal. Chem.*** 63:2232–2237.

Germani, M.S. (1991). Evaluation of Instrumental Parameters for Automated Scanning Electron Microscopy/Gunshot Residue Particles Analysis. ***J. Forensic Sci.*** 331-342.

Ghio, A.J.; Kennedy, T.P.; Whorton, R.; Crumbliss, A.L.; Hatch, G.E.; Hoidal, J.R. (1992). Role of Surface Complexed Iron in Oxidant Generation and Lung Inflammation Induced by Silicates. ***Am. J. Physiology.*** 263:L511-L518.

Ghio, A.J.; Stonehuerner, J.; Prtichard, R.J.; Piantadosi, C.A.; Quigley, D.A.; Dreher, K.L.; Costa, D.L. (1996). Humic-like Substances in Air Pollution Particulates Correlate with Concentrations of Transition Metals and Oxidant Generation. ***Inhalation Toxicology*** 8:479-494.

Goldstein, J.I.; Newbury, D.E.; Echlin, P.; Joy, D.C.; Romig Jr., A.D.; Lyman, C.E.; Fiori, C.; Lifshin, E. (1992). *Scanning Electron Microscopy and X-ray Microanalysis,* Second Edition. Plenum Press, New York.

Grasserbauer, M. (1977). The Present State of Local Analysis: Analysis of Individual Small Particles. ***Mikrochimica Acta*** 1:329–350.

Hanna, R.B.; Karcich, K.J.; Johnson, D.L. (1980). Determination of Particle Identities Via a Computer Assisted SEM-EDXA System. ***Scanning Electron Microsc.*** 1:323–328.

Henry, R.C. Unmix Version 2.3 Manual; **2001**, available with Unmix software (rhenry@usc.edu).

Hock, J.L.; Lichtman, D. (1983). A Comparative Study of In-Plume and In-Stack Collected Individual Coal Fly Ash Particles. ***Atmos. Environ.*** 17:849–852.

Henry, R.C. History and Fundamentals of Multivariate Air Quality Receptor Models; *Chemom. Intell. Lab. Syst.* **1997**, *37*, 37-42.

Hopke, P.K.; Mi, Y. (1990). Use of a Rule-Building Expert System for Classifying Particles Based on SEM Analysis. In *Scientific Computing and Automation,* E.J. Karjalainen, Ed., Elsevier Science Publishers B.V., Amsterdam, pp 179–198.

Hopke, P.K.; Song, X.-H. (1997). Classification of Single Particles by Neural Networks Based on the Computer-Controlled Scanning Electron Microscopy Data. ***Analytica Chimica Acta*** 348:375-388.

Jambers, W.; Van Grieken, R. (1997). Single Particle Characterization of Inorganic Suspension in Lake Baikal, Siberia. ***Environ. Sci. Technol.*** 31:1525–1533.

John, W.; Reischl, G. (1980). A Cyclone for Size-Selective Sampling of Ambient Air. ***J. Air Poll. Control Assoc.*** 30:872-876.

Johnson, D.; Hunt, A. (1995). Analysis of Lead in Urban Soils by Computer Assisted SEM/EDX—Method Development and Early Results. In *Lead in Paint, Soil and Dust: Health Risks, Exposure Studies, Control Measures, Measurement Methods, and Quality Assurance,* Special Technical Publication 1226, M. Beard and S. Allen Iske, Eds., American Society for Testing and Materials, Philadelphia, PA, pp 283–299.

Johnson, D.L.; McIntyre, B.L.; Stevens, R.K.; Fortmann, R.C.; Hanna, R.B. (1981). A Chemical Element Comparison of Individual Particle Analysis and Bulk Chemical Method. ***Scanning Electron Microsc.*** 1:469–476.

Johnson, D.L.; Twist, J.P. (1982). Statistical Considerations in the Employment of SAX Results for Receptor Models. In *Receptor Models Applied to Contemporary Pollution Problems*, APCA Specialty Conference Proceedings SP-48, S.L. Dattner and P.K. Hopke, Eds., Air Pollution Control Association, Danvers, MA, pp 224–237.

Johnson, D.L.; Davis, B.L.; Dzubay, T.G.; Hasan, H.; Crutcher, E. R.; Courtney, W.J.; Jaklevic, J.M.; Thompson, A.C.; Hopke. P.K. (1984b). Chemical and Physical Analyses of Houston Aerosol for Interlaboratory Comparison of Source Apportionment Procedures. ***Atmos. Environ.*** 18:1539–1553.

Johnson, D.L.; McIntyre, B; Fortmann, R; Stevens, R.K.; Hanna, R.B. (1984a). Particle Analysis → Bulk Analysis. ***Chemtech*** November:678–683.

Katrinak, K.A.; Rez, P.; Buseck, P.R. (1992). Structural Variations in Individual Carbonaceous Particles from an Urban Aerosol. ***Environ. Sci. Technol.*** 26:1967–1976.

Katrinak, K.A.; Anderson, J.R.; Buseck, P.R. (1995). Individual Particle Types in the Aerosol of Phoenix, Arizona. ***Environ. Sci. Technol.*** 29:321–329.

Kelly, J.F.; Lee R.J.; Lentz, S. (1980). Automated Characterization of Fine Particulates. ***Scanning Electron Microsc.*** 1:3111.

Kim, D.S.; Hopke, P.K.; Massart, D.L.; Kaufman, L.; Casuccio, G.S. (1987). Multivariate Analysis of CCSEM Auto Emission Data. ***The Science of the Total Environment*** 59:141–155.

Kim, D.S.; Hopke, P.K. (1988b). Source Apportionment of the El Paso Aerosol by Particle Class Balance Analysis. ***Aerosol Sci. Technol.*** 9:221–235.

Kim, D.S.; Hopke, P.K. (1988a). Classification of Individual Particles Based on Computer-Controlled Scanning Electron Microscopy Data. ***Aerosol Sci. Technol.*** 9:133–151.

Lee, R.J.; Fasiska, E.J.; Janocko, P.; McFarland, D.; Penkala, S. (1979). Electron-Beam Particulate Analysis. ***Ind. Res. Dev.*** June:25–28.

Lee, R.J.; Kelly, J.F. (1980). Applications of SEM-Based Automated Image Analysis. In *Microbeam Analysis*, D.B. Wittry, ed., San Francisco Press, San Francisco, CA.

Lewis, C.; Norris, G.; Henry, R.; Conner, T. Source Apportionment of Phoenix $PM_{2.5}$ Aerosol with the Unmix Receptor Model; *Journal of the Air and Waste Association* (in press.)

Linton, R.W.; Williams. P.; Evans, C.A. Jr.; Natusch, D.F.S. (1977). Determination of the Surface Predominance of Toxic Elements in Airborne Particles by Ion Microprobe Mass Spectrometry and Auger Electron Spectrometry. ***Anal. Chem.*** 49:1514–1521.

Mamane, Y. (1988). Estimate of Municipal Refuse Incinerator Contribution to Philadelphia Aerosol Using Single Particle Analysis—I. Source Analysis. ***Atmos. Environ.*** 22:2411–2418.

Mamane, Y.; Willis, R.; Conner, T. (2001). Evaluation of Computer-Controlled Scanning Electron Microscopy Applied to an Ambient Urban Aerosol Sample. ***Aerosol Sci. Technol.*** 34:97-107.

Mamane, Y.; de Pena, R. (1978). A Quantitative Method for the Detection of Individual Submicrometer Size Sulfate Particles. ***Atmos. Environ.*** 12:69–82.

Mamane, Y. (1990). Estimate of Municipal Refuse Incinerator Contribution to Philadelphia Aerosol Using Single Particle Analysis—II. Ambient Measurements. ***Atmos. Environ.*** 24B:127–135.

Mamane, Y. (1984). Characterization of Individual Particles Collected During the Deep Creek Lake Experiment. Paper 84-58.6, presented at the 77th Annual Meeting of the Air Pollution Control Association, San Francisco, 24–29 June.

Mamane, Y.; Miller, J.L.; Dzubay, T.G. (1986). Characterization of Individual Fly Ash Particles Emitted from Coal- and Oil-Fired Power Plants. ***Atmos. Environ.*** 20:2125–2135.

Mamane, Y.; Dzubay, T.G.; Ward, R. (1992). Sulfur Enrichment of Atmospheric Minerals and Spores. ***Atmos. Environ.*** 26A:1113–1120.

Mamane, Y.; Willis, R.; Stevens, R.; Miller, J. (1995). Scanning Electron Microscopy/X-ray Fluorescence Characterization of Lead-Rich Post-Abatement Dust. In *Lead in Paint, Soil and Dust: Health Risks, Exposure Studies, Control Measures, Measurement Methods, and Quality Assurance*, Special Technical Publication 1226, M. Beard and S. Allen Iske, eds., American Society for Testing and Materials, Philadelphia, PA, pp 268–282.

Marjamcki, M.J.; Keskinen, D. Chen; Pui, D. (1997). Calibration of the Electrical Low Pressure Impactor (ELPI). Abstracts of the 16th Annual Conference of the American Association for Aerosol Research, 63.

Martello, D.V.; Anderson, R.R.; White, C.M.; Casuccio, G.D.; Schlaegle, S.F. (2001). Quantitative Scanning Electron Microscopy Methods to Characterize Ambient Air $PM_{2.5}$. American Chemical Society, Fuel Chemistry Division Preprints 46(1).

Mészáros, A.; Vissy, K. (1974). Concentration, Size Distribution and Chemical Nature of Atmospheric Aerosol Particles in Remote Oceanic Areas. ***J. Aerosol Sci.*** 5:101–109.

Michaud, D.; Baril, M.; Perrault, G. Characterization of Airborne Dust from Cast Iron Foundries by Physico-Chemical Methods and Multivariate Statistical Analyses; *J. Air & Waste Manage. Assoc.* **1993**, *43*, 729-735.

Novakov, T.; Chang, S.G.; Harker, A.B. (1974). Sulfates as Pollution Particulates: Catalytic Formation on Carbon (Soot) Particles. ***Science*** 186:259–261.

Obrusnik, I; Starkova, B.; Blazek, J. (1989). Composition and Morphology of Stack Emission from Coal and Oil Fuelled Boilers. ***J. Radioanalytical and Nuclear Chemistry*** 133:377–390.

Paatero, P; Tapper, U. (1994). Positive Matrix Factorization: A Non-Negative Factor Model with Optimal Utilization of Error Estimates of Data Values. ***Environmetrics*** 5:111-126.

Paatero, P. (1997). Least Squares Formulation of Robust Non-Negative Factor Analysis. ***Chemometrics and Intelligent Laboratory Systems*** 37: 23-35.

Palotás, Á.B.; Rainey, L.C.; Sarofim, A.F.; Vander Sande, J.B.; Flagan, R.C. (1998). Where Did That Soot Come From? ***Chemtech*** July:24–30.

Parungo, F.; Nagamoto, C.; Hoyt, S.; Bravo, H. (1990). The Investigation of Air Quality and Acid Rain Over the Gulf of Mexico. ***Atmos. Environ.*** 24A:109–123.

Pope III, C.A.; Dockery, D.W.; Schwartz, J. (1995). Review of Epidemiological Evidence of Health Effects of Particulate Air Pollution. ***Inhal. Toxicol.*** 7(1):1–18.

Parungo, F.; Nagamoto, C.; Rosinski, J.;. Haagenson, P.L. (1986). A Study of Marine Aerosols over the Pacific Ocean. ***J. Atmos. Chem.*** 4:199–226.

Pósfai, M.; Anderson, J.R.; Buseck, P.R; Sievering, H. (1999). Soot and Sulfate Particles in the Remote Marine Troposphere. ***J. Geophys. Res.*** 104:21,685–21,693.

Pósfai, M.; Anderson, J.R.; Busick, P.R.; Shattuck, T.W.; Tindale, N.W. (1994). Constituents of a Remote Pacific Marine Aerosol: a TEM Study. ***Atmos. Environ.*** 28:1747–1756.

Post, J.E.; Buseck, P.R. (1984). Characterization of Individual Particles in the Phoenix urban Aerosol Using Electron Beam Instruments. ***Environ. Sci. Technol.*** 18:35–42.

Pueschel, R.F. (1976). Aerosol Formation During Coal Combustion: Condensation of Sulfates and Chlorides on Flyash. ***Geophys. Res. Lett.*** 3:651–653.

Ramadan, Z.; Song, X.-H.; Hopke, P.K. Identification of Sources of Phoenix Aerosol by Positive Matrix Factorization; *J. Air & Waste Manage. Assoc.* **2000**, *50*, 1308-1320.

Rothenberg, S.J.; Denee, P.; Holloway, P. (1980). Coal Combustion Fly Ash Characterization: Electron Spectroscopy for Chemical Analysis, Energy Dispersive X-ray Analysis, and Scanning Electron Microscopy. ***Appl. Spectroscopy*** 34:549–555.

Sampson, P.J., Moody, J.L., 1981. Trajectories as two-dimensional probability fields In: Air Pollution Modeling and its Application, Plenum Press, New York, pp. 43-54.

Saucy, D.A.; Anderson, J.R.; Buseck, P.R. (1991). Aerosol Particle Characteristics Determined by Combined Cluster and Principal Component Analysis. ***J. Geophys. Res.*** 96:7407–7414.

Saucy, D.A.; Anderson, J.R.; Buseck, P.R. (1987). Cluster Analysis Applied to Atmospheric Aerosol Samples from the Norwegian Arctic. ***Atmos. Environ.*** 21:2191–2206.

Schwartz, J. (1994). Air Pollution and Daily Mortality: A Review and Meta-Analysis. ***Environ. Res.*** 64:36–52.

Shattuck, T.W.; Germani, M.S.; Buseck, P.R. (1991). Multivariate Statistics for Large Data Sets: Applications to Individual Aerosol Particles. ***Anal. Chem.*** 63:2646–2656.

Small, M.; Germani, M.S.; Small, A.M.; Zoller, W.H.; Moyers, J.L. (1981). Airborne Plume Study of Emissions from the Processing of Copper Ores in Southeastern Arizona. ***Environ. Sci. Technol.*** 15:293–299.

Song, X.-H.; Hopke, P.K.. Solving the Chemical Mass Balance Problem Using an Artificial Neural Network. ***Environ. Sci. Technol.*** 30:531-535.

Song, X.-H.; Hadjiiski, L.; Hopke, P.K.; Ashbaugh, L.; Carvacho, O.; Casuccio, G.S.; Schlaegle, S. (1999). Source Apportionment of Soil Samples by the Combination of Two Neural Networks Based on Computer-Controlled Scanning Electron Microscopy. ***J. Air & Waste Manage. Assoc.*** 49:773-783.

U.S. Environmental Protection Agency. *National Emissions Trends Air Pollution Point Sources Database (1996).* http://www.epa.gov/air/data/index.html

Van Cleef, M.; Holt, S.A.; Watson, G.S.; Myhra, S. (1996). Polystyrene Spheres on Mica Substrates: AFM Calibration, Tip Parameters and Scan Artefacts. ***J. Microsc.*** 181:2–9.

Van Borm, W.A.; Adams, F.C; Maenhaut, W.A. (1989). Characterization of Individual Particles in the Antwerp Aerosol. ***Atmos. Environ.*** 23:1139–1151.

Vander Wood, T.; Brown, R. (1992). The Application of Automated Scanning Electron Microscopy/Energy Dispersive X-ray Spectrometry to the Identification of Sources of Lead-Rich Particles in Soil and Dust. ***Environmental Choices Technical Supplement.*** 1:July/August.

Watt, J. (1990). Automated Feature Analysis in the Scanning Electron Microscope. ***Microscopy and Analysis***, January.

Wienke, D; Xie, Y; Hopke, P.K. (1994). An Adaptive Resonance Theory Based Artificial Nueral Network (ART-2a) for Rapid Identificaiton of Airborne Particle Shapes from Hteir Scanning Electron Microscopy Images. ***Chemometrics and Intelligent Laboratory Systems*** 25:367–387.

Williams, R., Suggs, J., Zweidinger, R., Evans, G., Creason, J., Kwok, R., Rodes, C., Lawless, P., Sheldon, L., 2000a. The 1998 Baltimore particulate matter epidemiology-exposure study: part 1 - comparison of ambient, residential outdoor, indoor and apartment particulate matter monitoring. Journal of Exposure Analysis and Environmental Epidemiology, 10: 518-532.

Williams, R., Suggs, J., Creason, J., Rodes, R., Lawless, P., Kwok, R., Zweidinger, R., Sheldon, L., 2000b. The 1998 Baltimore particulate matter epidemiology-exposure study: part 2 - personal exposure assessment associated with an elderly study population. Journal of Exposure Analysis and Environmental Epidemiology, 10: 533-543.

Willis, R.D.; Ellenson, W.D.; Conner, T.L. (2001). Monitoring and Source Apportionment of Particulate Matter near a Large Phosphorus Production Facility. ***J. Air Waste Manage. Assoc.*** 51:1142–1166.

Wurster, R.; Ocker, B. (1993). Investigation of Nanoparticles by Atomic and Lateral Force Microscopy. ***Scanning*** 15:130–135.

Xhoffer, C.; Wouters, L.; Van Grieken, R. (1992). Characterization of Individual Particles in the North Sea Surface Microlayer and Underlying Seawater: Comparison with Atmospheric Particles. ***Environ. Sci. Technol.*** 26:2151–2162.

Xie, Y.; Hopke, P.K.; Wienke, D. (1994). Airborne Particle Classification with a Combination of Chemical Composition and Shape Index Utilizing an Adaptive Resonance Artificial Neural Network. ***Environ. Sci. Technol.*** 28:1921-1926.

Zayed, J.; Hong, B.; L'Esperance, G. Characterization of Manganese-Containing Particles Collected from the Exhaust Emissions of Automobiles Running with MMT Additive; *Environ. Sci. Technol.* **1999**, *33 (19)*, 3341-3346.

Appendix A

- **Example of LEO/PGT Output**
- **Example of PSEM Output**

Example of LEO/PGT Data Output

```
Sample: Brownsville 159609    Units: micrometers

Number of features:
   Total:                          323
   Excluded by selection formula:  99* (See note at bottom)
   Deleted manually:                0
   Remaining in analysis:         224

Area of all fields:
   Total    :   7.2256e+04
   Remaining:   7.0033e+04

Area of all features:
   Total    :   6.5718e+03 (  9.10% of field)
   Remaining:   4.3491e+03 (  6.02% of field)
                (  6.21% of the remaining field)

Area of all features filled:
   Total    :   6.6053e+03 (  9.14% of field)
   Remaining:   4.3615e+03 (  6.04% of field)
                (  6.23% of the remaining field)


Feature classification report:
   Class name    Total    % of Analyzed  % of All
   Al_Si:          42          18.75        18.75
   Quartz:         16           7.14         7.14
   Ca_rich:        25          11.16        11.16
   Ca_S:           19           8.48         8.48
   Organic:        22           9.82         9.82
   Metal_rich:      2           0.89         0.89
   trace_metals:    1           0.45         0.45
   Na_Cl:          11           4.91         4.91
   Mixed_mineral:  45          20.09        20.09
   Na_enriched:    29          12.95        12.95
   Mg_enriched:    17           7.59         7.59
   S_enriched:     18           8.04         8.04
   Cl_enriched:    50          22.32        22.32
   No class match: 47          20.98        20.98
```

* Note added by authors: The “selection formulas” are user-defined rules which determine whether a given feature will be included or excluded in the feature analysis report above. Selection formulas use a comprehensive set of arithmetic operators and functions and basic logic operators and can be applied to virtually any measurable physical (not chemistry) particle parameter (e.g., feature number, x and y coordinates, feature diameters, area, perimeter, volume, aspect ratio, circularity, roughness). The conditions in the selection formulas are tested and if they are false for a given feature, then the feature is excluded. If they are true, then the feature is included in the feature analysis report. A common application of the selection formula is to exclude features that are either too small or too large.

Sample: Brownsville 159609 Units: micrometers

Measurement	Average	Median	Minimum	Maximum	1 Std. Deviation
Avg Diameter	5.61	4.71	3.01	14.56	2.61

Sample: Brownsville 159609 Units: micrometers

Field	Area	#Features	Area of Features	#/Area	Area Fraction	um/Pixel	1
72256		323	6605	0.00447	0.0910	0.5940	

Sample: Brownsville 159609 Units: micrometers

Feature#*	Field	Avg Diameter	Circularity	Volume	Classes
1	1	3.39	1.77	9.0	Organic Mixed_mineral
2	1	3.01	2.05	5.16	Na_enriched Cl_enriched
5	1	7.58	2.08	90.24	not classified
6	1	3.14	2.24	5.52	not classified
7	1	3.02	1.67	7.81	not classified
10	1	8.01	1.6	143.64	Ca_rich S_enriched
11	1	3.21	2.12	6.29	not classified
13	1	4.99	1.84	27.24	Organic
14	1	7.22	2.86	47.75	Organic
16	1	8.16	1.90	119.57	Ca_rih
17	1	4.24	1.89	18.83	Cl_enriched
18	1	10.76	2.33	189.79	Mixed_mineral Cl_enriched
21	1	4.52	2.43	17.45	Na_Cl

*Note added by authors: "Feature number" is simply the number, in sequential order, assigned to each particle as it is identified by the image-processing software. Each particle identified in a field image is assigned a unique number, but only those particles which meet the criteria set in the selection formulas are included in the feature report. Thus, particles 3, 4, 8, 9, 12, 15, 19, and 20 were identified by the image processing software but excluded by the selection formula.

Example of PSEM Data Output

Client_Name	mukerjee
Client_Number	
Project_Number	0001
Sample_Number	159601
Analysis_Date	11/22/96
Operator	rdw
Instrument	Personal SEM

Mag	Fields	Grid
600	4.3584	0.579
2000	39.1068	0.174

Classes	#	Number %	Area %	Vol %	Wt %	Counts	Area Fr.	Num/cm^2*
Calcite	366	16.76	37.12	38.80	41.87	2687	0.1358812	3.920E+005
Ca-silicate	103	4.63	14.13	13.69	13.38	3833	0.0517038	1.084E+005
Silicate	150	6.83	14.77	15.07	13.31	3516	0.0540556	1.598E+005
Si/CaCl	65	2.94	7.38	6.92	6.91	3789	0.0270002	6.868E+004
CaCl	250	12.71	7.75	6.31	6.68	2239	0.0283688	2.974E+005
Quartz	58	2.59	6.10	8.07	6.42	2797	0.0223359	6.062E+004
Misc.	49	2.42	3.21	3.31	3.59	2923	0.0117516	5.669E+004
Ca-sulfate	256	13.92	1.28	1.74	1.54	2110	0.0047001	3.256E+005
Salt/CaCl	39	1.87	1.64	1.40	1.49	3628	0.0060083	4.375E+004
MgSi	4	0.19	0.52	1.24	1.12	2952	0.0018956	4.430E+003
Si/Salt	18	0.81	1.35	1.07	1.07	3500	0.0049276	1.906E+004
Na-silicate	15	0.68	0.88	0.69	0.66	3989	0.0032083	1.593E+004
Salt	289	15.65	1.35	0.47	0.51	2783	0.0049404	3.661E+005
Fe-rich	4	0.18	0.29	0.31	0.50	3012	0.0010538	4.181E+003
Cl-rich	141	7.61	0.85	0.29	0.33	1953	0.0031066	1.780E+005
Na-rich	29	1.47	0.36	0.24	0.25	2536	0.0013047	3.429E+004
Sulfate	115	6.21	0.53	0.21	0.19	1928	0.0019496	1.453E+005
Salt/CaSO4	42	2.20	0.31	0.11	0.11	2245	0.0011334	5.137E+004
AlSi	2	0.09	0.14	0.05	0.05	1411	0.0005012	2.090E+003
Barite	1	0.04	0.02	0.01	0.01	2508	0.0000840	1.045E+003
Fe-silicate	1	0.04	0.01	0.00	0.01	3620	0.0000385	1.045E+003
Si/CaSO4	1	0.04	0.01	0.01	0.00	3270	0.0000499	1.045E+003
Dolomite	1	0.06	0.01	0.00	0.00	1855	0.0000190	1.294E+003
Fe-spheres	1	0.06	0.00	0.00	0.00	2329	0.0000012	1.294E+003
Totals	2000	100.00	100.00	100.00	100.00	2666	0.3660194	2.339E+006

* Note added by authors: "Num / cm^2", last column of data, is the number of particles per square cm of sample for the listed class. Typically, only a small fraction of a square cm of a sample is analyzed. Therefore the values in this column are simple extrapolations based on the number of particles in the listed class which were identified in the area of sample actually analyzed. The extrapolated Num/cm^2 therefore assumes a uniform particle loading over the entire sample.

Client_Name mukerjee
Client_Number
Project_Number 0001
Sample_Number 159601
Analysis_Date 11/22/96
Operator rdw
Instrument Personal SEM

Aerodynamic Mass Distribution by Aerodynamic Diameter (microns)

Classes	Mass %	<<< 0.0	0.7	1.3	2.0	2.7	3.3	4.0	4.7	5.3	6.0	6.7	7.3	8.0	8.7	9.3	10.0 >>>
Calcite	41.9	0.0	0.0	0.0	0.0	0.1	0.1	0.4	0.6	0.8	0.7	1.3	2.0	1.5	2.1	1.7	1.9 86.8
Ca-silicate	13.4	0.0	0.0	0.0	0.0	0.0	0.1	0.3	0.2	0.6	1.2	0.9	2.0	3.4	3.3	1.9	3.0 83.0
Silicate	13.3	0.0	0.0	0.0	0.1	0.0	0.2	0.8	0.7	1.2	2.3	3.1	2.6	3.4	3.8	3.9	7.4 70.6
Si/CaCl	6.9	0.0	0.0	0.0	0.0	0.1	0.0	0.2	0.1	0.5	2.8	2.7	0.9	6.5	3.1	5.0	2.7 75.4
CaCl	6.7	0.0	0.0	0.2	0.4	0.5	0.4	1.0	1.2	2.1	1.8	3.8	1.9	0.7	3.8	3.6	2.3 76.4
Quartz	6.4	0.0	0.0	0.0	0.0	0.2	0.5	0.2	1.1	2.5	1.2	1.8	1.8	1.1	1.2	1.1	5.6 81.7
Misc.	3.6	0.0	0.0	0.0	0.2	0.1	0.1	0.0	0.4	0.7	2.3	0.6	2.8	1.2	5.3	0.0	0.0 86.2
Ca-sulfate	1.5	0.0	0.1	1.7	1.3	1.1	1.4	0.3	0.9	0.4	0.0	0.0	0.0	4.4	0.0	0.0	8.9 79.5
Salt/CaCl	1.5	0.0	0.0	0.1	0.1	0.1	0.4	0.4	1.7	3.2	2.6	2.1	11.9	11.3	0.0	4.6	6.8 54.6
MgSi	1.1	0.0	0.0	0.0	0.0	0.0	0.0	1.0	0.0	0.0	0.0	0.0	0.0	0.0	0.0	0.0	0.0 98.9
Si/Salt	1.1	0.0	0.0	0.0	0.1	0.0	0.4	0.8	0.9	3.1	0.6	2.4	0.0	5.2	18.1	0.0	0.0 68.4
Na-silicate	0.7	0.0	0.0	0.0	0.0	0.0	1.3	1.6	4.4	2.6	6.3	2.6	0.0	0.0	9.9	0.0	0.0 71.2
Salt	0.5	0.0	0.0	5.6	10.7	6.3	4.5	5.4	0.0	3.8	1.2	0.0	0.0	0.0	0.0	0.0	0.0 62.6
Fe-rich	0.5	0.0	0.0	0.0	0.0	0.0	0.0	0.6	0.0	0.0	0.0	7.4	4.7	0.0	0.0	0.0	0.0 87.3
Cl-rich	0.3	0.0	0.0	4.6	7.4	4.5	2.1	3.4	0.0	0.0	13.9	0.0	0.0	0.0	0.0	0.0	0.0 64.2
Na-rich	0.3	0.0	0.0	0.8	1.1	1.7	3.7	3.0	4.0	2.8	7.8	0.0	22.8	0.0	0.0	0.0	0.0 52.4
Sulfate	0.2	0.0	0.3	5.8	7.6	3.9	1.3	9.8	8.5	8.7	10.6	0.0	0.0	0.0	43.6	0.0	0.0 0.0
Salt/CaSO4	0.1	0.0	0.0	3.2	5.7	3.7	14.8	13.4	9.2	0.0	0.0	0.0	0.0	50.0	0.0	0.0	0.0 0.0

Appendix B

- **Submittal Form for SEM/EDX Samples**
- **Assignment of SEM IDs**
- **Sample Log-In/Log-Out**

Submittal Form for SEM/EDX Samples

Project Name (8 characters or less): _____ Date: _____

6-digit XRFID (if assigned by the XRF Lab): _____

OR Your 6-digit Sample ID: _____

Description (*what are they, how collected, particle size, chemistry, etc. If samples have been prepped, sieved, or deposited on filters or substrates, please describe*): ***Respond in the expanding boxes below.***

NOTE: Samples must be vacuum-compatible. Loose samples not collected on appropriate substrates will require additional prepping by us -- SUGGESTIONS?

What information do you want SEM/EDX to provide?

_____ Quick evaluation?
_____ Particle size distribution (*specify upper and lower size limits*)
_____ Chemical class distribution
_____ Pretty pictures (*Polaroids and/or .TIF files*)
_____ Search for specific type of particle
_____ Please call me to discuss
_____ Special requests or requirements (describe):

How do you want the results? (Specify desired electronic format).

_____ Hard copy _____ Electronic copy
_____ Text report _____ Spreadsheet _____ Photomicrographs
_____ Size distribution histograms _____ Oral debriefing _____ Other (specify)

Contact person: _____

Tel: _____ Fax: _____ E-mail: _____

When do you need results? _____

Sample disposition: return to client _____ archive in SEM lab _____ discard _____

SUBMIT ELECTRONIC FORM TO TERI CONNER, SEM WORK ASSIGNMENT MANAGER
Tel: (919) 541-3157 email: Conner.Teri@epamail.epa.gov

ASSIGNMENT OF SEM IDs

First 3 Digits	Study Name	Sub Studies 0	1	2	3	4	5	6	7	8	9
019	EC Quartz filters carbon coat G. Norris										
020	AGEVAL Si/Al spheres D. Heist 5-9-00										
021	SEA-Salt PM 2.5-10µm 2-27-01	12-18-01									
022	WTC NYC Bulk 10-17-01										
023	WTC 1 NHeeRL										
024	Mauna Loa Quartz 12-18-01										

Sample Log-In/Log-Out

		SAMPLE	LOG-IN	LOG-OUT			
Date Samples Received	Sample Description	Number Of Samples	Delivered To Lab By	SEMIDs PSEM	SEMIDs LEO/PGT	Sample Numbers Returned	Samples Returned To
4-9-99	NHEERL P. EVANSKY ZINC OXIDE	17	P. Evansky	✓			
4-19-99	BALT. Ret. Home PM 2.5 Teflo	9	G. Norris	✓			
6-30-99	Balt. Ret. Home PM 2.5 Teflo	8	G. Norris	✓			
10-29-99	Porous Media SFE EXTRACTIONS	17	Dan Valleio	✓			
2-8-00	5mm. Nickel mesh Discs. Coated with Gold	19	Bob Quintz	✓			Bob Quintz
3-1-00	Phoenix T. Conner XRF Filters	6	T. Conner	✓			
3-14-00	EC Quartz filters CARBON COAT G. Norris	3	T. Conner	✓			
5-16-00	AGEVAL SI/AL Spheres Nuc/greased.	18	D. Heist	✓			
2-27-01	SEA-SALT PM 2.5-10 um Polycarbonate	19	T. Conner	✓			
10-17-01	WTC NYC BULK	6	F. Blanchard	✓			
12-1-01	WTC 1 Polycarbonate 47 mm NHEERL	4	Fred Blanchard	✓			
12-18-01	Sea-Salt	2	T. Conner	✓			

Appendix C

- **Particle classification rules for $PM_{10-2.5}$ (coarse) particles**
- **Particle classification rules for $PM_{2.5}$ (fine) particles**

Particle classification rules for $PM_{10-2.5}$ (coarse) particles

Particle Class	Classification Rule
aerodiam	AeroDia[a] < 2.495
Fly Ash	Aspect[b] < 1.5 and Al > 20 and Al < 50 and Si > 40 and Si < 60 and K >= 2 and K < 8 and Mg <= 5 and Na < 3 and Cl < 3 and Fe >= 1.15 and counts >= 1000
Pb containing	Pb >= 20 and counts >= 1000 or Pb >= 20 and video[c] >= 120
Cr rich	Cr >= 50 and counts >= 1000 or Cr >= 50 and video >= 120
Zn rich	Zn >= 50 and counts >= 1000 or Zn >= 50 and video >= 120
Cu rich	Cu >= 50 and counts >= 1000 or Cu >= 50 and video >= 120
Mn rich	Mn >= 50 and counts >= 1000 or Mn >= 50 and video >= 120
Other Mn	Mn >= 20 and counts >= 1000 or Mn >= 20 and video >= 120
High Ti	Ti >= 70 and counts >= 1000
Ti rich	Ti >= 50 and counts >= 1000 or Ti >= 50 and video >= 120
Ti rich al-silicates	Al >= 10 and Si >= 20 and Ti >= 10 and Si >= Ti and counts >= 800 and video >=80
Other Ti	Ti >= 20 and Ti > Ca and Ti > Fe and counts >= 800 and video >= 80
Ni and/or V	Ni + V >= 20 and counts >= 1000 or Ni + V >= 20 and video >= 120
Ba containing	Ba >= 10 and Ba > Fe and counts >= 1000 or Ba >= 10 and Ba > Fe and video >= 120
High Fe	Fe >= 70 and counts >= 1000
Fe rich	Fe >= 50 and Ca < 25 and S < 25 and Cl < 25 and Si < 10 and Al < 10 and Ba < 10 and counts >= 1000 or Fe >= 50 and Ca < 25 and S < 25 and Cl < 25 and Si < 10 and Al < 10 and Ba < 10 and video >= 120
Fe rich al-silicates	Al >= 10 and Si >= 20 and Fe >= 10 and Si >= Fe and Fe > Ca and counts >= 800 and video >=80
Other Fe	Fe >= 20 and counts >= 800 or Fe >= 20 and video >= 80
Ca and Mg rich	Mg >= 10 and Ca >= 25 and Mg > S and Mg > Si and Ca > Si and counts >= 800 and video >= 80
Ca and S rich	Ca + S >= 50 and Ca >= 20 and S >= 20 and Ca > Si and counts >= 800 and video >= 80 or S >= 30 and Ca >= 30 and Ca > Si and counts >= 800 and video >= 80
High Ca	Ca >= 70 and counts >= 800 or Ca >= 70 and video >= 80
Ca rich	Ca >= 50 and counts >= 800 or Ca >= 50 and video >= 80
Ca rich al-silicates	Al >= 10 and Si >= 20 and Ca >= 10 and Si >= Ca and counts >= 800 and video >=80
Other Ca	Ca >= 20 and counts >= 800 and video >= 80
K and S rich	S >= 10 and S > P and K >= 20 and K + S >= 40 and counts >= 800 and video >= 80
K and P rich	P >= 40 and K >= 10 and K + P >= 60 and counts >= 800 and video >= 80
Quartz	Si >= 75 and Al < 10 and counts >= 1000
Al-Zr-Cl	Al >= 30 and Zr >= 20 and Cl >= 3 and video >= 100 and counts >= 1000
Al rich	Al >= 50 and counts >= 800 or Al >= 50 and video >= 80
Talc	Mg >= 10 and Al < 10 and Si >= 40 and Ca < 10 and Fe < 10 and counts >= 800 and video >= 80 or Mg >= 15 and Si >= 40 and counts >= 500
Mixed al-silicates	Al >= 10 and Si >= 20 and counts >= 800 and video >= 80 or Si >= 40 and counts >= 800 and video >= 80
Salt	Na + Cl >= 40 and counts >= 1000 or Na + Cl >= 40 and video >= 120
Other - High Counts	Counts >= 1000
Other - Mid Counts	Counts < 1000 and counts >= 500
Other - Low Counts	Counts < 500

[a]aerodynamic diameter
[b]aspect ratio (ratio of maximum diameter to perpendicular diameter)
[c]grayscale brightness value

Particle classification rules for $PM_{2.5}$ (fine) particles

Particle Class	Classification Rule
aerodiam	AeroDia[a] >= 2.495
Salt/Marine	Na >= 5 and Cl >= 20 and Cl > Si and Cl > Al or Na + Cl >= 30 and Cl > Si and Cl > Al or S >= 10 and Cl >= 10 and Ca >= 10 and Cl > Si and Cl > Al or Na + Mg + S + Cl + Br >= 70 and Ca < 20
Sulfate	S >= 40 and counts >= 250 and Dave[b] >= 0.3 and Na < 10 and Mg < 10 and Al + Br < 10 and Si < 10 and Cl 10 and K < 10 and Ca < 10 and Fe < 10
Other - Low Counts	Counts < 500
Fly Ash	Aspect[c] < 1.5 and Al + Br > 20 and Al + Br< 50 and Si > 40 and Si < 60 and K >= 2 and K < 8 and Mg <= 5 and Na < 3 and Cl < 3 and Fe >= 1.15 and Fe < 10 and Ca < 10
Pb rich	Pb >= 50 and video[d] >= 100 and counts >= 1000
Other Pb	Pb >= 20 and counts >= 750 and video >= 90
Bi rich	Bi >= 50 and video >= 100 and counts >= 1000
Other Bi	Bi >= 20 and counts >= 750 and video >= 90
Cr rich	Cr >= 50 and counts >= 1000 or Cr >= 50 and video >= 80
Other Cr	Cr >= 20
Zn rich	Zn >= 50 and counts >= 1000 or Zn >= 50 and video >= 80
Other Zn	Zn >= 20
Cu rich	Cu >= 50 and counts >= 1000 or Cu >= 50 and video >= 80
Other Cu	Cu >= 20
Mn rich	Mn >= 50 and counts >= 1000 or Mn >= 50 and video >= 80
Other Mn	Mn >= 20
High Ti	Ti >= 70 and counts >= 750 and video >= 90 or Ti >= 70 and counts >= 1000 or Ti >= 70 and video >= 100
Ti rich	Ti >= 50 and counts >= 750 or Ti >= 50 and video >= 80
Other Ti	Ti >= 20
High Fe	Fe >= 70 and counts >= 750 and video >= 90 or Fe >= 70 and counts >= 1000 or Fe >= 70 and video >= 100
Fe rich	Fe >= 50 and counts >= 750 or Fe >= 50 and video >= 80
Ca and Mg rich	Mg >= 10 and Ca >= 25 and Mg > S and Mg > Si
Ca and S rich	Ca + S >= 50 and Ca >= 20 and S >= 20 or S >= 30 and Ca >= 30
High Ca	Ca >= 70 and counts >= 1000 or Ca >= 70 and video >= 80
Ca rich	Ca >= 50 and counts >= 1000 or Fe >= 50 and video >= 80
K-S-P rich	K + S + P >= 60 and K >= 10 and K > Ca or K + S >= 40 and K >= 10 and K > Ca or K + P >= 40 and K >= 10 and K > Ca
Quartz	Si >= 75 and Al + Br < 10 and counts >= 1000 or Si >= 75 and Al + Br < 10 and video >= 80
Fe rich al-silicates	Si >= 10 and Al + Br >= 10 and Fe >= 10 and Si > S and Fe > Ti and video >= 80 or Si >= 10 and Al + Br >=10 and Fe >= 10 and Si > S and Fe > Ti and counts >= 1000
Other Fe	Fe >= 20
Ba containing	Ba >= 10 and Ba > Fe and counts >= 1000 or Be >= 10 and Ba > Fe and video >= 80
Ni and/or V	Ni + V >= 20 and counts >= 1000 or Ni + V >= 20 and video >= 80
Al-Zr-Cl	Al + Br >= 30 and Zr >= 20 and Cl >= 3
Al rich	Al + Br >= 50 and counts >= 750 or Al + Br >= 50 and video >= 90
Talc	Mg >= 10 and Al + Br < 10 and Si >= 40 and Ca < 10 and Fe <
Other Ca	Ca >= 20
Mixed al-silicates	Al + Br + Si >= 30 and Al + Br >= 10 and Si >= 20 or Si >= 40
Other - High Counts	Counts >= 1000
Other - Mid Counts	Counts < 1000 and counts >= 500

[a]aerodynamic diameter
[b]average diameter
[c]aspect ratio (ratio of maximum diameter to perpendicular diameter)
[d]grayscale brightness value

Appendix D

- **Particles from ambient air sample collected in NYC near WTC site**

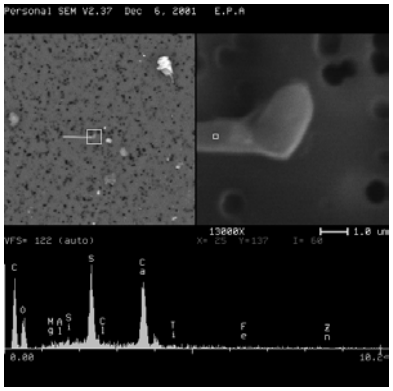
Personal SEM V2.37 Dec 6, 2001 E.P.A
13000X
1.0 um
0.00
10.24

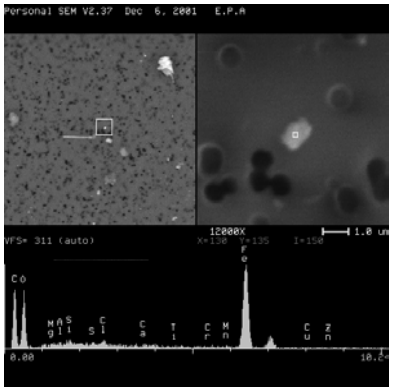
Personal SEM V2.37 Dec 6, 2001 E.P.A
12000X
1.0 um
0.00
10.24

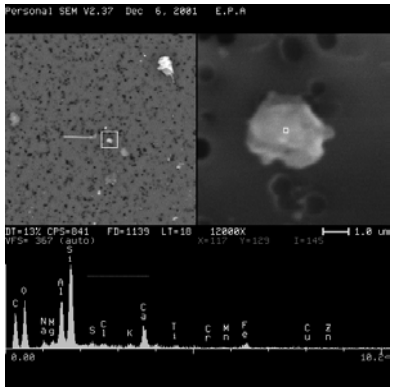
Personal SEM V2.37 Dec 6, 2001 E.P.A
12000X
1.0 um
0.00
10.24

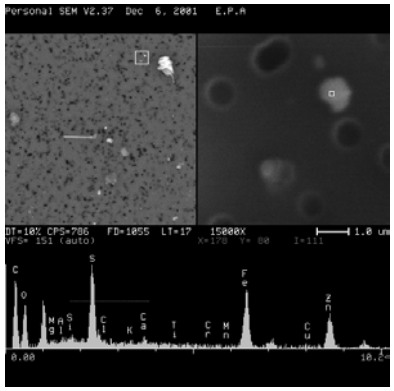
Personal SEM V2.37 Dec 6, 2001 E.P.A
15000X
1.0 um
0.00
10.24

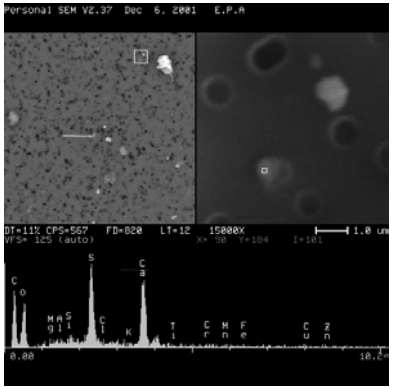
Personal SEM V2.37 Dec 6, 2001 E.P.A
15000X
1.0 um
0.00
10.24

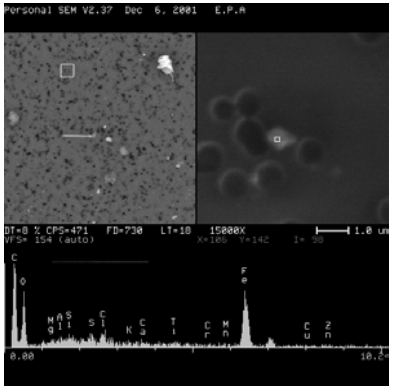
Personal SEM V2.37 Dec 6, 2001 E.P.A
15000X
1.0 um
0.00
10.24

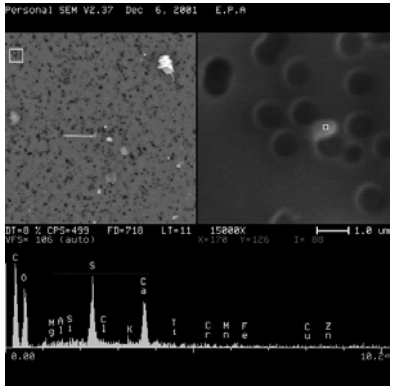
Personal SEM V2.37 Dec 6, 2001 E.P.A
15000X
1.0 um
0.00
10.24

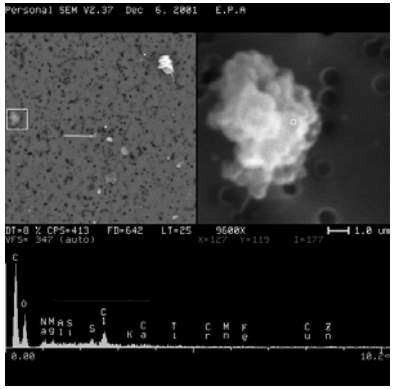
Personal SEM V2.37 Dec 6, 2001 E.P.A
9600X
1.0 um
0.00
10.24

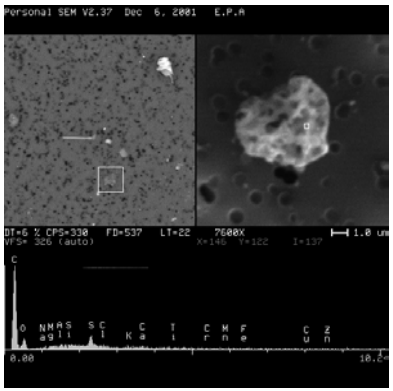
Personal SEM V2.37 Dec 6, 2001 E.P.A
7600X
1.0 um
0.00
10.24

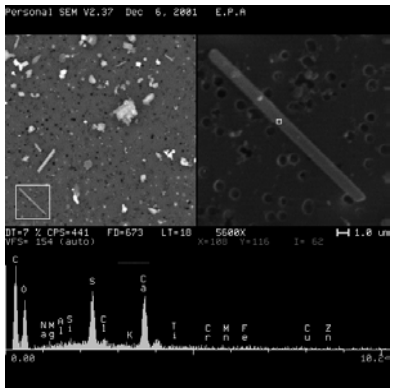
Personal SEM V2.37 Dec 6, 2001 E.P.A
5600X
1.0 um
0.00
10.24

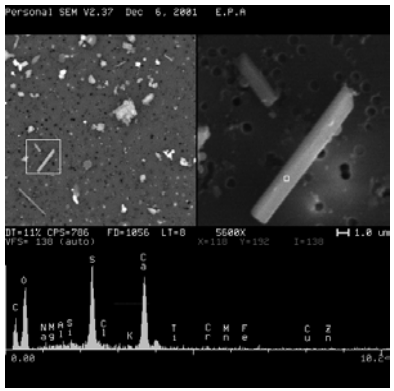
Personal SEM V2.37 Dec 6, 2001 E.P.A
5600X
1.0 um
0.00
10.24

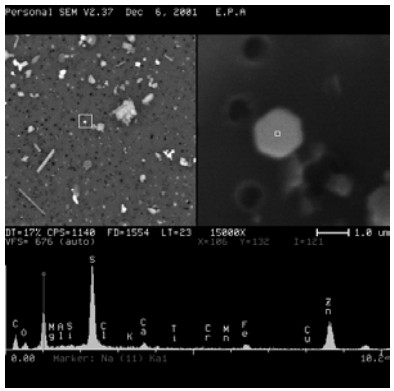
Personal SEM V2.37 Dec 6, 2001 E.P.A
15000X
1.0 um
0.00
10.24

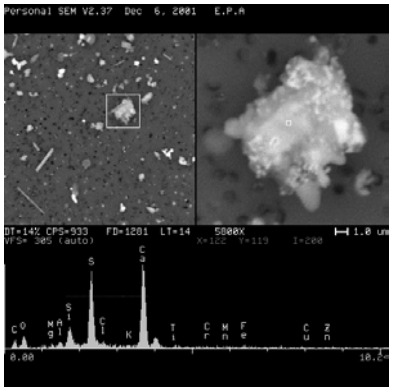
Personal SEM V2.37 Dec 6, 2001 E.P.A
DT=14% CPS=933 FD=1201 LT=14 5800X
VFS= 305 (auto) X=122 Y=119 I=200
1.0 um
0.00
10.24

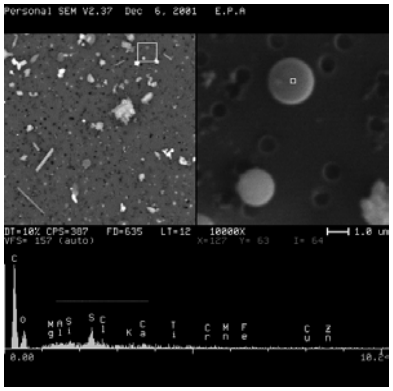
Personal SEM V2.37 Dec 6, 2001 E.P.A
DT=10% CPS=387 FD=635 LT=12 10000X
VFS= 157 (auto) X=127 Y= 63 I= 64
1.0 um
0.00
10.24

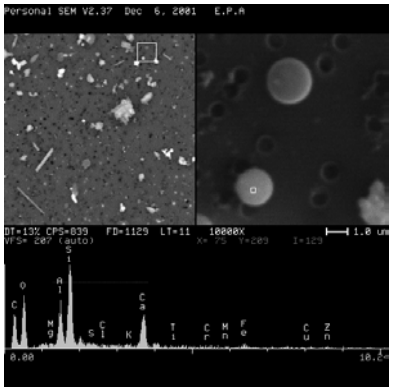
Personal SEM V2.37 Dec 6, 2001 E.P.A
DT=13% CPS=839 FD=1129 LT=11 10000X
VFS= 287 (auto) X= 75 Y=203 I=129
1.0 um
0.00
10.24

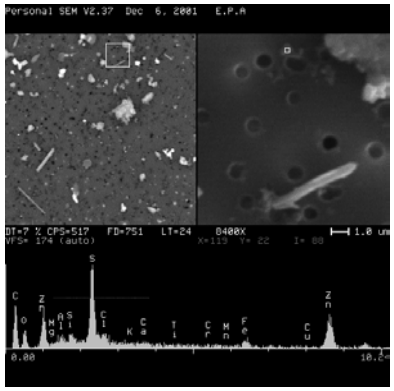
Personal SEM V2.37 Dec 6, 2001 E.P.A
DT=7 % CPS=517 FD=751 LT=24 8400X
VFS= 174 (auto) X=119 Y= 22 I= 88
1.0 um
0.00
10.24

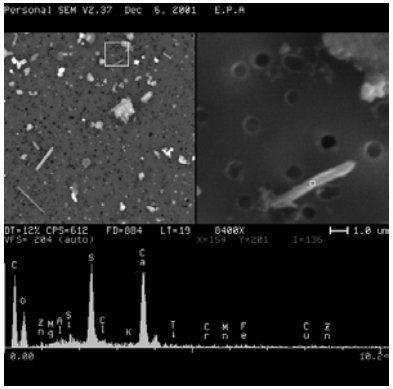
Personal SEM V2.37 Dec 6, 2001 E.P.A
DT=12% CPS=612 FD=884 LT=19 8400X
VFS= 204 (auto) X=154 Y=201 I=136
1.0 um
0.00
10.24

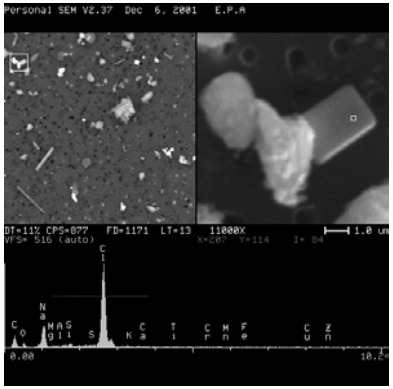
Personal SEM V2.37 Dec 6, 2001 E.P.A
DT=11% CPS=877 FD=1171 LT=13 11000X
VFS= 316 (auto) X=207 Y=114 I= 84
1.0 um
0.00
10.24

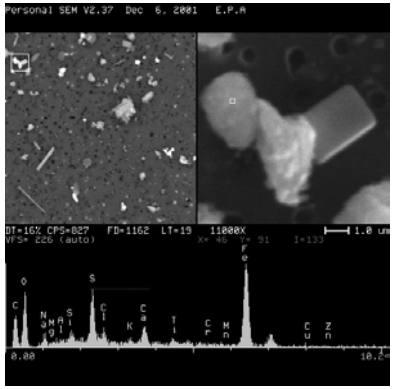
Personal SEM V2.37 Dec 6, 2001 E.P.A
DT=16% CPS=827 FD=1162 LT=19 11000X
VFS= 226 (auto) X= 46 Y= 91 I=133
1.0 um
0.00
10.24

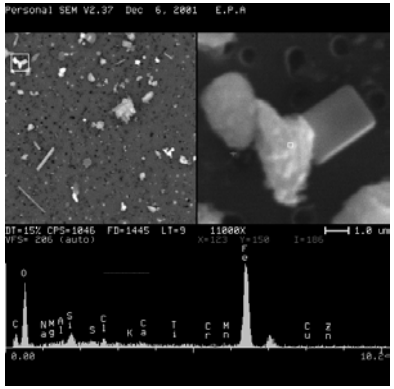
Personal SEM V2.37 Dec 6, 2001 E.P.A
DT=15% CPS=1046 FD=1445 LT=9 11000X
VFS= 286 (auto) X=123 Y=150 I=186
1.0 um
0.00
10.24

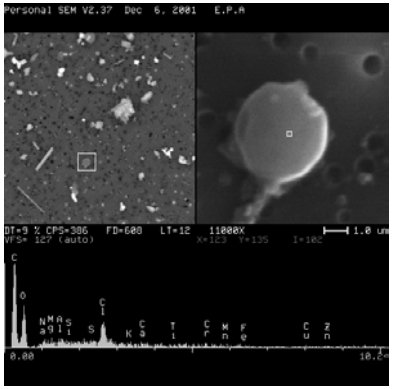
Personal SEM V2.37 Dec 6, 2001 E.P.A
DT=9 % CPS=386 FD=680 LT=12 11000X
VFS= 127 (auto) X=123 Y=135 I=182
1.0 um
0.00
10.24

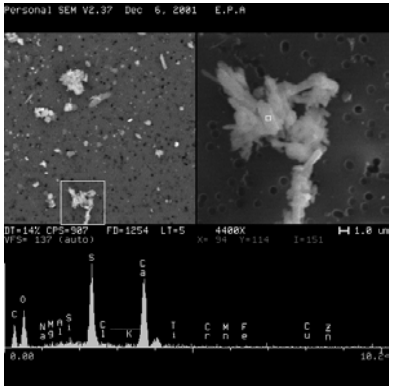
Personal SEM V2.37 Dec 6, 2001 E.P.A
DT=14% CPS=987 FD=1254 LT=5 4400X
VFS= 137 (auto) X= 94 Y=114 I=151
1.0 um
0.00
10.24

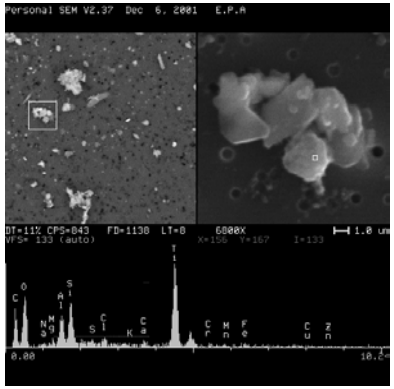
Personal SEM V2.37 Dec 6, 2001 E.P.A
DT=11% CPS=843 FD=1138 LT=8 6000X
VFS= 133 (auto) X=158 Y=167 I=133
1.0 um
0.00
10.24

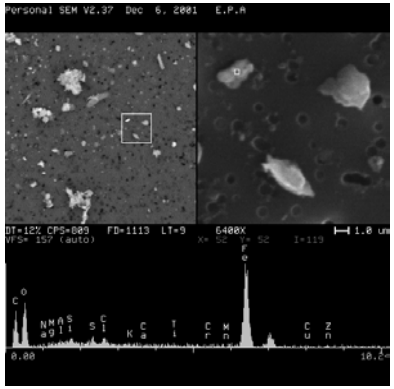
Personal SEM V2.37 Dec 6, 2001 E.P.A
DT=12% CPS=883 FD=1113 LT=9 6400X
VFS= 157 (auto) X= 52 Y= 52 I=119
1.0 um
0.00
10.24

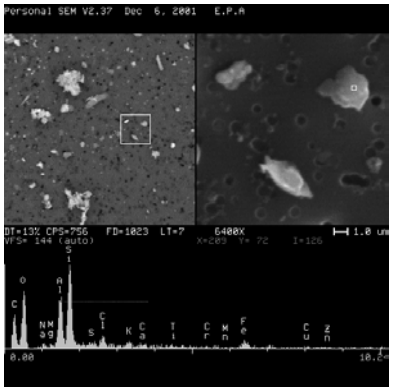
Personal SEM V2.37 Dec 6, 2001 E.P.A
DT=13% CPS=756 FD=1023 LT=7 6400X 1.0 um
VFS= 144 (auto)

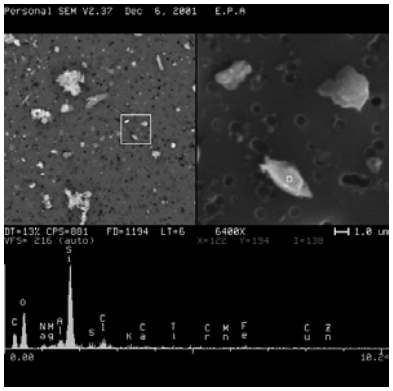
Personal SEM V2.37 Dec 6, 2001 E.P.A
DT=13% CPS=881 FD=1194 LT=6 6400X 1.0 um
VFS= 216 (auto)

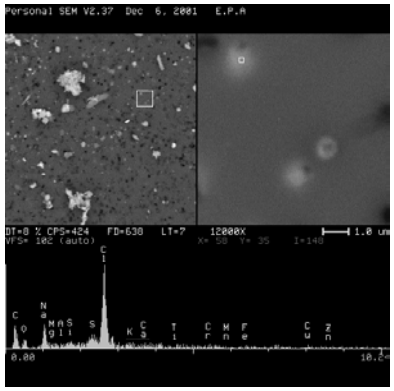
Personal SEM V2.37 Dec 6, 2001 E.P.A
DT=8 % CPS=424 FD=638 LT=7 12800X 1.0 um
VFS= 102 (auto)

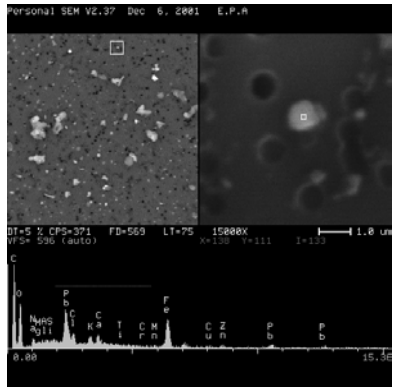
Personal SEM V2.37 Dec 6, 2001 E.P.A
DT=5 % CPS=371 FD=569 LT=75 15000X 1.0 um
VFS= 596 (auto)

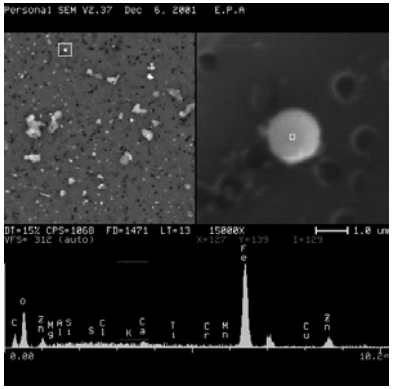
Personal SEM V2.37 Dec 6, 2001 E.P.A
DT=15% CPS=1060 FD=1471 LT=13 15000X 1.0 um
VFS= 312 (auto)

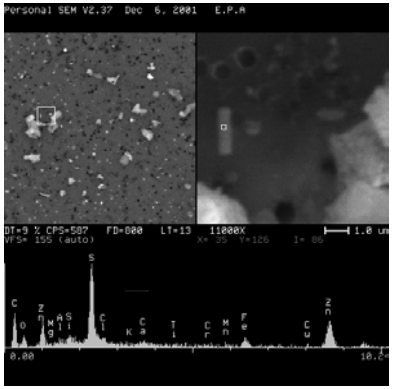
Personal SEM V2.37 Dec 6, 2001 E.P.A
DT=9 % CPS=587 FD=880 LT=13 11000X 1.0 um
VFS= 155 (auto)

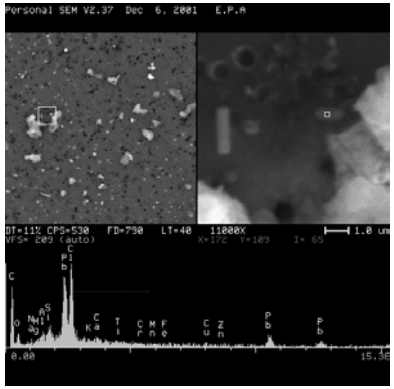
Personal SEM V2.37 Dec 6, 2001 E.P.A
DT=11% CPS=530 FD=790 LT=40 11000X 1.0 um
VFS= 209 (auto)

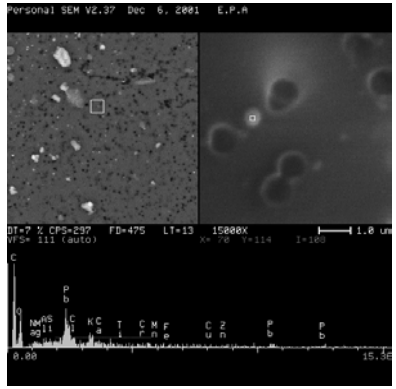
Personal SEM V2.37 Dec 6, 2001 E.P.A
DT=7 % CPS=297 FD=475 LT=13 15000X 1.0 um
VFS= 111 (auto)

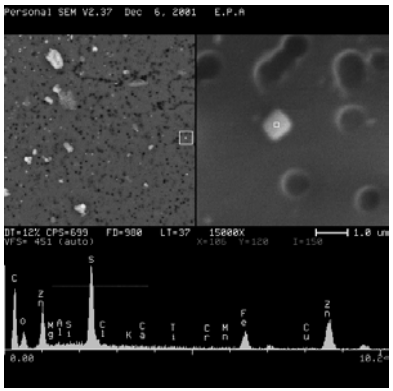
Personal SEM V2.37 Dec 6, 2001 E.P.A
DT=12% CPS=699 FD=980 LT=37 15000X 1.0 um
VFS= 451 (auto)

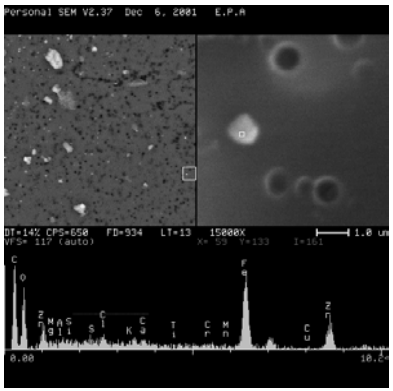
Personal SEM V2.37 Dec 6, 2001 E.P.A
DT=14% CPS=658 FD=934 LT=13 15000X 1.0 um
VFS= 117 (auto)

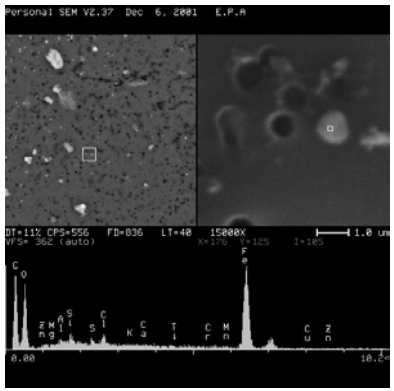
Personal SEM V2.37 Dec 6, 2001 E.P.A
DT=11% CPS=556 FD=836 LT=40 15000X 1.0 um
VFS= 362 (auto)

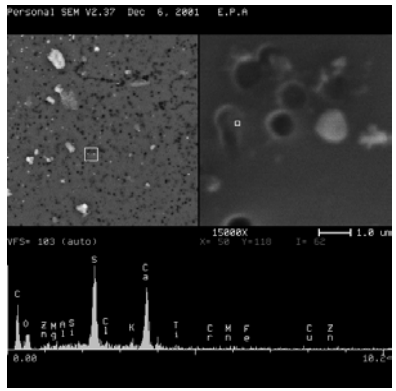
Personal SEM V2.37 Dec 6, 2001 E.P.A
15000X 1.0 um
VFS= 103 (auto)

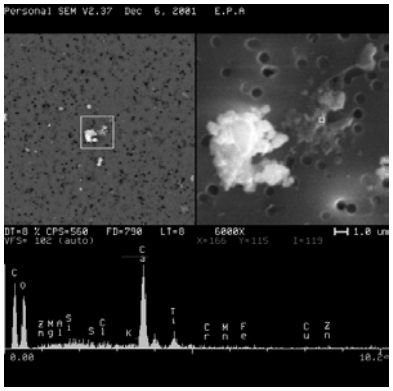
Personal SEM V2.37 Dec 6, 2001 E.P.A
DT=8 % CPS=560 FD=790 LT=8 6000X 1.0 um
VFS= 102 (auto)
0.00
10.24

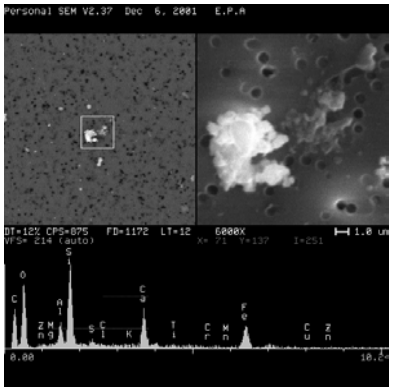
Personal SEM V2.37 Dec 6, 2001 E.P.A
DT=12% CPS=875 FD=1172 LT=12 6000X 1.0 um
VFS= 214 (auto)
0.00
10.24

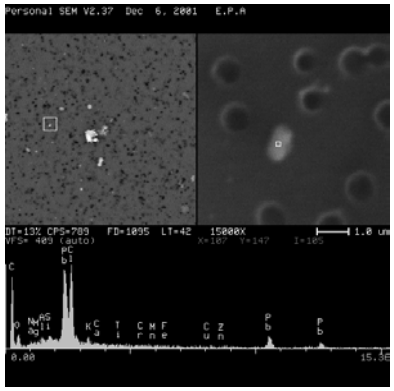
Personal SEM V2.37 Dec 6, 2001 E.P.A
DT=13% CPS=709 FD=1095 LT=42 15000X 1.0 um
VFS= 403 (auto)
0.00
15.36

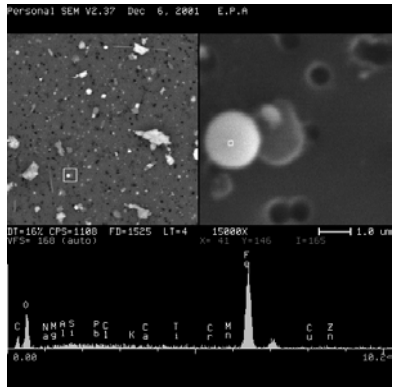
Personal SEM V2.37 Dec 6, 2001 E.P.A
DT=16% CPS=1108 FD=1525 LT=4 15000X 1.0 um
VFS= 168 (auto)
0.00
10.24

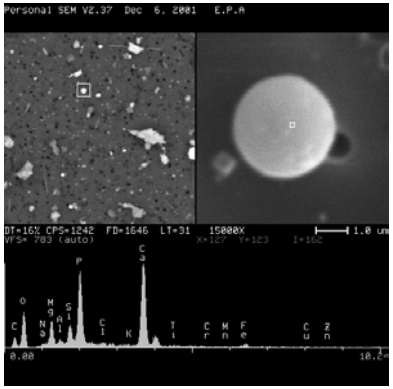
Personal SEM V2.37 Dec 6, 2001 E.P.A
DT=16% CPS=1242 FD=1646 LT=31 15000X 1.0 um
VFS= 783 (auto)
0.00
10.24

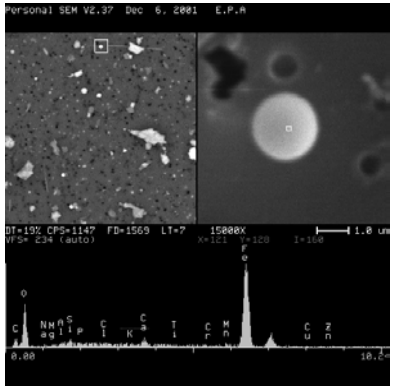
Personal SEM V2.37 Dec 6, 2001 E.P.A
DT=19% CPS=1147 FD=1569 LT=7 15000X 1.0 um
VFS= 234 (auto)
0.00
10.24

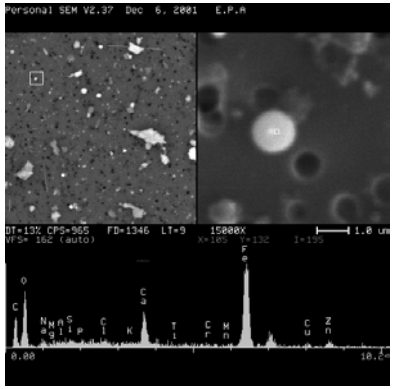
Personal SEM V2.37 Dec 6, 2001 E.P.A
DT=13% CPS=965 FD=1346 LT=9 15000X 1.0 um
VFS= 162 (auto)
0.00
10.24

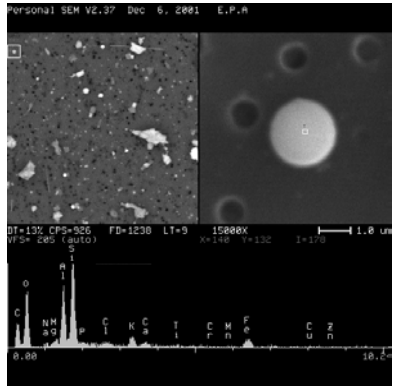
Personal SEM V2.37 Dec 6, 2001 E.P.A
DT=13% CPS=926 FD=1238 LT=9 15000X 1.0 um
VFS= 205 (auto)
0.00
10.24

Appendix E

- **Source particle atlas**

Tire Wear Debris

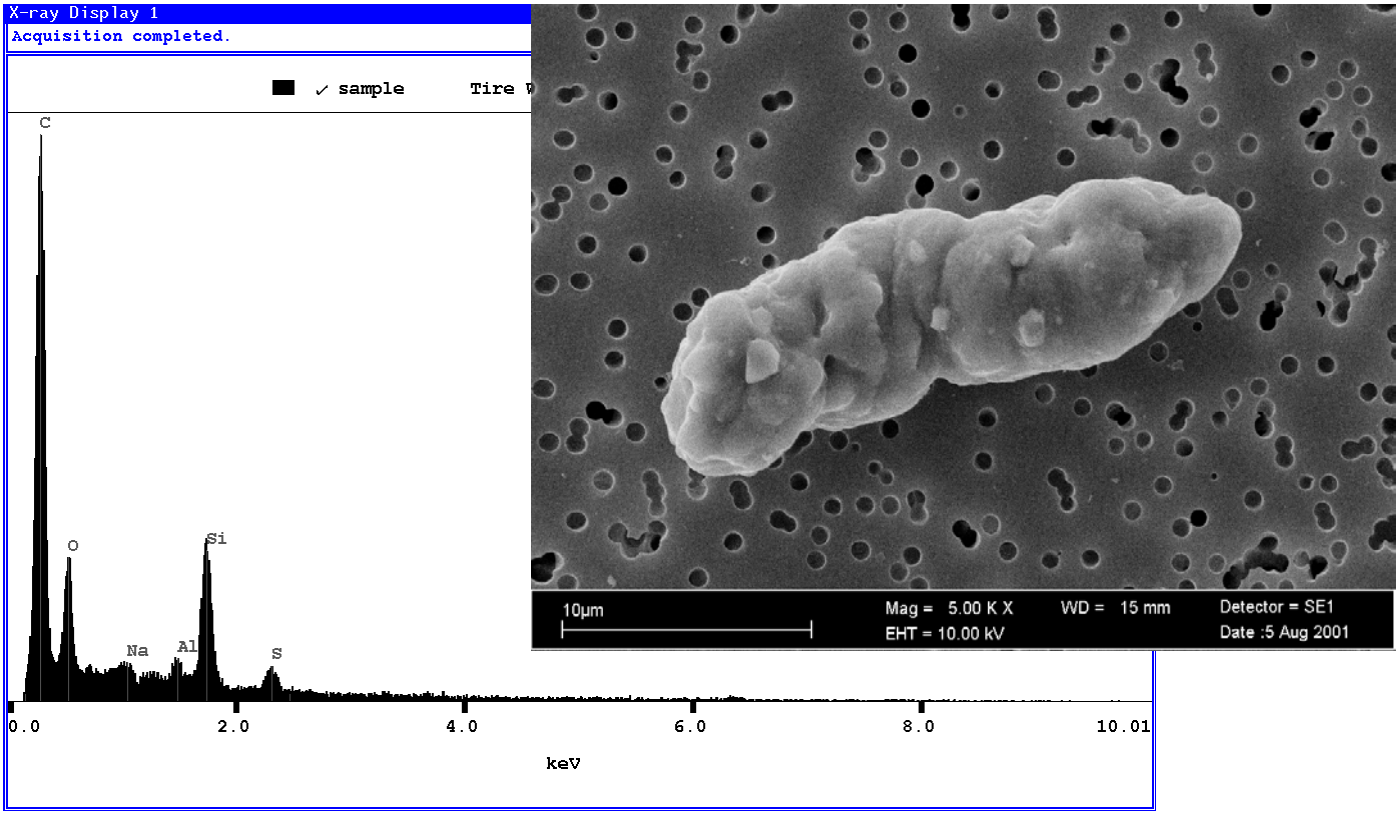

Sample Collection: Sample was collected following a routine auto emissions test in the EPA dynamometer facility. The 1-hr test simulated stop and go driving (brakes were applied during the test), and highway driving. The sample was collected from the front-axle roller which was wiped clean before the dynamometer test. At the conclusion of the test, the portion of the roller which had been under the front passenger wheel was wiped with a 47-mm nuclepore filter. A section of the filter was removed for SEM/EDX analysis.

Particle Description: Particles tend to be elongated, elliptical or cigar-shaped. Bright inclusions in BSE image are Fe-rich aluminum silicates or pure iron.

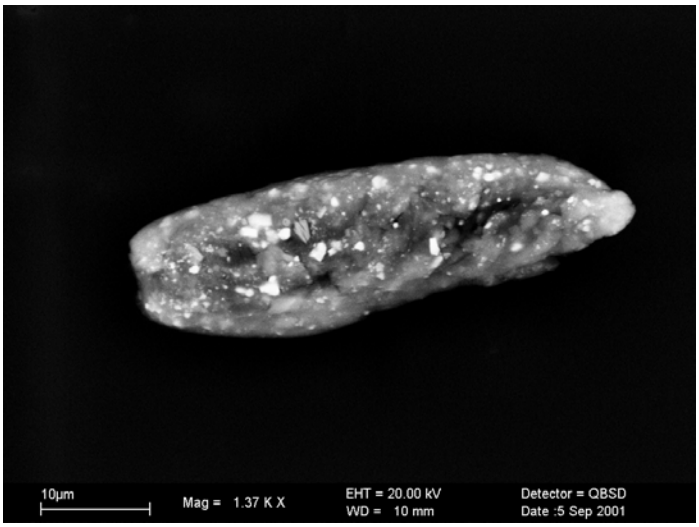

Submitted by: Bob Willis
Date: August 27, 2001

Tire Wear Debris, Page 2

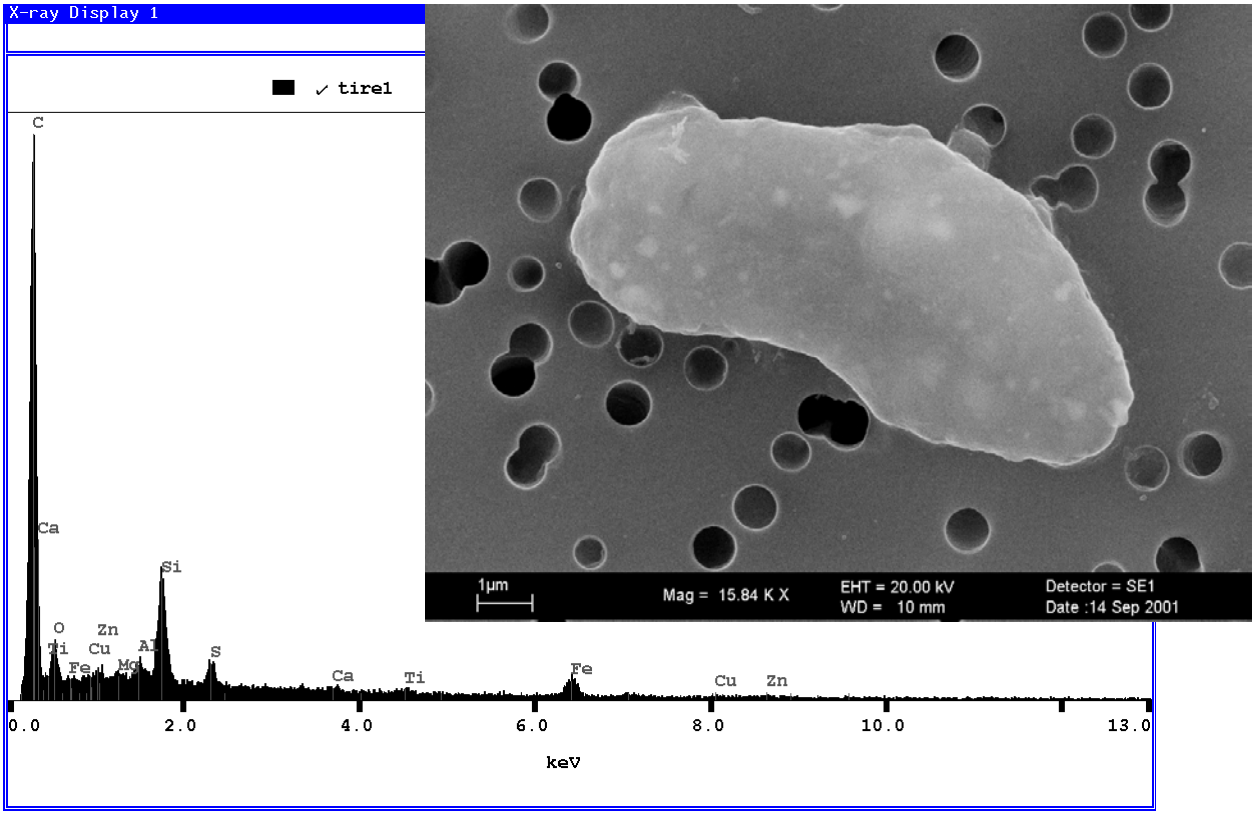

Bright inclusions are mostly rich in Fe or Fe-Si. Occasional Ti-rich inclusions

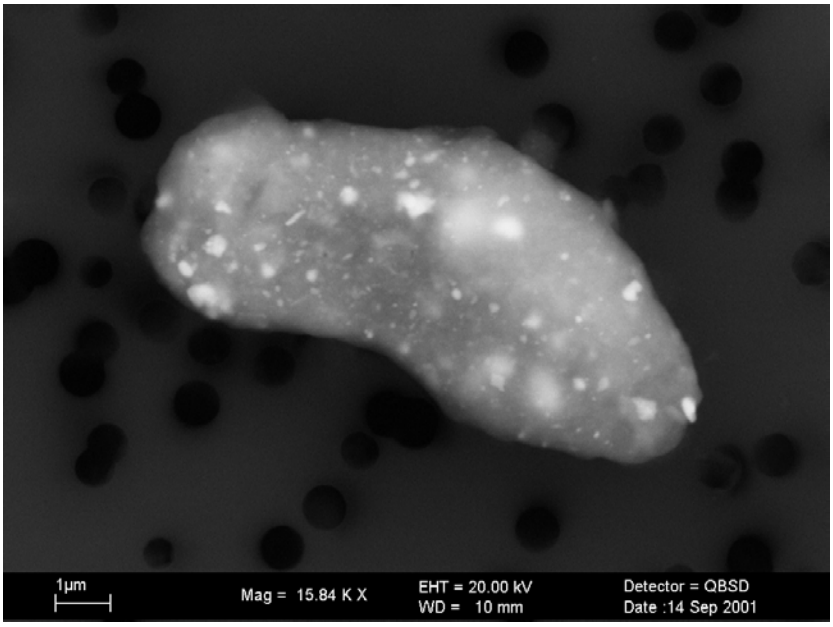

Tire Wear Debris, Page 3

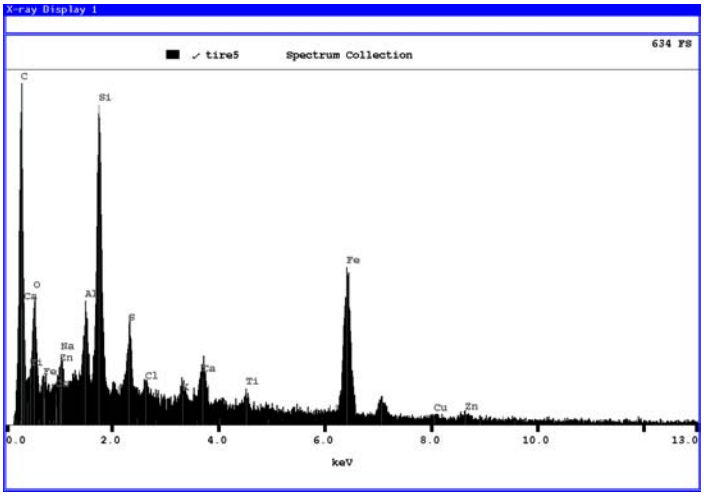

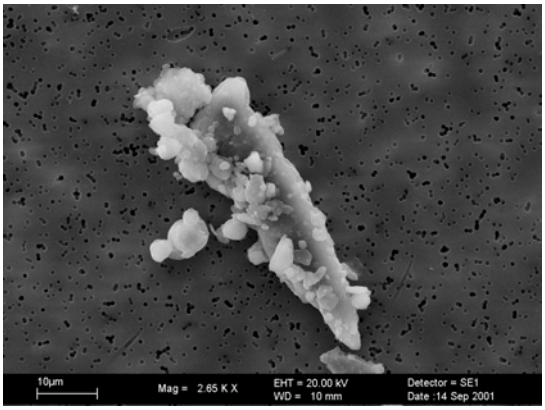

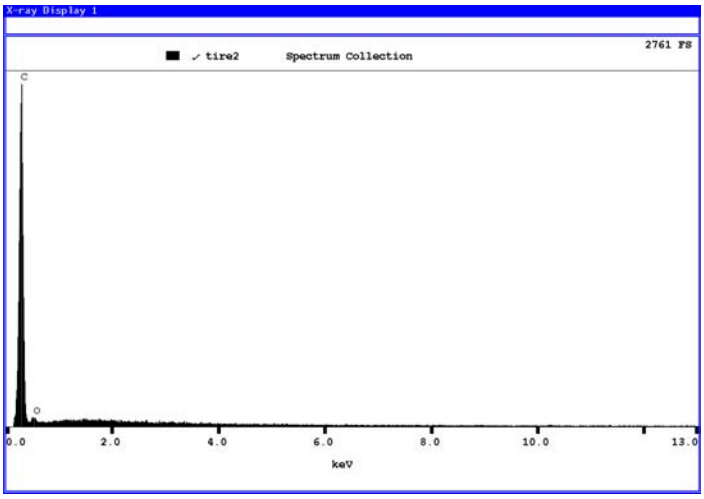

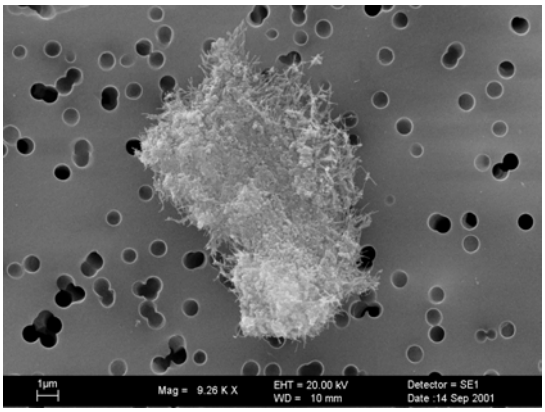

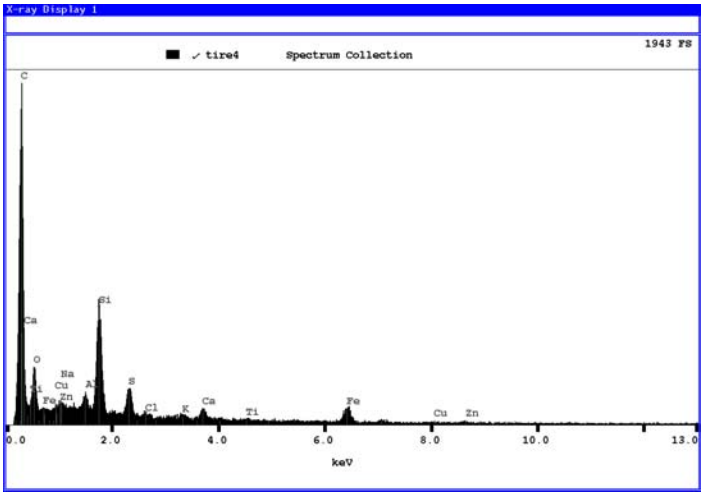

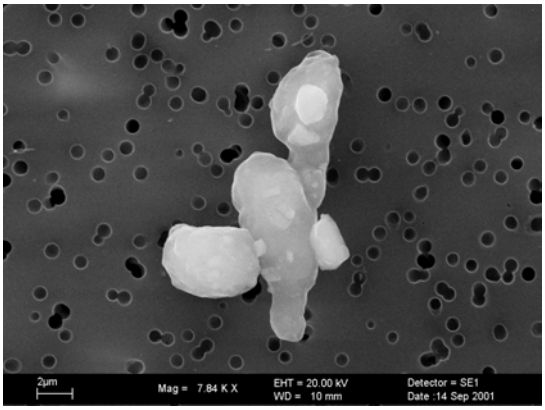

Mushroom Spores (Chloropyllum molybdites)

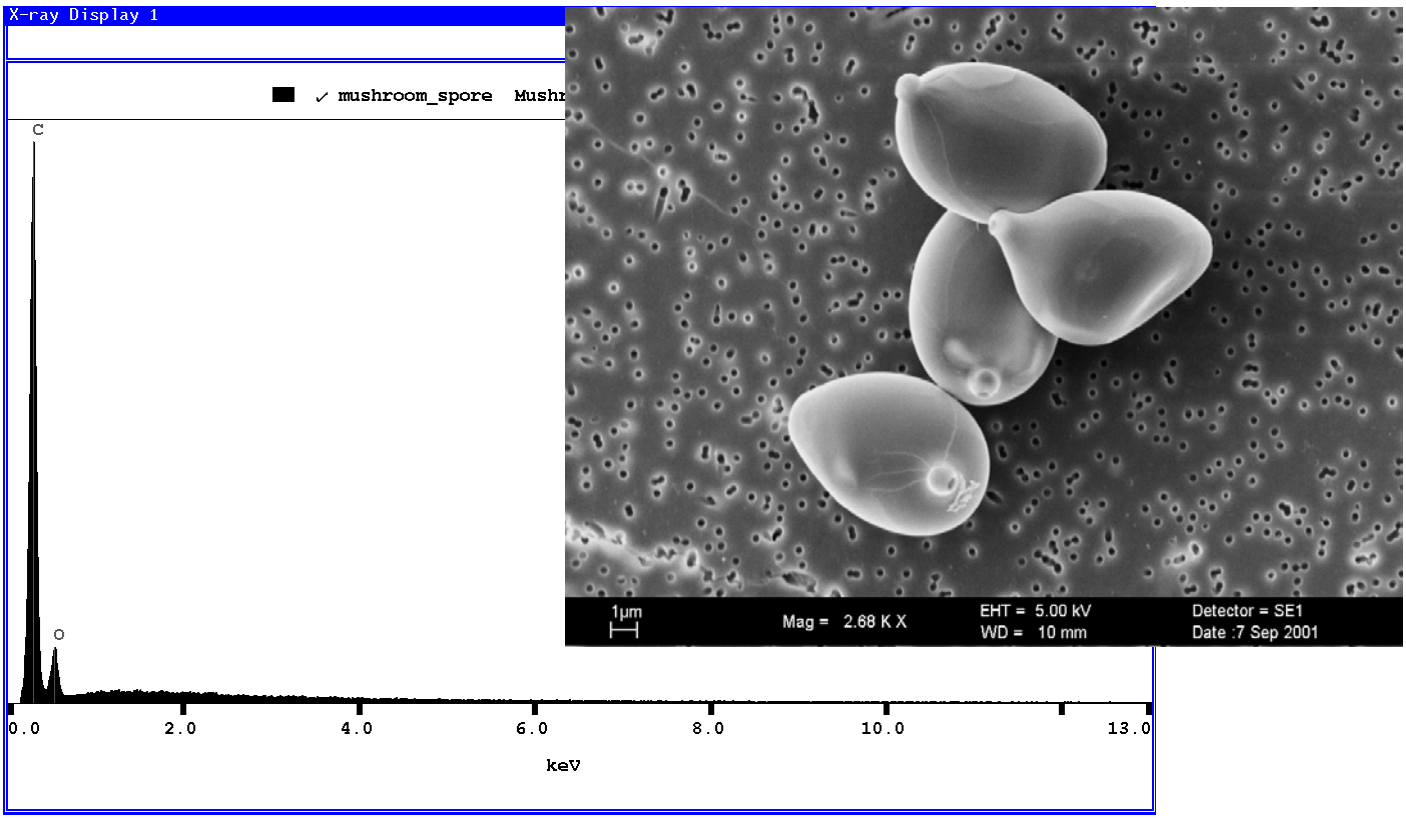

Sample Collection: Contributed by Herb Jacumin.

Particle Description: Spores seem to hold up well to beam heating and vacuum.

Submitted by: Bob Willis
Date: September 7, 2001

Ragweed Pollen

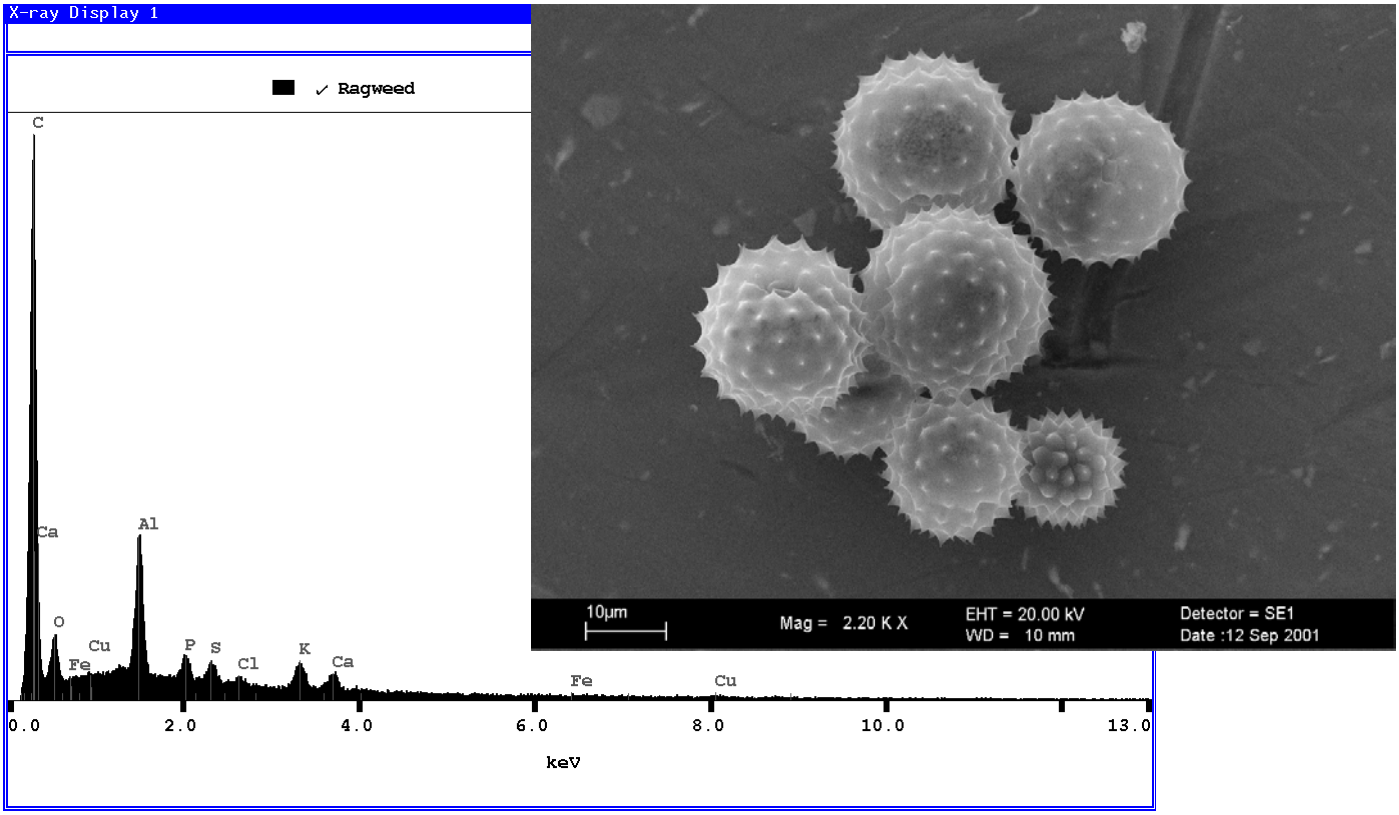

Sample Collection: Southern ragweed. Collected by John Miller.

Particle Description: EDX spectrum is mostly C and O with minor P,S, C, K, Ca. The Al peak is generated by the underlying Al stub.

Submitted by: Bob Willis
Date: September 7, 2001

Calcite Powder

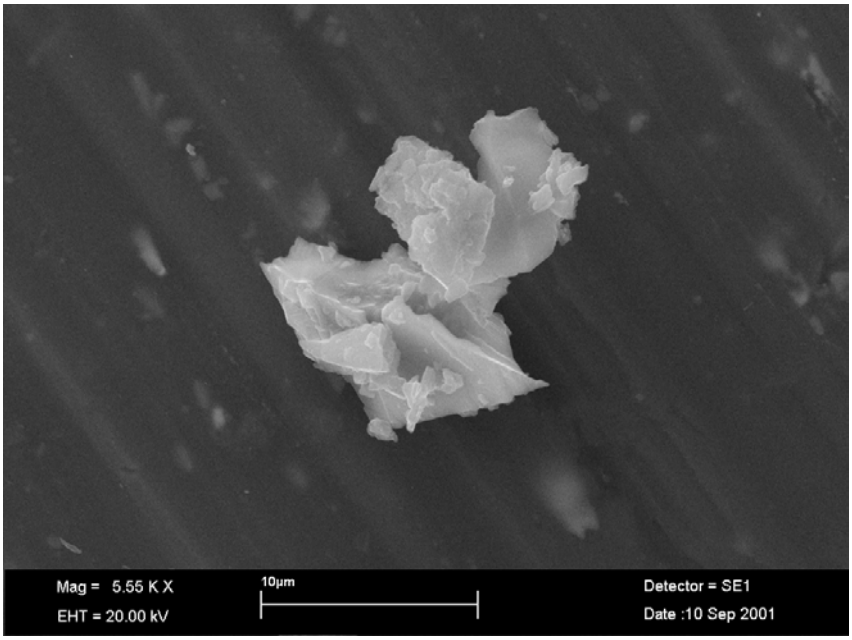

Sample Collection:

Particle Description: Aluminum is contaminant in calcite powder. Particles show rectangular cleavage.

Submitted by: Bob Willis
Date: September 13, 2001

Dandelion Pollen

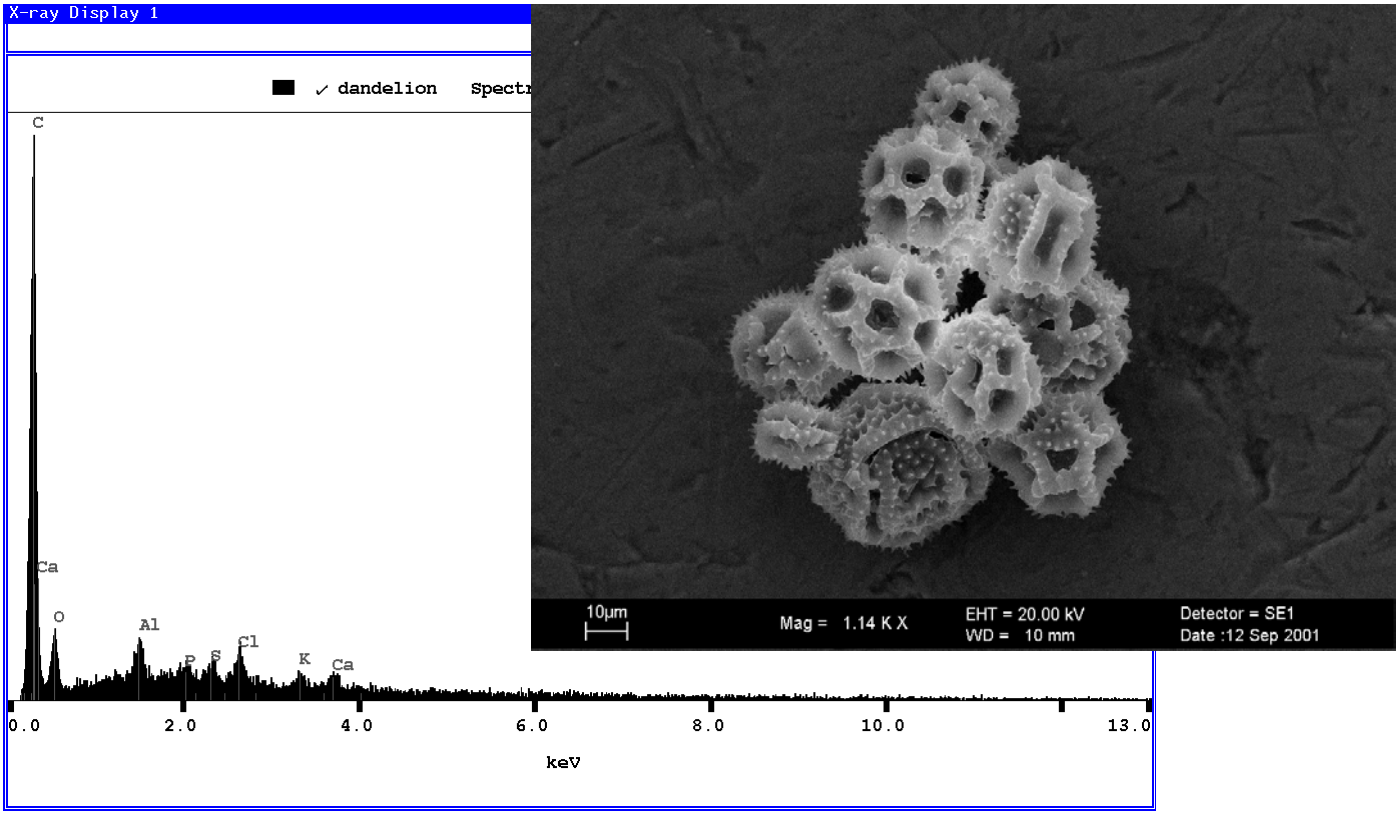

Sample Collection:

Particle Description: EDX spectrum is mostly C and O with minor P, S, Cl, K, and Ca. The Al peak is generated by the stub.

Submitted by: Bob Willis
Date: September 13, 2001

Flyash #8730 (Superfine)

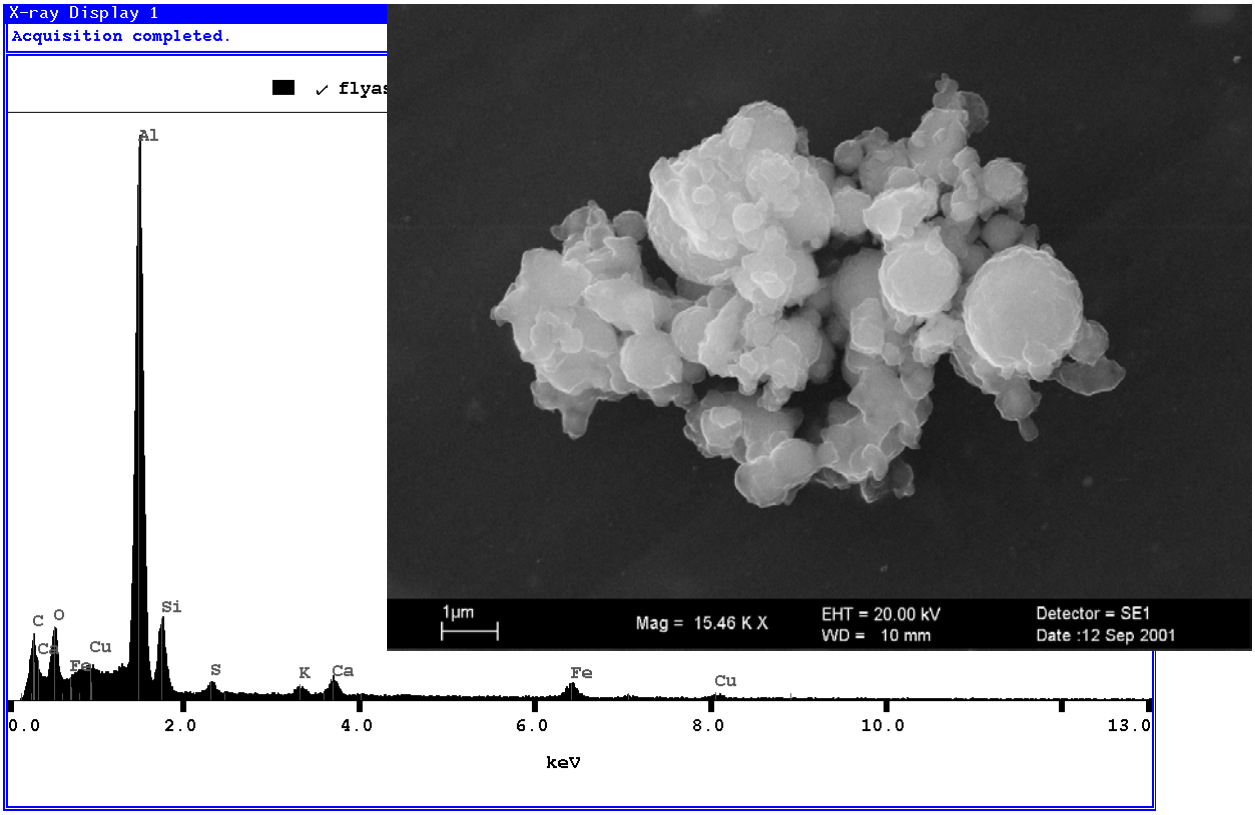

Sample Collection: Sample provided by John Miller. Source unknown.

Particle Description: EDX spectrum is dominated by Aluminum. BSE image shows that spheres have different composition. Brightest spheres are very Fe-rich. Medium bright spheres approach pure Al. Dull spheres are Aluminum-silicates with composition similar to spectrum above.
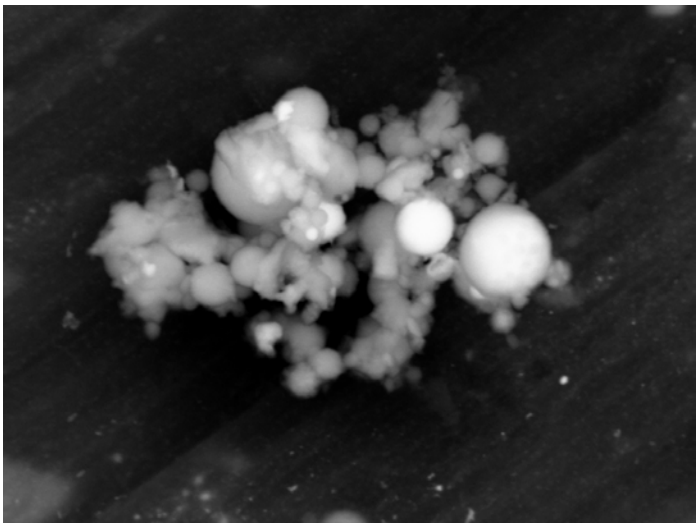
Submitted by: Bob Willis
Date: September 13, 2001